AFRL-PR-WP-TR-2004-2011

SCRAMJET COMBUSTOR SIMULATIONS USING REDUCED CHEMICAL KINETICS FOR PRACTICAL FUELS

Bradley R. Adams, Marc A. Cremer, Christopher J. Montgomery, and Wei Zhao

Reaction Engineering International (REI)
77 West 200 South, Suite 210
Salt Lake City, UT 84101

Dean R. Eklund and C.J. Tam

Taitech, Inc.

J.-Y. Chen

University of California, Berkeley

DECEMBER 2003

Final Report for 08 May 2001 – 08 December 2003

THIS IS A SMALL BUSINESS INNOVATION RESEARCH (SBIR) PHASE II REPORT.

STINFO FINAL REPORT

PROPULSION DIRECTORATE
AIR FORCE MATERIEL COMMAND
AIR FORCE RESEARCH LABORATORY
WRIGHT-PATTERSON AIR FORCE BASE, OH 45433-7251

NOTICE

USING GOVERNMENT DRAWINGS, SPECIFICATIONS, OR OTHER DATA INCLUDED IN THIS DOCUMENT FOR ANY PURPOSE OTHER THAN GOVERNMENT PROCUREMENT DOES NOT IN ANY WAY OBLIGATE THE U.S. GOVERNMENT. THE FACT THAT THE GOVERNMENT FORMULATED OR SUPPLIED THE DRAWINGS, SPECIFICATIONS, OR OTHER DATA DOES NOT LICENSE THE HOLDER OR ANY OTHER PERSON OR CORPORATION; OR CONVEY ANY RIGHTS OR PERMISSION TO MANUFACTURE, USE, OR SELL ANY PATENTED INVENTION THAT MAY RELATE TO THEM.

THIS REPORT HAS BEEN REVIEWED BY THE OFFICE OF PUBLIC AFFAIRS (ASC/PA) AND IS RELEASABLE TO THE NATIONAL TECHNICAL INFORMATION SERVICE (NTIS). AT NTIS, IT WILL BE AVAILABLE TO THE GENERAL PUBLIC, INCLUDING FOREIGN NATIONS.

THIS TECHNICAL REPORT HAS BEEN REVIEWED AND IS APPROVED FOR PUBLICATION.

/s/

DOUGLAS L. DAVIS
AFRL/PRAS, Project Engineer
Propulsion Sciences Branch
Aerospace Propulsion Division

/s/

CAPT. BRIAN C. MCDONALD
Branch Chief
Propulsion Sciences Branch
Aerospace Propulsion Division

/s/

THOMAS A. JACKSON
Deputy for Science
Aerospace Propulsion Division
Propulsion Directorate

/s/

PARKER L. BUCKLEY
Division Chief
Aerospace Propulsion Division
Propulsion Directorate

Do not return copies of this report unless contractual obligations or notice on a specific document require its return.

REPORT DOCUMENTATION PAGE

Form Approved
OMB No. 0704-0188

1. REPORT DATE *(DD-MM-YY)*	2. REPORT TYPE	3. DATES COVERED *(From - To)*
December 2003	Final	05/08/2001 – 12/08/2003

4. TITLE AND SUBTITLE
SCRAMJET COMBUSTOR SIMULATIONS USING REDUCED CHEMICAL KINETICS FOR PRACTICAL FUELS

5a. CONTRACT NUMBER
F33615-01-C-2124

5b. GRANT NUMBER

5c. PROGRAM ELEMENT NUMBER
65502F

6. AUTHOR(S)
Bradley R. Adams, Marc A. Cremer, Christopher J. Montgomery,
and Wei Zhao (Reaction Engineering International)
Dean R. Eklund and C.J. Tam (Taitech, Inc.)
J.-Y. Chen (University of California, Berkeley)

5d. PROJECT NUMBER
3005

5e. TASK NUMBER
02

5f. WORK UNIT NUMBER
HF

7. PERFORMING ORGANIZATION NAME(S) AND ADDRESS(ES)

Reaction Engineering International (REI)
77 West 200 South, Suite 210
Salt Lake City, UT 84101

Taitech, Inc.

University of California, Berkeley

8. PERFORMING ORGANIZATION REPORT NUMBER

9. SPONSORING/MONITORING AGENCY NAME(S) AND ADDRESS(ES)

Propulsion Directorate
Air Force Research Laboratory
Air Force Materiel Command
Wright-Patterson AFB, OH 45433-7251

10. SPONSORING/MONITORING AGENCY ACRONYM(S)
AFRL/PRAS

11. SPONSORING/MONITORING AGENCY REPORT NUMBER(S)
AFRL-PR-WP-TR-2004-2011

12. DISTRIBUTION/AVAILABILITY STATEMENT
Approved for public release; distribution is unlimited. Report contains color.

13. SUPPLEMENTARY NOTES
This is a Small Business Innovation Research (SBIR) Phase II report.

14. ABSTRACT

This report covers work performed to make hydrocarbon combustion modeling simulations for scramjet flow fields practical. Several approaches were combined and demonstrated to greatly improve the time required for simulating complex hydrocarbon combustion reactions in scramjet-type flows. A code that converts a large set of reactions to a FORTRAN subroutine that computes reaction rates for a reduced set of species was refined and applied. An efficient methodology for storing and reusing reaction rate computations via a multidimensional adaptive table was developed and applied. A methodology for limiting reaction rates based on fine scale molecular mixing was incorporated into the tabular methodology and applied. A code for evaluating the impact of subgrid scale nonuniformity in temperature and species on reaction rate was also developed.

15. SUBJECT TERMS
hydrocarbon scramjet combustion kinetics modeling

16. SECURITY CLASSIFICATION OF:			17. LIMITATION OF ABSTRACT:	18. NUMBER OF PAGES	19a. NAME OF RESPONSIBLE PERSON (Monitor)
a. REPORT	b. ABSTRACT	c. THIS PAGE			Douglas L. Davis
Unclassified	Unclassified	Unclassified	SAR	90	19b. TELEPHONE NUMBER *(Include Area Code)* (937) 255-7302

Standard Form 298 (Rev. 8-98)
Prescribed by ANSI Std. Z39-18

Table of Contents

Table of Contents (Concluded)

List of Figures

List of Figures (Continued)

List of Figures (Concluded)

List of Tables

1.0 Executive Summary

This project focused on improving the realism of combustion chemistry models used in existing state-of-the-art computational fluid dynamics (CFD) software that is currently used in the design of scramjet combustors. The result is a modeling tool that is a significant improvement over existing capabilities and the ability to create chemistry models suitable for use in CFD from published detailed chemical kinetic mechanisms.

Capabilities were developed and demonstrated for 1) creating accurate reduced chemical kinetic mechanisms for hydrocarbon fuels of interest for high speed propulsion, 2) integrating the reduced mechanisms with *in-situ* adaptive tabulation (ISAT) and the eddy dissipation concept (EDC) turbulence-chemistry interaction model into the high-speed CFD code VULCAN (**V**iscous **U**pwind A**L**gorithm for **C**omplex Flow **AN**alysis), and 3) simulating combusting flows with complex aviation fuel chemistry in scramjet combustor geometries.

The key results from the Phase II work included the following:

- Development of accurate reduced mechanisms for combustion kinetics of hydrogen, ethylene, *n*-heptane, and a six-specie surrogate blend representing JP-8.
- Improvements to the CARM (Computer Aided Reduction Mechanism) software for automated reduction of chemical kinetic mechanisms, resulting in improved robustness and decreased computational times.
- Implementation of four reduced mechanisms into VULCAN.
- Implementation of ISAT chemical rate tabulation technique into VULCAN.
- Implementation of EDC turbulence model (with ISAT) into VULCAN.
- Completion of scramjet combustor simulations demonstrating improved chemical descriptions from reduced mechanisms compared to previously used global chemistry models.
- ISAT results showing speed increases up to a factor of 36 for the ethylene case.
- Two-dimensional combustion simulations in VULCAN demonstrating mechanism reduction and implementation for hydrogen, ethylene, *n*-heptane, and JP-8 (up to 35 species in the reduced mechanism).
- Three-dimensional scramjet combustor simulations run for ethylene and *n*-heptane (up to 20 species in the reduced mechanism), demonstrating that reduced mechanisms and ISAT can be used for CFD simulations of realistic 3- dimensional scramjet geometries with hydrogen fuels.

Overall, the research completed during this project has demonstrated newly developed mechanism reduction techniques applied to newly acquired knowledge of hydrocarbon combustion kinetics. These techniques were integrated into a practical engineering tool to produce a method for calculation of realistic combustion chemistry in high-speed CFD. This capability allows the U.S. Air Force to better address the needs of its high- speed propulsion programs, specifically the simulation of hydrocarbon fuels in a scramjet combustor.

2.0 Introduction

2.1 Purpose of Work

Computational modeling has become a central analytical tool used in the design of practical combustion systems for increased performance, improved efficiency, and low emissions. CFD simulation is particularly important in the aerospace industry in reducing prototype and testing costs and the time needed to bring products to market. Accurate simulation of chemical processes in aircraft engines is critical because chemistry determines the rate of heat release, flame stability, ignition, extinction, and pollutant emissions. However, fully detailed chemical kinetic descriptions of hydrocarbon oxidation may require the tracking of hundreds of chemical species and thousands of reaction steps. CPU and memory limitations prohibit implementation of full detailed chemistry of practical fuels into 3-D CFD simulations, even using the latest massively parallel computers.

Improved methods for computing combustion in high speed flows are of particular interest to the U.S. Air Force. In particular, the U.S. Air Force HyTech program (Mercier and Ronald, 1996) is one example of the need for a reliable representation of reduced kinetic models within CFD simulations. The goal of the HyTech program is to develop and demonstrate a hydrocarbon-fueled engine capable of accelerating an air-launched missile to Mach 8. The development of a successful scramjet combustor has proven to be difficult due in large part to structural limitations caused by high heat transfer rates, and short residence times for fuel and air mixing (Heiser and Pratt, 1994, and Curran et al., 1996). CFD is routinely used to analyze the combustor geometry concepts for these vehicles both before and after tests (Baurle et al., 1997, 1998a, 1998b, 2000). A large portion of the design phase of these combustors must rely heavily on CFD because of difficulties in measuring all of the relevant flow parameters that affect scramjet combustor performance.

The grid requirements for solving the Reynolds-averaged Navier-Stokes equations on scramjet combustor geometries can easily exceed several million grid points. This limitation places a significant constraint on the size of the chemistry models that can be considered. Calculations have shown that existing global mechanisms, even for simple hydrocarbon fuels such as ethylene, are woefully inadequate (Baurle et al., 1998b). Thus, previous CFD modeling of scramjet combustion has been very limited in terms of including adequate chemical representations of the combusting flow. Further, the effect of turbulence on chemical reactions has not been adequately addressed. The inclusion of turbulence-chemistry interactions in simulations further exacerbates the CPU and memory limitations.

Recent advances in chemical and numerical techniques have helped to address some of these simulation challenges. Detailed chemical kinetic descriptions of the oxidation of hydrocarbon blends representing practical fuels are rapidly improving (Dagaut, 1994; Maurice, 1996; Curran et al., 1998; and Violi et al., 2002). These detailed mechanisms, though impractical for implementation into a CFD simulation, are the starting point for creating reduced chemical kinetic mechanisms which can be implemented into CFD

simulations. Furthermore, techniques are now available to automatically create reduced mechanisms that approximate the results of detailed chemical kinetic descriptions using many fewer species, and thus less CPU time and memory. These advances have the potential to be combined with new numerical techniques, such as ISAT, to further reduce CPU time and thus promote tractable solutions for 3-D, high-speed, chemically reacting flows.

This program was designed specifically to utilize recent advances in chemical kinetic descriptions and numerical techniques to enhance modeling capabilities for scramjet engines firing hydrocarbon jet fuels. Beyond this, the capabilities developed in this program can also be applied to other aspects of the U.S. Air Force's high-speed propulsion programs as well as to CFD modeling of combusting flows in general. Two examples of additional applications that could benefit from program results are ignition delay studies for supersonic flows and prediction of atmospheric pollutants from fossil fuel combustion.

A more general area where the need for improved representations of finite-rate chemistry is particularly evident is in predicting the emission of atmospheric pollutants, such as oxides of nitrogen (NO_x), from the combustion of fossil fuels. Identifying methods for reducing NO_x emissions from combustion devices such as gas turbines, internal combustion engines, fossil fuel-fired utility boilers, and industrial process heaters has become tremendously important to U.S. industry in an effort to meet continually tightening air quality standards. Integration of more accurate representations of chemistry into specialized CFD tools, based on information gained from this research, helps improve the ability to solve complex industrial combustion problems and related pollutant emission concerns.

2.2 Related Research

This SBIR Phase II work builds on research previously completed in Phase I as well as research performed in parallel programs at Reaction Engineering International (REI) funded by the U.S. Army, National Science Foundation (NSF), and U.S .industry.

The historical reasons that CFD codes have typically incorporated only grossly simplified descriptions of the chemistry, as outlined in the previous section, are not as valid today as they were in the past. Advancements have been made in computer software, numerical methods and hardware that provide a framework for increasingly detailed chemistry to be implemented into 3-D CFD simulations to address practical engineering problems. Validated, detailed mechanisms for the large hydrocarbons that comprise aviation fuels have been available for some time now (Dagaut, 1994; Maurice, 1996; Curran et al., 1998; and Violi et al., 2002). These mechanisms represent the state of the art in terms of a chemical kinetic description of the combustion of large hydrocarbons. However, use of fully detailed mechanisms for hydrocarbon fuels in such simulations is still unreachable for the foreseeable future. Great strides have been made that improve our capability to

rapidly develop reduced descriptions of detailed chemical mechanisms while retaining the necessary fidelity to the detailed chemistry.

The Phase I SBIR program successfully demonstrated that a chemical kinetic mechanism for a large hydrocarbon fuel, such as those that comprise aviation fuels, can be quickly reduced to a size amenable for implementation in CFD codes using automated techniques such as CARM (Chen, 1997). The success of the reduction strategy in the Phase I program was demonstrated by

- Successful application to a range of large detailed mechanisms for practical fuels
- Comparison to experiments
- Comparison to results of full mechanisms for simple, spatially homogeneous combustion configurations such as perfectly stirred reactors (PSRs) and plug flow reactors (PFRs)
- The ability of the reduced mechanism to capture heat release, stability, and ignition delay behavior.

During the Phase I program, which concluded in March 1999, REI successfully produced reduced mechanisms with various numbers of species and reaction steps for ethylene and from two different detailed mechanisms for *n*-heptane, a large hydrocarbon fuel similar to aviation fuel constituents. More complex fuels (heavier alkanes and aromatics) require more species to accurately represent their chemistry. However, since large hydrocarbons break down rapidly into smaller pieces under combustion conditions, the number of scalars needed for accurate description of the reaction kinetics can be expected to increase slowly with increasing fuel molecular weight.

Beyond the Phase I program, REI has led research projects in several related areas between the end of the Phase I effort and the present. These include the following:

- A U.S. Department of Defense (DoD) Army Phase II SBIR for the development of detailed and reduced mechanisms and application in CFD codes for problems of interest to the DoD (Denison et al., 2003)
- U.S. industry-funded development and application of reduced mechanisms for prediction of NOx reduction in fossil-fuel fired utility boilers (Cremer et al., 2000a, 2000b, 2001)
- NSF Phase I and II SBIRs for investigation of advanced Newton-Krylov solver techniques to reduce computational times in chemically reacting flow simulations, especially those using reduced mechanisms created using CARM (Bockelie et al., 2003)
- A U.S. DoD Air Force Phase I SBIR for numerical and experimental investigation of soot-reducing fuel additives in JP-8 jet fuel combustion, including implementation of reduced JP-8 kinetics and soot models into the UNICORN CFD code (Montgomery et al., 2003a)
- NSF Phase I and II SBIRs for development of a computer-assisted reduction mechanism problem solving environment (CARM-PSE) that allows easy and automated comparison of detailed and reduced chemistry over a multidimensional

parameter space of interest (Montgomery et al., 2002a). During Phase II, automated reduced mechanism optimization capability was added and optimized reduced mechanisms integrated into the commercial CFD code, Fluent, and the internal combustion engine research code, KIVA .

Information and techniques developed in these programs has helped further the research on this Phase II program, particularly with respect to the development and application of reduced mechanisms in chemically reacting flows.

2.3 Phase II Objectives

The overall goal for this SBIR Phase II program was to provide the U.S. Air Force with an improved computational tool for simulating jet fuel combustion in a scramjet combustor. This goal was met by achieving the following objectives:

Identify detailed mechanisms best describing oxidation of hydrocarbon fuels for scramjets

Produce reduced mechanisms for the detailed hydrocarbon mechanisms and verify reduced mechanism accuracy by comparison with detailed mechanism results

Implement the reduced mechanisms into a CFD code suitable for performing 2-D and 3-D scramjet combustor simulations

Validate the implementation against available experimental data and with detailed chemistry in simplified geometries

Implement and test new chemistry tabulation techniques to reduce computation times in the CFD code

Evaluate the impact of turbulence-chemistry interactions on predictions.

2.4 Key Accomplishments of Phase II Work

The Phase II objectives were addressed by focusing on the following five areas of research and development:

Identification of detailed chemical kinetics mechanisms for simple and complex hydrocarbon fuels appropriate for use in simulating scramjet combustion

Formulation of reduced chemical kinetic mechanisms that represent the detailed kinetic behavior of hydrocarbon fuels using many fewer species than the detailed mechanism

Implementation of a chemical rate tabulation technique (ISAT) that significantly reduces CPU time when computing chemical reactions with reduced mechanisms

Implementation of reduced mechanisms and tabulation techniques into the VULCAN CFD code

Preliminary evaluation of turbulence-chemistry impacts on VULCAN simulations based on the EDC modeling and a probability density function (PDF) post-processing technique.

The Phase II objectives were accomplished by integrating key technologies, developed and/or implemented as part of the process outlined above, to develop a capability for modeling turbulent reactive flows that has not, as yet, been fully realized for high-speed reacting flow applications. The improved simulation capabilities were evaluated using 2-

D simulations to verify implementation and test result sensitivities and 3-D simulations to demonstrate predictions for a scramjet combustor.

Key results from the Phase II work included the following:

- Development of reduced mechanisms for combustion kinetics of hydrogen, ethylene, *n*-heptane, and a six-specie surrogate blend representing JP-8
- Comparison with detailed results showed excellent agreement over a wide range of temperatures and equivalence ratios
- Improvements to CARM software for automated reduction of chemical kinetic mechanisms resulting in improved robustness and decreased computational times
- Implementation of four reduced mechanisms into VULCAN
- Implementation of ISAT chemical rate tabulation technique into VULCAN
- Implementation of EDC turbulence model (with ISAT) into VULCAN
- Utilization of PDF post-processing technique for estimation of turbulence-chemistry interaction
- Simulation results showing chemical kinetic effects missing from simpler global chemistry models
- ISAT timing results showing speed increases up to a factor of 36
- Turbulence-chemistry interactions showing significant impact on the flame front;
- 2-D combustion simulations run for hydrogen, ethylene, n-heptane and JP-8 (up to 35 species in the reduced mechanism)
- 3-D scramjet combustor simulations run for ethylene and *n*-heptane (up to 20 species in the reduced mechanism).

This research has demonstrated the application of newly developed mechanism reduction and rate tabulation techniques to newly developed hydrocarbon combustion kinetics and the subsequent integration of these techniques into a practical engineering tool to produce a method for calculation of realistic chemistry in CFD. This capability allows the U.S. Air Force to better address the needs of its high-speed propulsion programs, specifically the simulation of hydrocarbon fuels in a scramjet combustor.

3.0 Technical Approach

This section provides an overview of the technical approach and key technical tasks in this research. Figure 1 illustrates conceptually the technical approach and task dependencies for this program. The technical research and code development were divided into five development tasks plus the evaluation of 2-D and 3-D combustion simulation results.

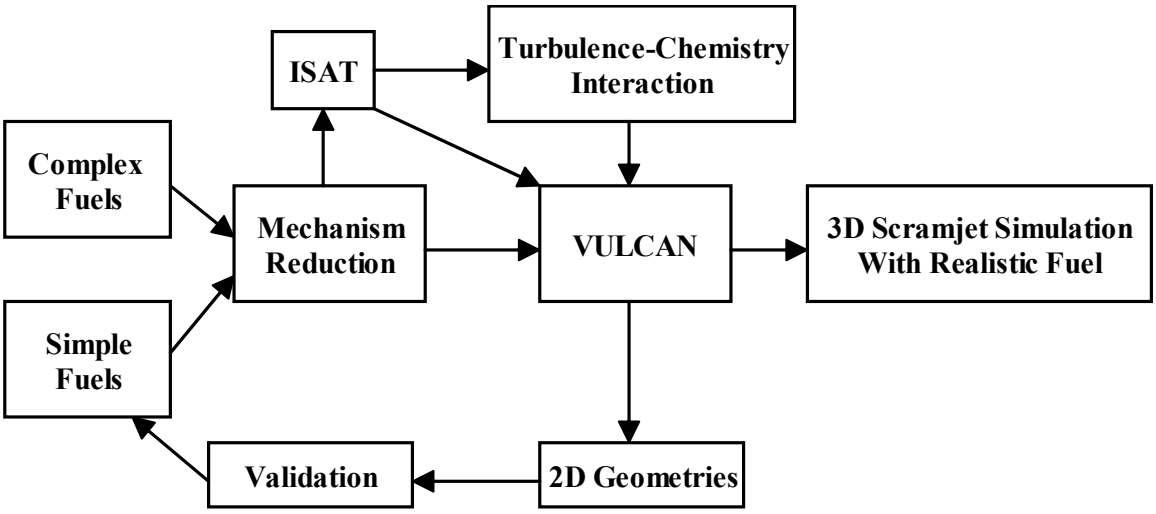

Figure 1. Technical Approach Used in Program.

The five development tasks were as follows:

1. Selection of detailed chemical kinetic mechanisms for fuels of interest
2. Formulation of reduced chemical kinetics mechanisms using CARM
3. Implementation of ISAT routines for use with reduced mechanisms and VULCAN
4. Implementation of EDC routines for use with reduced mechanisms and VULCAN
5. Implementation of reduced mechanisms, ISAT and EDC into VULCAN.

Once the development and implementation tasks were completed, VULCAN simulations were run to evaluate the performance of the reduced mechanism, ISAT, and EDC routines, respectively. The following sections provide a summary of each of the development, implementation, and simulation tasks for this program.

3.1 Detailed Mechanism Selection

This task involved the selection of detailed chemical kinetic mechanisms for simple and complex aviation fuels. Reduced mechanisms can be no more accurate than the detailed chemical kinetic models on which they are based. Thus, accurate description of detailed chemical kinetic mechanisms is a necessary first step for each fuel of interest. Identification of detailed mechanisms was divided into two categories, simple fuels (hydrogen and ethylene) and complex fuels (heptane and JP-8). Section 4 of this report describes the selection of detailed mechanisms for reduction and eventual incorporation into VULCAN. Detailed mechanisms were taken from existing literature. Some modifications for compatibility with CARM software were required depending on original detailed mechanism format.

3.2 Formulation of Reduced Mechanisms

The detailed chemical kinetic mechanisms identified in the previous task were utilized to formulate reduced chemical kinetic mechanisms using CARM. This allows a great deal of chemical kinetic information contained in the detailed mechanisms to be replicated in a computationally tractable form. Reduced mechanisms were developed for simple

(hydrogen, ethylene) and complex (heptane and JP-8) hydrocarbon fuels. Accuracy of the reduced mechanisms was validated by comparison to detailed chemistry over a range of conditions and, where available, experimental data. Details of the formulation approach and results are given in Section 5 of this report.

3.3 Implementation of ISAT Routines

The ISAT technique provides a method for accessing chemical properties without resorting to direct calculation of reaction rates or direct tabulation of properties. This results in significant CPU savings. The ISAT subroutines, developed originally for a PDF method (Chen et al., 2000), were modified and used to tabulate the chemical reaction rates from both the CARM-produced reduced mechanisms and the EDC model. Background on the ISAT approach is given in Section 6 of this report.

Since this was the first use of ISAT for this type of CFD application, numerous timing and accuracy studies were conducted for different ISAT settings. VULCAN timing studies were performed with and without ISAT for many of the reduced mechanisms in order to develop a sense of appropriate accuracy and tolerance settings to be used within ISAT.

3.4 Turbulence-Chemistry Interactions

The modeling of the mean chemical source term has often been considered to be the main problem in CFD simulations of turbulent combustion (Peters, 2000). Turbulent combustion models can be placed into one of following categories: eddy-breakup (EBU) and eddy-dissipation models, PDF model (including assumed PDF method and transport PDF method), laminar flamelet models, conditional moment closure, and the linear eddy model (LEM). Transport PDF and LEM models are accurate, but they are also extremely expensive. Application of the laminar flamelet model is limited when more than one fuel stream is present. The CPU cost of the assumed PDF model increases dramatically when applied to the chemical mechanisms without an analytical reaction rate expression, such as the CARM-created reduced mechanisms. In this project, the turbulence-chemistry interactions are assessed via two approaches.

First, an EDC model was implemented into VULCAN and configured to work with ISAT. This was used to test the sensitivity of VULCAN predictions to turbulence-chemistry interactions within the limitations of the EDC model (see Section 7.1). Second, a PDF post-processor technique was applied to VULCAN results. This technique is described in Section 7.2. The PDF post-processor code reads the flow field from the VULCAN results and recalculates the turbulent species concentrations and temperature field with a PDF model, while the velocity and density are not updated. The results obtained with the EDC and PDF models are then compared with those from laminar chemistry to estimate the impact of turbulence effects on flow properties and CPU times.

3.5 Implementation into VULCAN

The simulation software utilized in this research for modeling scramjet combustion was VULCAN. VULCAN is a time-dependent, compressible, Navier-Stokes flow solver that

is currently maintained and distributed (restricted to the U.S.) by the Hypersonic Airbreathing Propulsion Branch of NASA Langley Research Center. VULCAN is a multigrid, multiblock, structured, finite-volume code, developed for solving the spatially elliptic and parabolized forms of the equations governing 3-D, turbulent, calorically perfect and nonequilibrium chemically reacting flows. The reduced chemical mechanisms, ISAT chemical property routines, and EDC turbulence model routines developed for this research were implemented into VULCAN (see VULCAN web page).

Implementation of reduced mechanisms in the VULCAN code focused in two areas. First, a numerical Jacobian capability was implemented in VULCAN. This was necessary to allow VULCAN to use the (nonanalytical) chemical rate source terms from CARM-formulated reduced mechanisms. Second, the reduced mechanisms for various hydrocarbon fuels were implemented and tested for numerical accuracy and robustness.

The ISAT routines functioned as an interconnection between VULCAN and the reduced mechanism routine from CARM. The ISAT subroutine provided not only the reaction rate vector, but also the Jacobian matrix required by VULCAN. This provided an opportunity for significant CPU savings over direct evaluation of the reaction rates.

Implementation of the EDC model into VULCAN was very similar to the implementation of the reduced mechanism with ISAT. In this formulation, the target functions of ISAT were the turbulent mean reaction rates, and the independent variables for ISAT were the species mass fractions, pressure, temperature and the life time of the fine-scale structures. This required only one more variable than that of ISAT with laminar chemistry. This allowed manageable CPU times for the EDC calculations.

The PDF post-processor utilized information from the VULCAN flow field results to calculate turbulence-chemistry effects as a post-processor. Thus there was no VULCAN implementation required.

3.6 2-D and 3-D Simulations

2-D VULCAN simulations were used to verify correct implementation of the reduced mechanism, ISAT and EDC routines in VULCAN, and to test the sensitivity of predicted results (accuracy, CPU time) to variations in new routine parameters such as search tolerances and numerical convergence. Most of the project simulations completed were 2-D. Once the correct implementation and usage of the new routines in VULCAN were established with the 2-D simulations, a few 3-D simulations were performed to demonstrate the capabilities of the newly combined technologies. 3-D cases were run for ethylene and *n*-heptane fuels in a scramjet cavity flameholder.

4.0 Selection of Detailed Mechanisms

Reduced mechanisms can be no better than the detailed chemical kinetic models on which they are based. This section describes our selection of detailed mechanisms for reduction and eventual incorporation into VULCAN.

4.1 Detailed Mechanisms for Simple Fuels

4.1.1 Hydrogen

The reduced mechanism was based on H_2-O_2 reactions extracted from the large hydrocarbon mechanism of Curran et al. (1998). The hydrogen-oxygen (H-O) reactions in most modern detailed mechanisms differ little and almost any detailed mechanism could have been chosen. The Curran mechanism is a widely used model of large hydrocarbon combustion, and the H-O subsystem is believed to be quite reliable. The H-O reactions are modeled using nine species and 27 reactions.

4.1.2 Ethylene

Calculations were performed to compare the ability of two detailed chemical kinetic mechanisms (Marinov et al., 1998, and Wang et al., 1999) to compute ignition delay of ethylene-oxygen mixtures as compared to experiments (Baker and Skinner, 1972, and Colket and Spadaccini, 1999). Three of the cases measured by Baker and Skinner were modeled. The initial pressure in all of these cases was 3 atm. The gas mixture for these cases consisted of 1 percent (by moles) ethylene with 3, 1.5, or 6 percent O_2, and the balance argon. These cases correspond to E.R.s of 1.0, 2.0, and 0.5, respectively. Baker and Skinner report only Arrhenius-form expressions fit to their data so individual data points can't be plotted. Figure 2 compares Baker and Skinner's measurements with calculations using the two detailed mechanisms and the 20-specie reduced mechanism described in Section 5.2.2. Three cases measured by Colket and Spadaccini were also compared to predictions of the detailed chemical kinetic mechanisms (not shown). These measurements have 0.7 percent ethylene with O_2 mole fractions of 4.2, 2.8, and 2.1 percent with the balance argon. This gives E.R.s of 0.5, 0.75, and 1.0, respectively. The initial pressures range from 5.27 to 7.89 atm. Similar levels of agreement for the detailed and reduced mechanisms were found for the Baker and Skinner measurements.

Both detailed mechanisms give reasonable agreement to the measurements. However, the Wang mechanism is noticeably superior for all of the measurements simulated. The Wang mechanism also has the advantage of containing fewer species: 75 species and 529 reactions versus 155 species and 689 reactions in the Marinov mechanism. Fewer species and reactions mean that the reduced mechanism is likely to run faster and to exhibit better numerical behavior and agreement with the detailed mechanism using fewer non-QSS species. Thus, the Wang mechanism was selected as the basis for the ethylene reduced mechanisms to be used in this work.

4.2 Complex Fuels

4.2.1 Heptane

Several chemical kinetic mechanisms for *n*-heptane combustion exist in the literature. One commonly used *n*-heptane mechanism is that of Curran et al. (1998), which is intended to cover the entire range of conditions from low-temperature (600 to 900 K) pyrolysis and oxidation to high-temperature combustion. During Phase I, a subset of this mechanism containing only those reaction steps and species that are only important at

higher temperatures (>900 K) was used as a basis for reduction. This high-temperature subset is still a large mechanism, with 105 species and 808 elementary steps.

In contrast, the *n*-heptane mechanism of Held et al. (1997) is considerably simpler. This mechanism compares well to experiments with comparatively very few species by empirically modeling the initial fuel breakdown. The Curran mechanism contains reaction steps for abstraction of H atoms from the fuel by a number of radical species to form several heptyl radical isomers. These heptyl radicals undergo isomerization reactions and decompose through a number of routes to form various species with two to five carbon atoms. Held et al. achieve considerable simplification by bypassing the formation, isomerization, and breakdown of the various heptyl radicals and by allowing the *n*-heptane fuel to decompose directly into smaller reaction products, often with three or four products on the right-hand side of an elementary reaction step. Because of its good comparison to experiments and comparative simplicity, the Held mechanism was chosen for reduction.

4.2.2 JP-8

The primary candidates for a detailed mechanism for JP-8 combustion are the mechanisms of Violi et al. (2002) and Mawid and Sekar (2002). We have chosen to use the Violi mechanism because of our access to it and because it compares very well to the limited data available on JP-8 and kerosene combustion. This mechanism was created by collaboration between the University of Utah and Italian researchers. One of the authors of the mechanism, Prof. Adel Sarofim, is a technical advisor to REI on this project, allowing us to actively engage in discussions regarding the development and use of this mechanism. The Violi mechanism was not originally in the Chemkin format needed for reduction by CARM. The Violi mechanism was converted to Chemkin format by REI as part of this project.

Experimental results (Douté et al., 1995) for kerosene combustion in a fuel-rich (equivalence ratio=1.7) PFR have been modeled successfully using the Violi mechanism. The comparison of the measured and calculated profiles is shown in Figure 3, where the surrogate is composed of 73.5 mol% *n*-dodecane, 5.5 mol% iso-octane, 10 mol% methylcyclohexane, 11 mol% toluene, and 1 mol% benzene. The mechanism reproduces the profiles of fuel components, products, and many intermediate species quite well.

Figure 4 compares ignition delay predictions made by the Violi, and Mawid and Sekar mechanisms with measurements from Mullins (1955) and Freeman and Lefebvre (1984). The Violi mechanism uses a six-specie surrogate blend to represent a typical batch of JP-8 fuel. The Mawid and Sekar mechanism uses 12 species. Having more species in the surrogate is a disadvantage for mechanism reduction because each species in the surrogate and some intermediates related to it must be kept in the reduced mechanism. Though the Violi mechanism has not been tuned to match these data, the agreement is somewhat better than that of Mawid and Sekar over the limited data range.

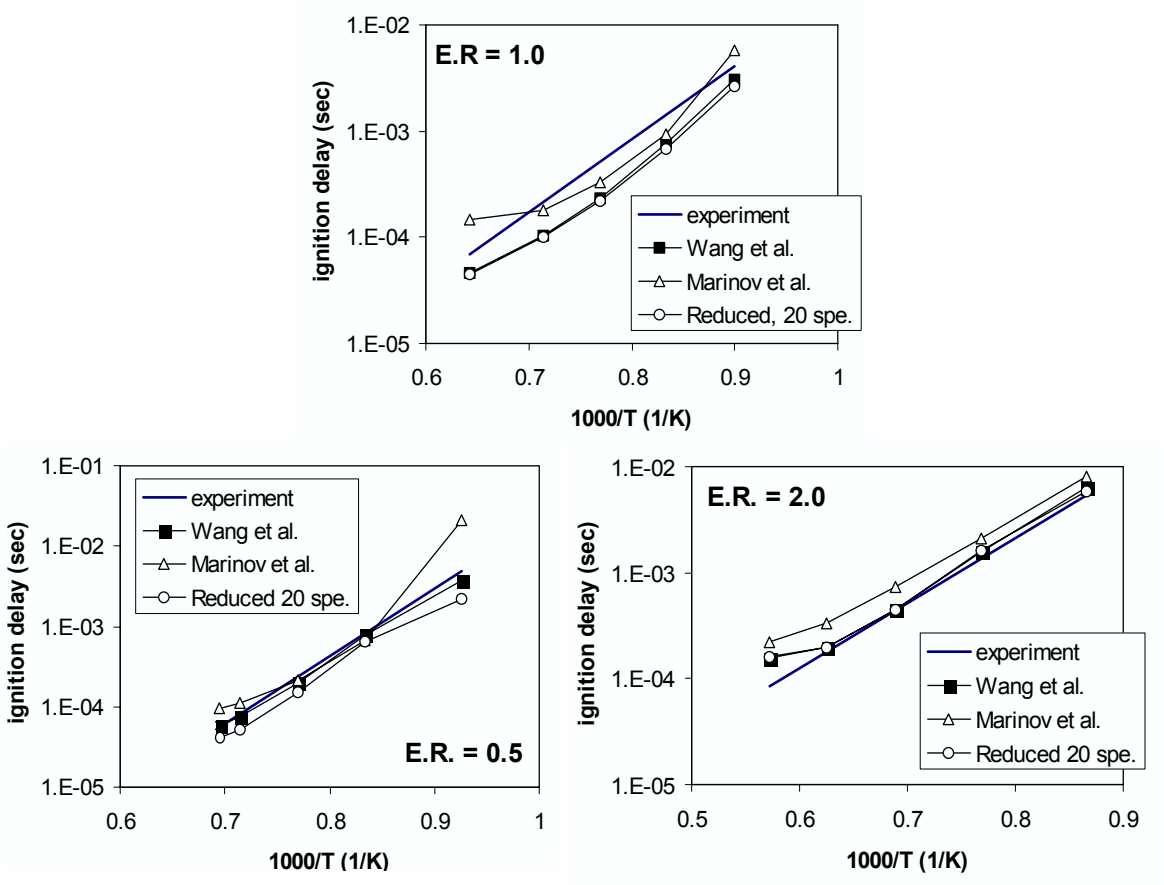

Figure 2. Comparison of Ignition Delay as a Function of Temperature for Experiments, Detailed Chemistry and the Reduced Mechanism for Ethylene-air Mixtures at E.R.s of 0.5, 1.0, and 2.0.

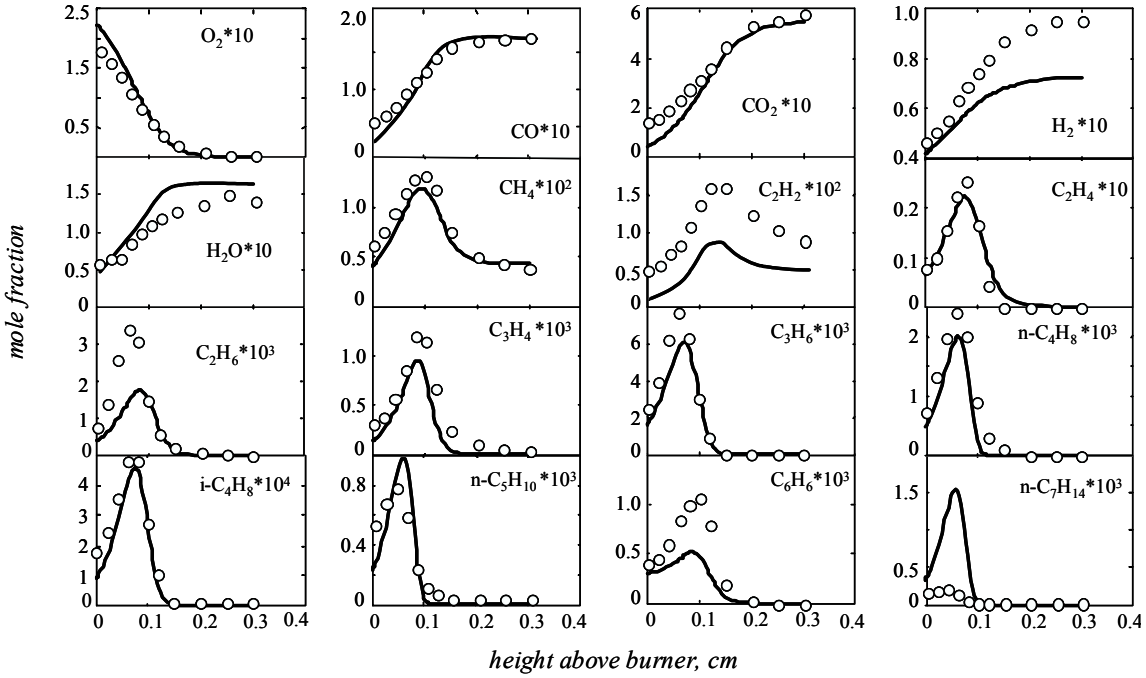

Figure 3. Comparison of the Violi Mechanism's Predictions to Experimental Results in a Kerosene-air PFR. T=1160 K, P=1 atm., E.R.=1.7.

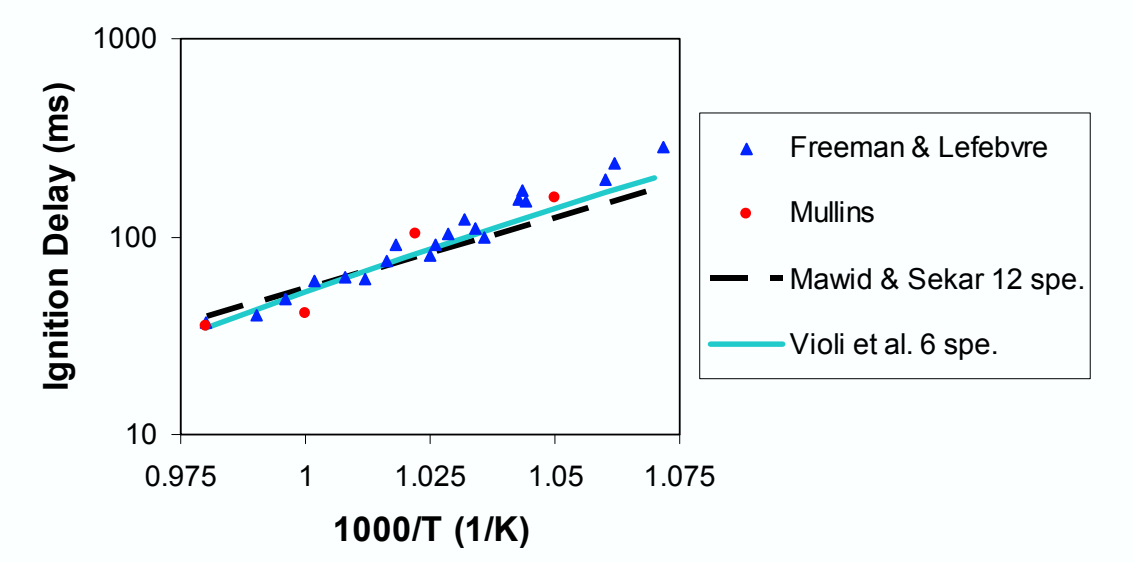

Figure 4. Comparison of the Mechanism Predictions for JP-8 (Freeman and Lefebvre, 1984) or Kerosene (Mullins, 1955) Ignition Delay. P = 1 atm, E.R. = 0.5.

5.0 Development of Reduced Mechanisms

In this section, the reduced mechanisms that have been created using CARM are described and compared to detailed chemistry and, where available, experimental data. Of primary interest for scramjet combustor simulations are the ignition delay and heat release rate. Ignition delay is very sensitive to the details of the chemical kinetics, while the overall heat release is a function of the thermodynamic properties of the fuel and major products. Ignition delay for reduced and detailed chemistry has been compared over a range of stoichiometries and temperatures for all the reduced mechanisms created and implemented in this project. It is believed that if the ignition delay is correctly modeled, then the heat release rates and distributions of important species will be modeled accurately as well.

5.1 CARM Phase I Background

There are four basic steps in the formulation of a reduced chemical kinetic mechanism: 1) identification of the appropriate detailed mechanism containing the essential species and elementary reaction steps, 2) identification of appropriate quasi-steady-state (QSS) approximations, 3) elimination of reactions through use of the algebraic relations obtained in step 2, and 4) solution of the coupled and nonlinear set of algebraic equations obtained in the previous steps to find the reaction rates of the remaining species. CARM automates steps 2 through 4, producing source code for the calculation of the chemical source terms defined by the reduced mechanism. As inputs, CARM uses a set of test problem results representing conditions of interest to rank species by the error introduced by assuming they are in steady state. The subroutine produced by CARM contains code that iteratively solves the coupled, nonlinear set of algebraic equations giving the concentrations of the quasi-steady-state species. These concentrations are used along with the rates of the elementary reactions from the detailed mechanism to calculate the chemical source terms for the non-QSS species.

During Phase I, the ability of the CARM software to create reduced mechanisms for hydrocarbon fuels (ethylene and *n*-heptane using two different mechanisms) was demonstrated. The ability of reduced mechanisms created using CARM to correctly predict temperatures and species concentrations in simple reactors calculations (Plug Flow Reactors (PFRs) and Perfectly Stirred Reactors (PSRs)) was examined. Before the Phase I work, CARM had only been demonstrated on methane.

5.2 CARM Software Improvements

During this project, several improvements were made to CARM. These improvements have been aimed at improving the speed and robustness of the subroutines produced by CARM, as well as allowing for nonstandard features of some detailed mechanisms of interest, such as the Violi mechanism.

5.2.1 Chemical Rate Table

Chemical rate expressions contain exponential functions of temperature only. Evaluation of exponential functions can be costly for repeated calculations as required by most CFD calculations. In the latest version of CARM, a new option is included for building a

chemical rate table as a function of temperature. This lookup table is built once. The chemical rates are determined from an efficient linear interpolation scheme. Nearly a factor of three speedup in the rate expression computations has been observed.

5.2.2 Acceptance of Nonstandard Mechanism Formatting

CARM was modified to work for detailed mechanisms that do not conform to standard Chemkin format. CARM can now operate on detailed mechanisms that have noninteger stoichiometric coefficients and up to 12 products on the right-hand side of an elementary reaction step. This modification was necessary for reduction of the Violi et al. (2002) JP-8 mechanism.

5.2.3 FORTRAN 90 Subroutine Output

CARM has been updated to provide a FORTRAN-90 compatible reduced mechanism source subroutine. This capability has been extensively tested. FORTRAN-90 subroutines are significantly easier to implement into VULCAN.

5.2.4 Newton Iteration for QSS Species

Reduced mechanisms produced by previous CARM versions used a fixed-point iteration scheme to solve for the QSS species concentrations. Occasional convergence failures have been observed when a limit is placed on the number of fixed-point iterations. This failure sometimes slows computation, and can impair the accuracy of the overall calculation. Since the fixed-point iteration scheme has a slow convergence rate on the order of unity (i.e., almost linear), modifications to CARM have been made to provide the capability of performing Newton iterations when the fixed-point scheme fails. The major coding effort of these modifications focused on automatic output of FORTRAN code to evaluate the Jacobian terms needed in the Newton iteration. Matrix inversion is the most expensive part of Newton iteration; a Lower-Upper (LU) matrix decomposition scheme is used. The automatically generated code is verified by comparisons of results obtained from a PSR model.

Several reduced mechanisms with different numbers of steady-state species have been developed for assessment of the performance of the combined scheme. Table 1 compares the ratio of CPU times used by Newton and fixed-point iteration along with the percentage of CPU time used for matrix inversion. As expected, the CPU time required for Newton iteration is larger than that required by the fixed-point scheme and the majority of the time is used for matrix inversion. Matrix inversion uses over 90 percent of the CPU time when the total number of steady-state species exceeds 20.

Table 1. Comparison of Ratio of CPU Times Used by Newton Iteration and by the Fixed-point Iteration Along with the Percentage of CPU Time Used for Matrix Inversion.

Reduced mech.	Number of species	Number of steady-state species	CPU Newton/ CPU fixed-point	Percent CPU for matrix inversion
H_2+ NOx	11	11	15.9	61.6
Skeletal CH_4	5	11	6.79	83.8
GRI 2.11	12	33	37.2	92.2
GRI 3.0	42	10	3.4	84.6
GRI 3.0	32	20	19.2	92.5
GRI 3.0	19	33	27.9	94.5
GRI 3.0	12	40	33.9	92.1

Figure 5 presents the CPU times used by the matrix inversion versus the number of variables (the steady-state species) showing the expected cubic dependence. Figures 6 and 7 plot the ratio of CPU times used by Newton and by fixed-point iteration based on a PSR calculation on linear and log-log scales, respectively. Due to the CPU times used by other parts of the PSR code, the dependence of total CPU time on the number of steady-state species scales roughly as $\sim(N_{ss})^{1.6}$, where N_{ss} stands for the total number of steady-state species. Figure 8 compares the number of iterations required to reach convergence by the two schemes. As can be seen in the figure, the fixed-point scheme requires a large number of iterations compared to the Newton method. On average, the fixed-point scheme performs 22.6 iterations to reach convergence, while the Newton scheme requires only 3.01 iterations. However, due to the large CPU time required by the Newton method, the overall CPU time is much larger than that used by the fixed-point scheme. This conclusion is somewhat expected; the main motivation for performing Newton iteration is in case of convergence failure by the fixed-point scheme.

Application of combined fixed point and Newton iterations for steady state species was carried out using a well mixed reactor model. The reduced chemistry is based on Gas Institute Research (GRI)-3.0 (GRI Mech web site) CH_4-air combustion with 15 steps and 33 steady-state species. The stiff ordinary differential equation (ODE) integrator DDASAC (Double precision Differential Algebraic Sensitivity Analysis Code) made a total of 38,577 calls to the subroutine CKWYP; 2.2 percent of these calls with the fixed-point iterations failed to converge within 20 iterations. The average number of fixed point iteration was 6.3 while the average number of Newton iteration was 3.2. Figure 9 illustrates a sample set of calling statistics showing that when fixed-point iteration exceeds the assigned maximum limit, Newton iteration is called, leading to fast convergence. Although Newton iteration is expensive, many of the convergence failures of the fixed-point iteration method can be avoided.

An exploration run was conducted with the fixed-point iterations only. During this run, the stiff ODE integrator DDASAC made 46,143 calls to the subroutine CKWYP, about 20% more than using the combined scheme. This is due to the fact that more calls are needed when iteration to calculate the steady-state species fails to converge. It is

interesting that the actual CPU runtime with the fixed iteration scheme is about 1.3% more expensive than the combined scheme. This may be fortuitous under this special application as Newton iteration is more expensive. However, the speeding convergence offered by the Newton iteration can offset the computer time by having fewer overall iterations. This development provides a robust iteration scheme to achieve a converged solution when the fixed-point iteration scheme fails.

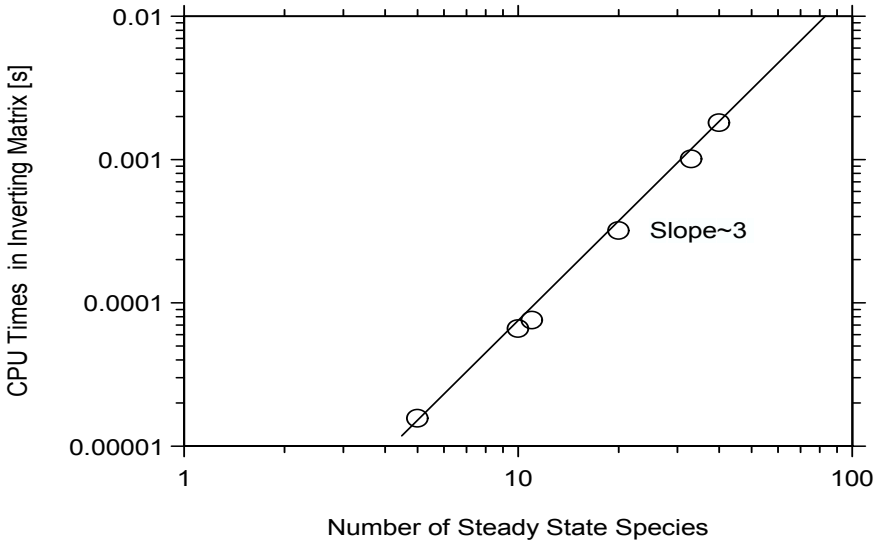

Figure 5. CPU Times Used in Inverting a Square Matrix Versus Number of Steady-State Species Showing the Statistics with the Expected Cubic Dependence.

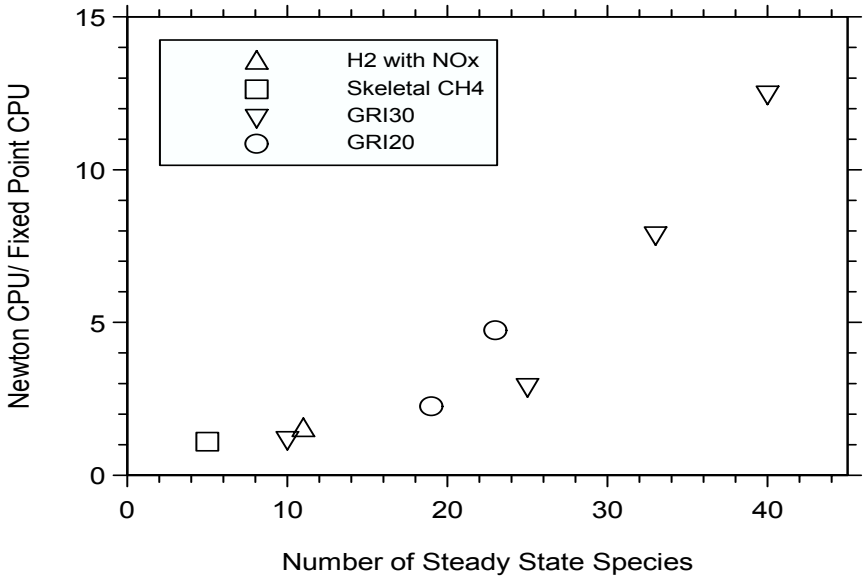

Figure 6. Ratio of Total CPU Time versus Number of Steady-State Species on a Linear Scale.

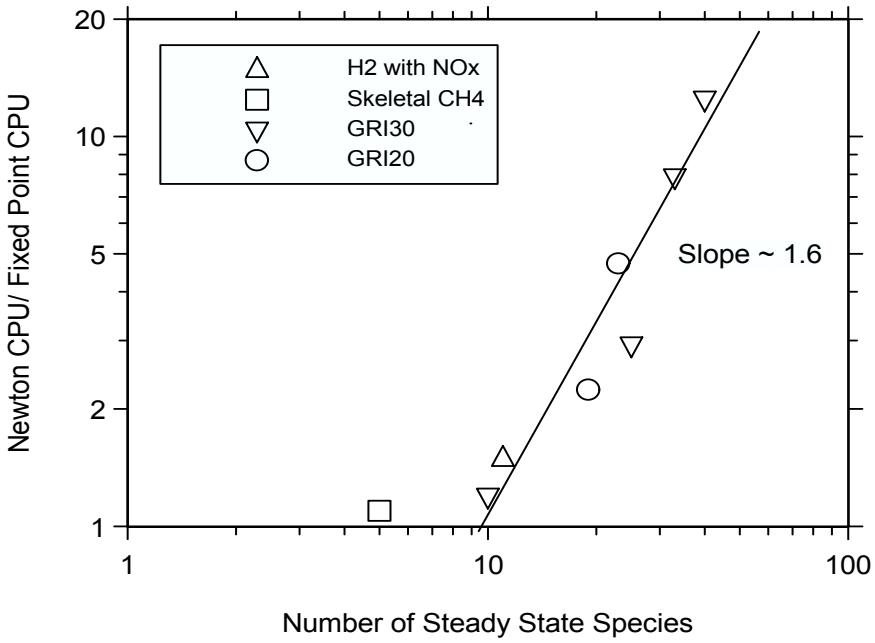

Figure 7. Ratio of Total CPU Time versus Number of Steady-State Species on a Log-log Scale.

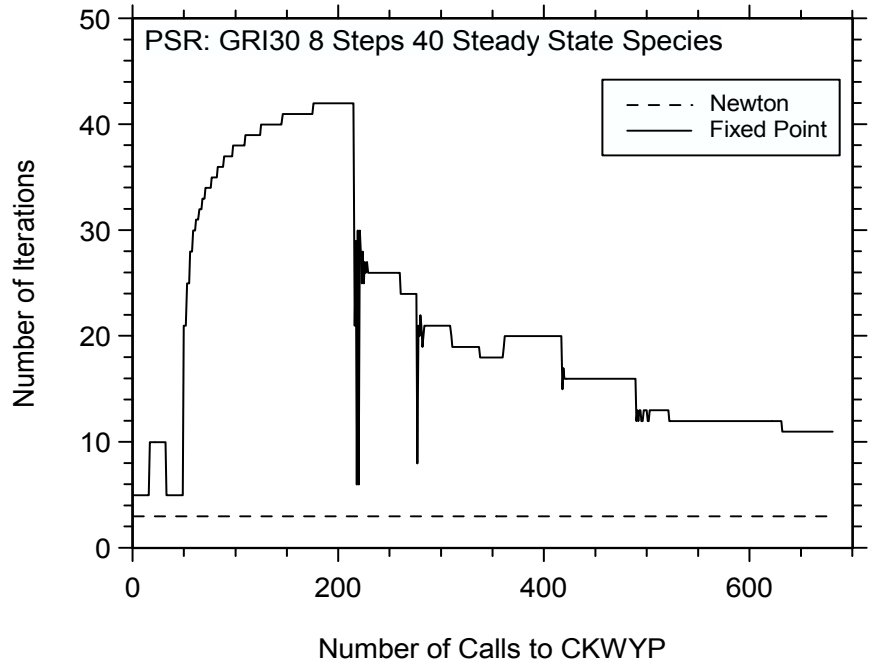

Figure 8. Comparison of the Number of Iterations to Reach Converged Solutions for the Fixed-Point Iteration Scheme and the Newton Iteration Method for a PSR Calculation.

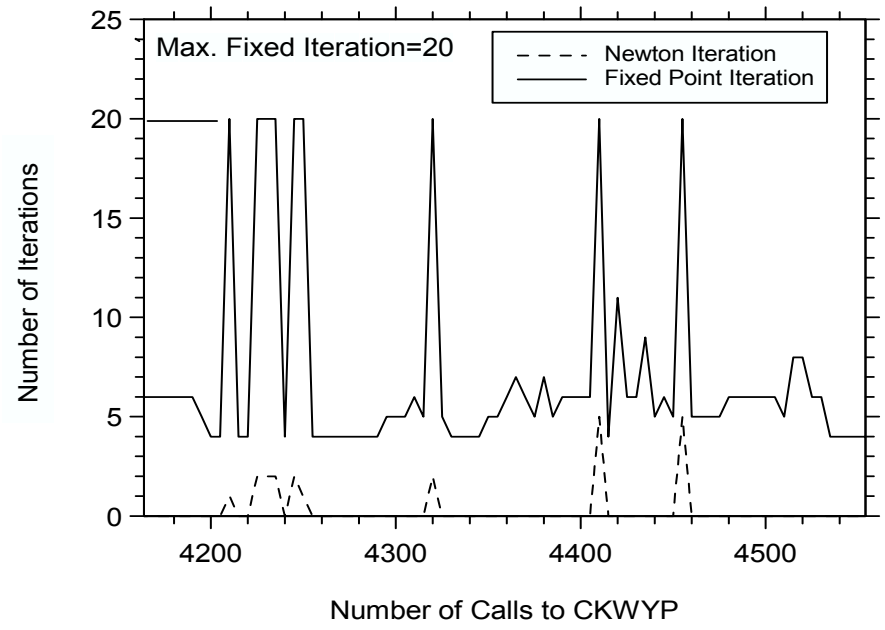

Figure 9. Number of Iterations in a Combined Fixed-Point and Newton Iteration Scheme.

5.2.5 Skeletal Mechanism Development

A skeletal mechanism is a smaller version of a detailed chemical kinetic mechanism with unimportant species and reactions deleted. For fuels requiring very large mechanisms, creation of a good skeletal mechanism is an important step in creating the reduced mechanism with CARM. Approaches for constructing accurate skeletal mechanisms were evaluated and new improvements to CARM were developed. Three different methods including detailed reduction (DR) (Wang and Frenklach, 1991), atomic flux analysis (Soyhan et al., 2001), and the original CARM scheme (Chen, 1997), were assessed for development of accurate skeletal mechanisms, especially for predictions of autoignition delay. Two features in the original CARM method were identified to be undesirable. One is the arbitrary threshold used for the initial selection of species to be kept in the skeletal mechanism. The other one is the required sensitivity information that is known to be time consuming to obtain, especially for large mechanisms. Furthermore, the large memory needed for storing sensitivity information presents a limiting factor on the number of combustion states that can be included during the development. Efforts have been made to remove these two undesirable features in the current CARM version by considering alternatives (Tham and Chen, 2003).

The atomic flux analysis method was explored as an alternative to the previously existing CARM approach for selecting the species to be kept in the skeletal mechanism. However, experience with large mechanisms, such as iso-octane, revealed that the atomic flux analysis can be quite time consuming and is unsuitable for running CARM interactively. Another alternative is reaction matrix analysis (Bendtsen, et al., 2001), which is similar to

atomic flux analysis but requires far less computation time for large mechanisms. Instead of a user-specified threshold value to distinguish species importance, a new method of tracing the most important reaction paths of major reactants and products is employed in the reaction matrix analysis. Our study of the reaction matrix analysis technique reveals that similar results to those from atomic flux analysis are obtained with much less computation time.

The DR approach focuses on the reaction rate and heat release rate of each step. On the other hand, the original CARM approach focuses on sensitivity information and construction/destruction rate of each species. The new version of CARM includes advantageous features from different approaches. The hybrid approach retains the heat release rate analysis from the DR approach along with the construction/destruction rate analysis from the CARM approach to efficiently produce a more accurate skeletal mechanism. The initial selection of species is performed using the newly developed tracing method.

Assessment of the performance of the latest CARM version is conducted for an autoignition study with a detailed hydrogen mechanism. Three methods, including DR, the original CARM, and the newly modified CARM, are used to create skeletal mechanisms with the constraint that they contain the same number of species. Comparisons of predicted temperature and H_2O_2 concentration during autoignition are presented in Figure 10. As seen in the comparisons, the original CARM approach predicts lower temperatures near the end of autoignition. The DR approach miscalculates the H_2O_2 mole fraction. The newly improved CARM approach (hybrid approach) gives a skeletal mechanism that agrees closely with the detailed mechanism in terms of both temperature and H_2O_2. This new capability has proven to be useful for creating reduced mechanisms for large hydrocarbons and blends representing real fuels.

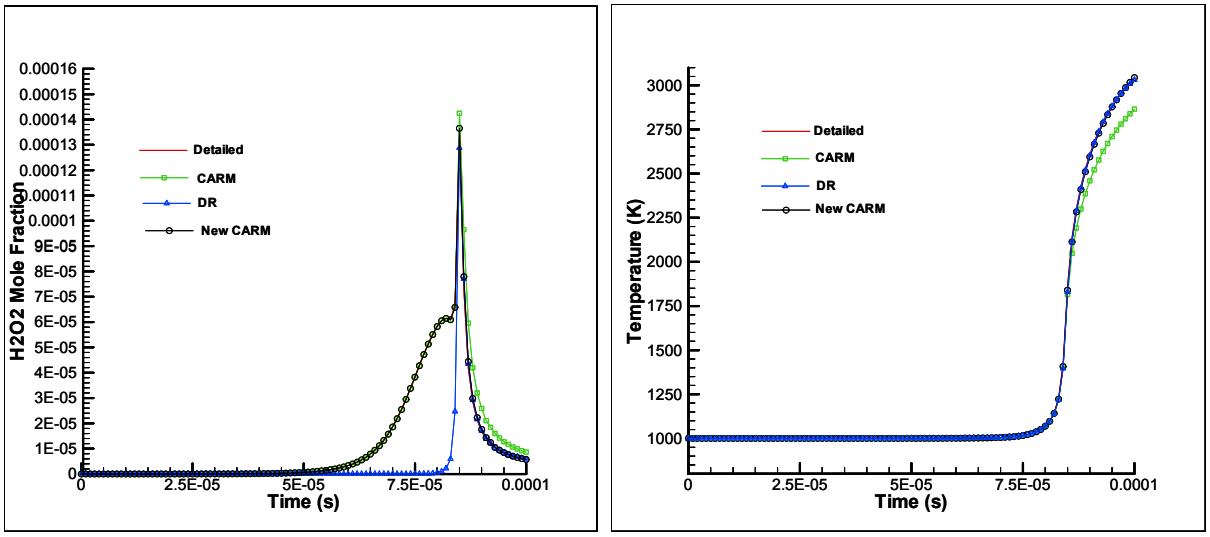

Figure 10. Comparisons of Three Different Approaches for Creating Skeletal Mechanisms.

5.3 Reduced Mechanisms for Simple Fuels

5.3.1 Reduced Mechanism for Hydrogen-Air Combustion

Using CARM, two reduced mechanisms designed to model ignition of hydrogen-air mixtures were created. The reduced mechanisms were based on H_2-O_2 reactions extracted from a large hydrocarbon mechanism (Curran et al., 1998). The reduced mechanisms reduce the number of species from nine in the detailed mechanism to six or seven, by assuming that OH and H_2O_2, or OH, H_2O_2, and HO_2 are in QSS. These reduced mechanisms have been tested against detailed chemistry in constant pressure ignition delay calculations for pressure = 1 atm, E.R. = 0.5, 1.0, and 2.0, and initial temperature = 1000 to 1400 K. Some of the results are plotted in Figure 11. The seven-specie reduced mechanism works very well. The six-specie mechanism results in some error in the computed ignition delay at the lower end of the temperature range QSS for OH and H_2O_2 makes almost no difference, but error begins to appear when HO_2 is assumed in QSS. The seven-species reduced mechanism shows excellent agreement with detailed chemistry and was selected for initial implementation into VULCAN. Reduction from nine to seven species is not a large reduction, but allowed the VULCAN implementation to be tested on a relatively simple case for which experimental data exist.

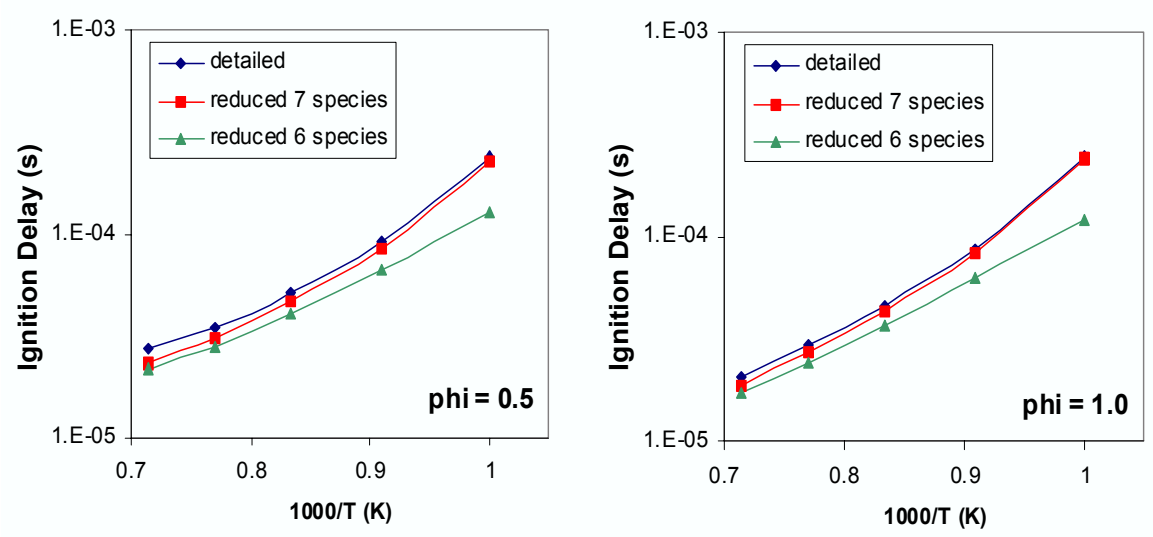

Figure 11. Comparison of Ignition Delay as a Function of Temperature for Detailed and Reduced Mechanisms for H_2-Air Mixture at E.R.s of 0.5 and 1.0, Respectively, P = 1 atm.

5.3.2 Reduced Mechanisms for Ethylene-Air Combustion

Ethylene (C_2H_4), is a small hydrocarbon which has been used previously in combustor simulations and experiments as a scramjet fuel (Baurle and Eklund, 2002). Based on the ethylene detailed mechanism comparisons, reduced mechanisms were created and tested based on the Wang et al. (1999) mechanism. A reduced mechanism with 20 species (cf. 75 in the detailed mechanism) gives excellent agreement with detailed chemistry and experimental results (see Figure 12). A 15-specie reduced mechanism, also based on the Wang detailed chemistry, did not perform satisfactorily, giving ignition delay errors for

some conditions of an order of magnitude or more. The 20-specie reduced mechanism has been implemented into VULCAN to further evaluate the numerical accuracy and robustness of the implementation.

The non-QSS species in this mechanism are H_2, H, O, O_2, OH, H_2O, HO_2, CH_3, CH_4, CO, CO_2, HCO, CH_2O, C_2H_2, C_2H_3, C_2H_4, HCCO, CH_2CO, CH_3CHO, and N_2. This new reduced mechanism is an improvement on previously published reduced mechanisms for ethylene combustion (Montgomery et al., 2002b), being based on a more up-to-date detailed mechanism and tuned for ignition delay under conditions of interest for a scramjet combustor.

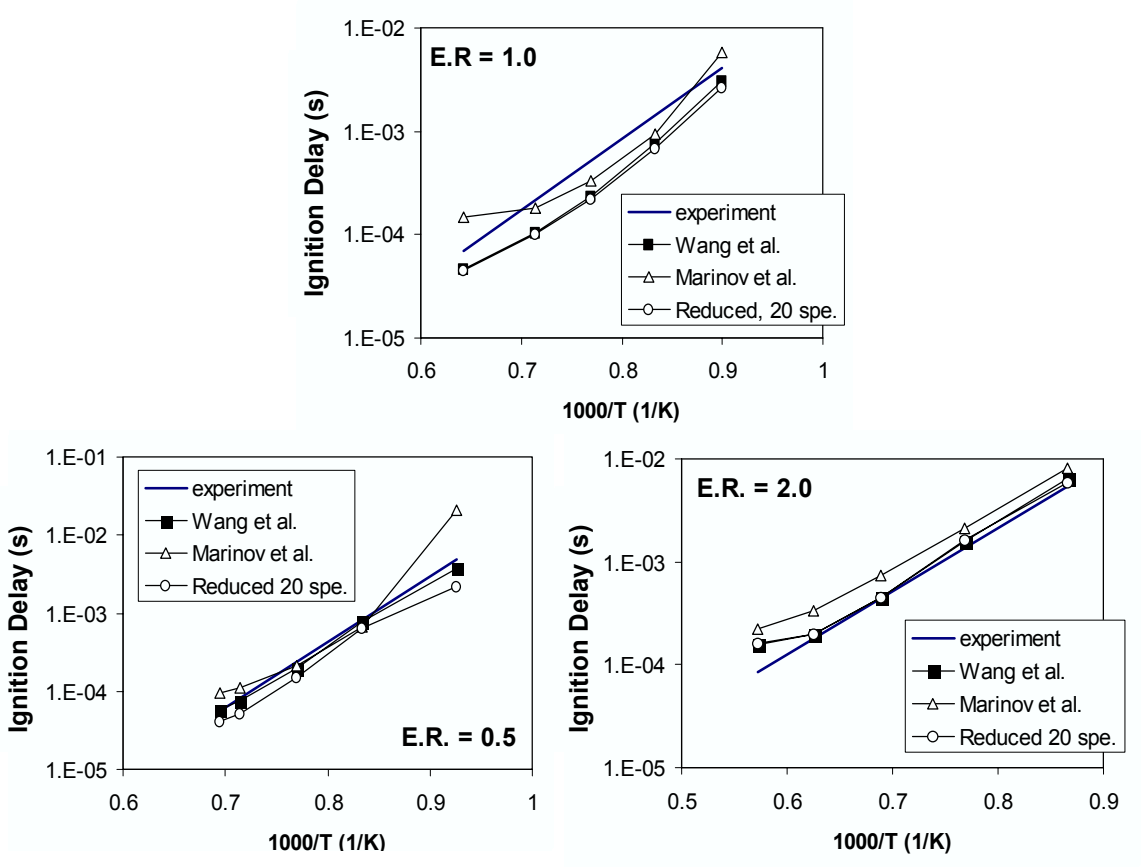

Figure 12. Comparison of Ignition Delay as a Function of Temperature for Experiments, Detailed Chemistry and the Reduced Mechanism for Ethylene-Air Mixtures.

5.4 Reduced Mechanisms for Complex Fuels

5.4.1 Reduced Mechanism for *N*-Heptane-Air Combustion

A 19-specie *n*-heptane reduced mechanism based on the detailed mechanism of Held et al. (1997) was created using CARM. Figure 13 compares calculated ignition delays for a range of E.R.s and temperatures for detailed and reduced chemistry. Despite the fact that *n*-heptane is a larger fuel with a more complex combustion process than ethylene, a

smaller reduced mechanism (19 species cf. 20 for ethylene) could be created with similar accuracy due to the reductions inherent in the semi-empirical mechanism of Held et al. (1997). The species contained in the reduced mechanism are *n*-C_7H_{16}, O_2, C_2H_4, CO, CO_2, C_3H_6, CH_4, C_2H_6, C_4H_8, C_5H_{10}, C_6H_{12}, C_2H_2, C_3H_5, CH_2O, H, H_2O_2, H_2, H_2O, and N_2.

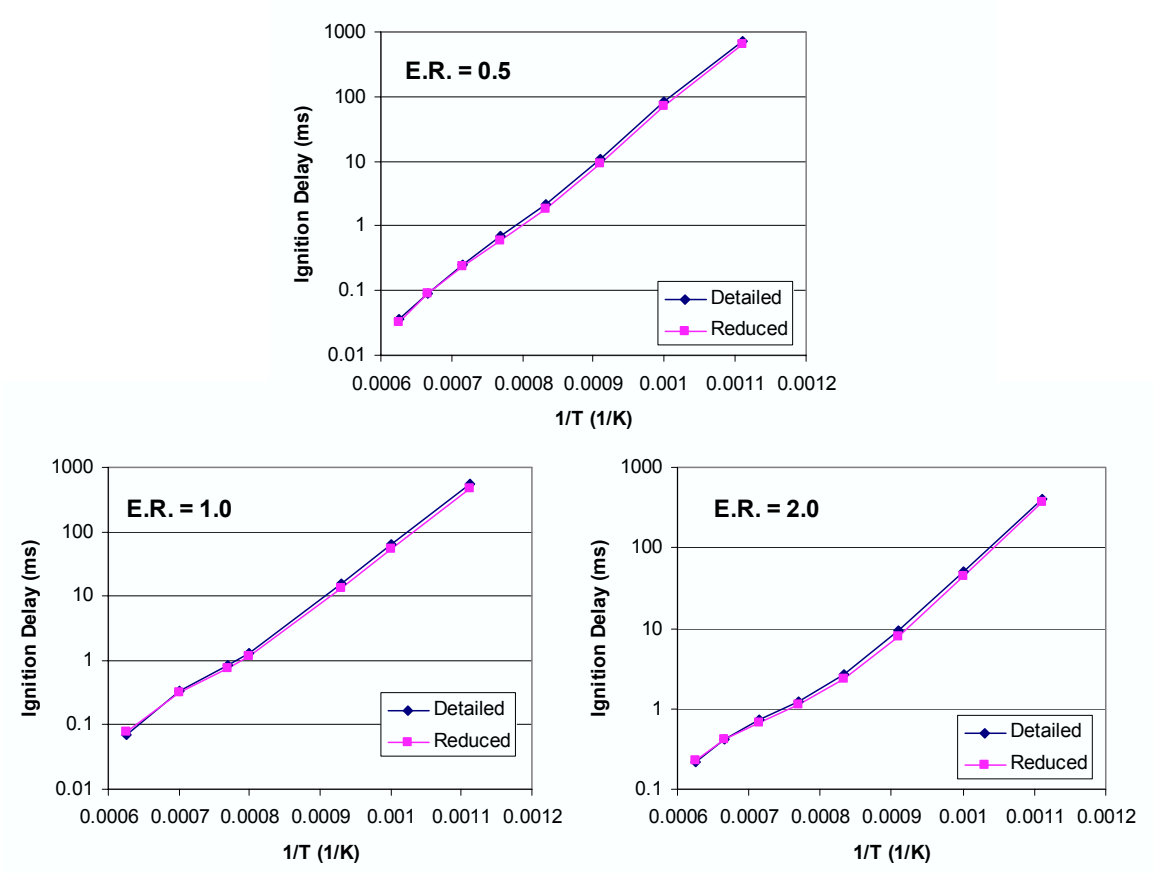

Figure 13. Ignition Delay Calculations for n-Heptane in Air for Detailed Chemistry and the 19-Specie Reduced Mechanism.

5.4.2 Reduced Mechanisms for JP-8-Air Combustion

JP-8 fuel is a complex mixture of thousands of hydrocarbon components that is manufactured to meet certain property standards. The exact composition varies in time and place depending on crude feedstocks and refinery processes. Modeling JP-8 combustion requires selection of a surrogate fuel blend containing a few species with known kinetics that reproduces the essential combustion behavior of a typical batch of the actual fuel (Edwards & Maurice, 2001). The newly upgraded CARM (with modifications described in Section 5.2.2) was used for development of a JP-8 reduced mechanism based on the semi-empirical mechanism developed by Violi et al. (2002) using a six-species surrogate JP-8 fuel mixture, which is listed in Table 2. This surrogate blend was developed to match the boiling curve of a batch of JP-8 and not for any combustion characteristics, yet was shown earlier to give excellent agreement to ignition

delay data (see Figure 4). The semi-empirical mechanism contains 216 species and 4,826 steps.

Table 2. JP-8 Surrogate Blend (Violi et al. 2002).

Compound	Formula	Mole Fraction
dodecane	$C_{12}H_{26}$	0.30
tetradecane	$C_{14}H_{30}$	0.20
iso-octane	C_8H_{10}	0.10
methyl-cylcohexane	C_7H_{14}	0.20
m-xylene	C_8H_{10}	0.15
tetralin	$C_{10}H_{12}$	0.05

A transient PSR was run with initial temperature of 1200 K and pressure of 1 atm to provide the needed information for development of skeletal mechanisms. Several trial versions with different sizes were tested, and the final version contains 147 species and 833 steps. Further reduction using CARM was carried out to develop reduced mechanism of various sizes. As the choice of the QSS species pool can impact the stiffness of the reduced chemistry, CARM was run iteratively with manageable QSS pools to meet the dual criteria of high accuracy without unmanageable stiffness. A 35-specie reduced mechanism was found to be quite accurate for a JP-8 surrogate fuel with six components. The non-QSS species contained in the 35-specie mechanism are H_2, CH_4, C_2H_2, *m*-xylene, C_2H_4, indenyl, C_2H_6, tetralin, H, O, *p*-C_3H_4, CH_3, *a*-C3H4, C_3H_6, $C_{12}H_{25}$, butadiene, butene, isobutane, C_5H_{10}, methyl-cylcohexane, H_2O, CO, CO_2, O_2, OH, H_2O_2, C_7H_{14}, CH_2O, CH_2CO, benzaldehyde, iso-octane, dodecane, tetradecane, C_8H_6, and N_2. A 33-specie reduced mechanism did not give sufficient accuracy. Figure 14 presents comparisons of the predicted ignition delay times among the detailed and reduced mechanisms showing excellent agreement. This reduced mechanism performs significantly better than those created previously (Montgomery et al., 2002c) from the Mawid and Sekar mechanism.

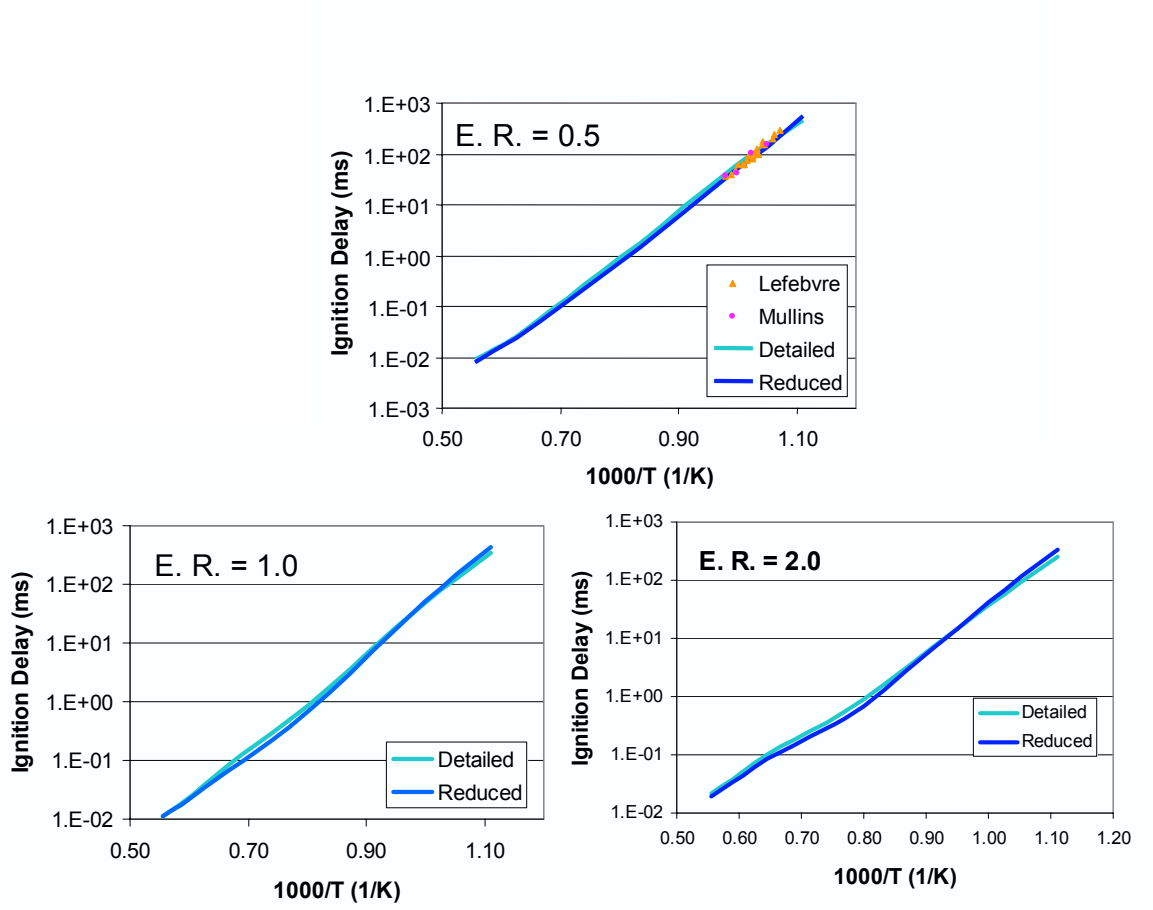

Figure 14. Comparison of Calculated Ignition Delays for JP-8 in Air.

In an attempt to create a reduced mechanism for JP-8 having significantly fewer than 35 species, further simplification was attempted. The Violi et al. (2002) mechanism uses a six-species fuel surrogate blend to represent JP-8. It was hypothesized that a significantly smaller reduced mechanism could be created by using a simpler fuel surrogate. Each species in the fuel surrogate plus some of its breakdown products must be included in the reduced mechanism. Through a trial-and-error process, we have created a two-species surrogate containing the normal dodecane (n-$C_{12}H_{26}$) and m-xylene (C_8H_{10}) that gives calculated ignition delay results that are indistinguishable from those found using the six-species surrogate as shown in Figure 15. The two species in the surrogate represent, respectively, the paraffin and aromatic components of the actual fuel.

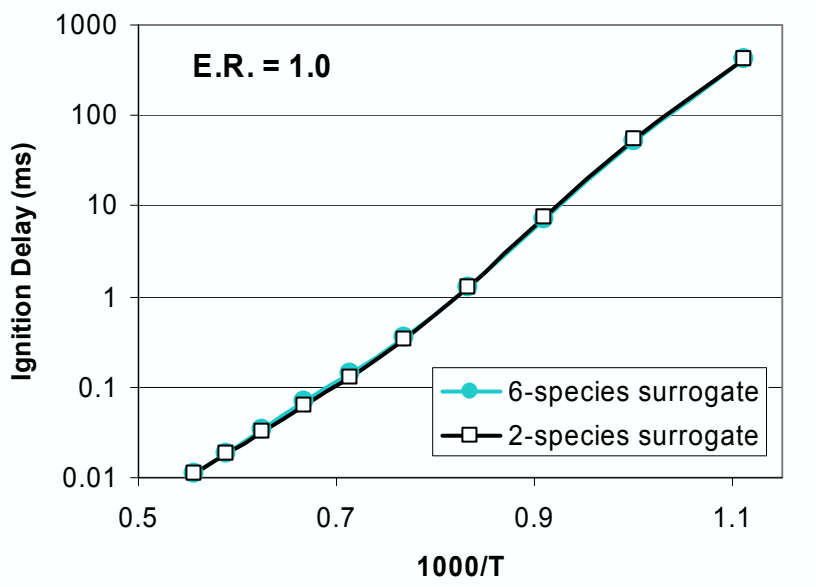

Figure 15. Comparison of Calculated Ignition Delays Using Six- and Two-Species Fuel Surrogates for JP-8.

However, satisfactory reduced mechanisms for the 2-specie surrogate having no fewer than 31 species could be created, not a particularly significant savings in comparison to the 35-specie mechanism. Therefore, it was decided to proceed with the implementation of the 35-specie reduced mechanism into the 2-D flame case in VULCAN. The 35-specie mechanism has been verified over a wide temperature range and for E.R.s ranging from nearly pure air to nearly pure fuel in a PFR. The mechanism does not present any numerical difficulties under these conditions. This reduced mechanism and surrogate blend give an excellent representation of the components of actual JP-8 fuel and their important combustion characteristics, such as heat release rate and ignition delay.

6.0 In Situ Adaptive Tabulation (ISAT)

The CARM produced reduced mechanism may require a great deal of CPU time to perform the iterative calculations to obtain the species reaction rates, depending on the number of steady-state species. For example, in a CFD simulation of a supersonic C_2H_4 diffusion flame with a 20-specie reduced mechanism (to be detailed later), more than 98% of the total CPU time is consumed by the reduced mechanism subroutine if the reaction rates are evaluated directly. In order to account for turbulence-chemistry interactions, evaluation of the turbulent reaction rates involves numerous calls to the reduced mechanism subroutine, which is even more expensive. Thus, significant CPU savings can be achieved by tabulating the chemical source terms.

Direct tabulation is efficient and accurate when there are only 2 or 3 independent variables. However, it is not feasible for a reduced mechanism that contains 10 or more species. *In situ* adaptive tabulation (ISAT), developed in the context of probability density function (PDF) methods (Pope, 1997), is reported to be able to achieve a speed-up factor of 1000.

The "accessed region" of the composition space is defined as the set of all compositions that occur in a reactive flow (or calculation of this flow). The basic idea of ISAT is based on a crucial observation: the accessed region is much smaller than the realizable region. It is sufficient to tabulate only the accessed region rather than the entire realizable region. An unstructured adaptive table is built up during the reactive flow simulation, which is referred as *in situ* tabulation.

In this research program, a scheme developed for the PDF method (Chen et al., 2000) was modified and implemented into VULCAN. The details of the development and implementation are discussed in the next two sections.

6.1 Mathematical Formulation

The ISAT algorithm employed here follows closely the principles proposed by Pope (1997), except that the target functions considered here are the species reaction rates instead of the species concentrations after a given time step. The reaction rates can be written as functions of mass fractions of species, temperature and pressure:

$$_i \quad _i(Y_1, Y_2, ..., Y_{ns}, T, p) \qquad i \quad 1,..., ns\ , \tag{1}$$

where *ns* is the number of species. More generally, in a vector form, we have R=R(Z) where $R=(R_1,\ldots,R_N)^T=(\ _1,\ldots,\ _{ns})^T$ and $Z=(Z_1,\ldots,Z_M)^T=(Y_1,\ldots,Y_{ns},T,p)^T$.

The interpolation formula used in ISAT is

$$\mathbf{R(Z^0 \quad Z)} \quad \mathbf{R}(\mathbf{Z}^0) \quad \frac{\mathbf{R}(\mathbf{Z}^0)}{\mathbf{Z}} \quad \mathbf{Z}\ , \tag{2}$$

where $\mathbf{Z}^0$ is the tabulation point, and $(\mathbf{Z}^0 \quad \mathbf{Z})$ is the query point.

The components of the Jacobian matrix, $\mathbf{R}(\mathbf{Z}^0)/\ \mathbf{Z}$, are calculated numerically:

$$\frac{R_i}{Z_j}(Z_1^0,...,Z_M^0) \quad \frac{1}{j} R(Z_1^0,...,Z_j^0 \quad {}_j,...,Z_M^0) \quad R(Z_1^0,...,Z_j^0,...,Z_M^0), \tag{3}$$

$$i \quad 1,..N, \qquad j \quad 1,...,M$$

Note that evaluation of the Jacobian matrix is expensive. It requires (M+1) times as much CPU as the evaluation of the reaction rate vector.

The interpolation error in ISAT is directly associated with the magnitude of $\mathbf{R} \quad (R_1,..., R_M)^T$. The error is controlled by setting a tolerance for all the components of $\mathbf{R}$. The ellipsoid of accuracy (EOA) of a tabulation point $\mathbf{Z}^0$ is defined as the domain surrounding the point such that

$$\text{Max} \ \frac{|\ R_j\ |}{R_{j,\text{nom}}} \qquad {}_{\text{tol}} \qquad\qquad j \quad 1,..., ns\ , \tag{4}$$

where $R_{j,\text{nom}}$ is the value for normalization, and ${}_{\text{tol}}$ is the tolerance.

6.2 Dynamic Tabulation

The table for ISAT is built as the calculation proceeds. Initially the table is empty. On receipt of the first query $\mathbf{Z}^q$, the first table entry is generated. As it receives the second query, the ISAT subroutine checks first if the query lies within the EOA of the existing table entry for an interpolation. If it is not, the second entry is generated. A cutting plane is also generated to divide the composition space into two parts. In our study, the cutting plane is defined as the plane perpendicular to the vector connecting the two tabulation points, as given in the following:

$$\mathbf{Z} \quad \frac{1}{2}(\mathbf{Z}_1 \quad \mathbf{Z}_2) \quad (\mathbf{Z}_1 \quad \mathbf{Z}_2) \quad 0\ , \tag{5}$$

where $\mathbf{Z}_1$ and $\mathbf{Z}_2$ are the two tabulation points. A sketch of the cutting plane in a 2D space is shown in Figure 16.

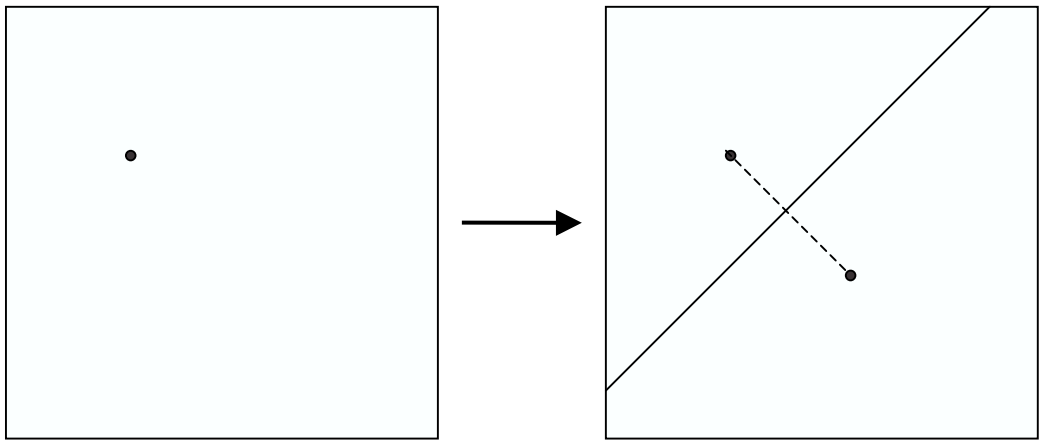

Figure 16. Sketch of Cutting Plane in Relation to the First and Second ISAT Table Entries.

For the third query point, it is first decided which side of the cutting plane the query point belongs to. Then the point is checked to determine whether the query is close enough to the table entry on the same side. If it is, interpolation is performed; if it is not, a new entry is generated and a new cutting plane is defined to separate the old entry and the new entry. The same algorithm repeats as more query points are received.

The dynamic table is stored in a binary tree, as sketched in Figure 17. Each leaf of the tree represents an entry of the table, where the tabulation point $\mathbf{Z}^0$, the reaction rates $\mathbf{R}(\mathbf{Z}^0)$, and the Jacobian matrix $\frac{\mathbf{R}(\mathbf{Z}^0)}{\mathbf{Z}}$ are stored. Each node of the tree represents a cutting plane.

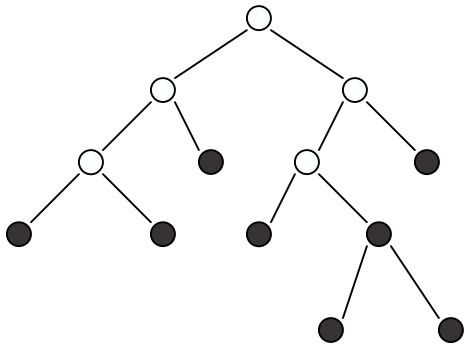

Figure 17. Sketch of the Binary Tree. Each leaf (black dot) contains a table entry; each node (circle) contains information about the cutting plane.

Each time a query point is received, the binary tree is traversed until a leaf is reached. Ideally, one would like to find the leaf $\mathbf{Z}^0$ that is closest to query point $\mathbf{Z}^q$ in the sense that the linear approximation error is minimized. However, it is computationally expensive to find the closest leaf. The binary search used instead is computationally inexpensive, and yields a leaf $\mathbf{Z}^0$ that is likely to be close to $\mathbf{Z}^q$.

7.0 Turbulence-Chemistry Interaction

The modeling of the mean chemical source term has often been considered to be the main problem in CFD simulations of turbulent combustion (Peters, 2000). Many turbulencechemistry interaction models have been developed and applied to various combustion simulations since Spalding (1971) proposed the eddy-break-up (EBU) model for turbulent premixed flames. Most of the models can be placed in one of the following categories: eddy-break-up and eddy-dissipation models, Probability Density Function (PDF) models (including assumed PDF method and transport PDF method), laminar flamelet models, conditional moment closures, and the linear eddy model (LEM). The transport PDF method and the LEM model are accurate, but they are also extremely expensive. Application of the laminar flamelet model is limited when more than one fuel stream is present. The CPU cost of the assumed PDF model increases dramatically when applied to the chemical mechanisms without an analytical form of the reaction rate.

Gran and Magnussen (1996) introduced a new method to implement finite-rate chemistry into the original eddy dissipation concept (EDC) model (Magnussen, 1989), for turbulent combustion which is an extension of Spalding s EBU model. Excellent agreement with experimental measurements was achieved for a bluff-body stabilized turbulent diffusion flame. We note that the case geometry is similar to that of a scramjet combustor. In this project, the model was slightly modified and coupled with the reduced mechanism. We also note that the formulation of the model can be directly coupled with ISAT in order to reduce the CPU cost.
The transport PDF method, where no closure is needed for the chemical source term, is considered as the most accurate method for turbulent reactive flow simulation. Due to the tremendous amount of work associated with implementing the PDF model into VULCAN and limited time frame of this project, the PDF method was only applied using a post-process approach. The density, velocity, and turbulent kinetic energy and dissipation rate were interpolated from VULCAN simulation results. The temperature and species concentrations are recalculated using the PDF method without updating the variables interpolated from VULCAN.

Details of the EDC model and PDF post-processor are described in the following sections.

7.1 Eddy Dissipation Concept Model

The eddy dissipation concept model employed in this project is an extension to the EDC model set forth by Gran and Magnussen (1996), which is related to the eddy-break-up model of Spalding (1976). The rationale of the EDC model was based on the assumption that chemical reaction occurs in the regions where the dissipation of turbulence energy takes place. In flows from moderate to intense turbulence, these regions are small and isolated, occupying only a small fraction of the flow. These regions consist of fine structures whose characteristic dimensions are of the order of the Kolmogorov length scale in one or two dimensions. An empirical expression for mean reaction rates is then given based on this assumption.
The fraction of flow occupied by the isolated fine structure regions is expressed as

$$C_D \overline{k^2}^{1/4}, \quad (6)$$

where k is turbulent kinetic energy, is turbulent kinetic energy dissipation rate , is the laminar kinematic viscosity, and C_D 2.80 is a model constant (Gran and Magnussen, 1996). Note that turbulent kinetic viscosity is $_t$ C k^2 / . The above formulation can also be written as

$$C_D C \left(\frac{l}{t}\right)^{1/4}, \quad (7)$$

where $_l$ is the laminar kinetic viscosity. This formula is more convenient when the turbulence model used in the simulation is not the k- model. In flows where turbulent viscosity is much larger than laminar viscosity, the fraction of fine structures is expected to be small. Magnussen (1989) argued that the volume fraction of the flow occupied by the fine structures should rather be modeled as ^{2} than ^{3} because one dimension of the fine structures is comparable to large vortex structures.

The time scale for the mass transfer between the fine structures and surroundings is estimated as

$$C_E \left(\frac{}{}\right)^{1/4}, \quad (8)$$

where C_E 0.167 is another model constant.

The mean reaction rate is then given by

$$\overline{} \quad \frac{}{}^2 (Y_i^0 \quad Y_i^*), \quad (9)$$

where Y_i^0 is the mean mass fraction and Y_i^* is the mass fraction within the fine structures. In this study, Y_i^* is computed from

$$Y_i^* \quad _0 \quad (Y_i, p, T)dt \ , \quad (10)$$

with initial conditions: Y_i Y_i^0 at t 0. The pressure and enthalpy are kept constant during the integration. The final form for the mean reaction rate is written as

$$\overline{} \quad \frac{}{}^2 \quad _0 \quad (Y_i, p, T)dt \quad Y_i^0 \ . \quad (11)$$

From Equation (11), the turbulent mean reaction rate given by the EDC model is indeed the averaged reaction rate during a time span, , times the volume fraction of the fine structures. The relation between the mean reaction rate and the parameter, , is obvious. The life time of the fine structures, , is also an important parameter in determining the turbulent mean reaction rate. The smaller the life time, the closer the averaged reaction

rate calculated from the integration is to the laminar reaction rate. In other words, smaller fine structure life results in less impact of turbulence chemistry interaction.
An Euler backward scheme was used to integrate Equation (10), which is given by

$$Y_i^{n\ 1} \quad Y_i^n \qquad t \ \ (Y_i^{n\ 1}, p, T^{n\ 1}) , \tag{12}$$

where t is the time step of the integration, Y_i^n and $Y_i^{n\ 1}$ are the species mass fractions at time steps n and $n \quad 1$, respectively. The nonlinear Equations (12) are solved using Newton's method.

The integration procedure of Equation (10) is very computationally expensive. The ISAT algorithm, which is discussed in Section 6, was applied to speed up the evaluation of the mean reaction rates. Note that the tabulation method does not need any change except for the inclusion of the parameter, as an independent variable.

7.2 PDF Post-Processor

Probability Density Function (PDF) methods have been under development for some time for modeling turbulence-chemistry interactions with some success. However CFD calculations with the PDF method are too CPU-intensive for modeling of practical 3D combustor geometries with realistic chemistry. In order to assess the importance of turbulence-chemistry interactions, a Monte Carlo analysis of the joint scalar PDF has been developed for use as a post-processing tool. The post-processing code reads in a CFD solution containing the mean flow field and turbulence properties including turbulence kinetic energy and dissipation rate. With a given flow field, Monte Carlo simulations are performed to solve for the joint scalar PDF evolution equation using fractional time steps.

Figure 18 presents an overview of the post-processing tool. The main routine PDFMC reads in the necessary information on the turbulent flows. As Monte Carlo simulations use notional particles to represent turbulence statistics, numerous calculations for the evolution of the chemical state are performed. The stiff kinetics integrator is initialized first. Second, the impact of turbulent convection and diffusion is determined in subroutine PDFCD as the flow field is assumed to remain unchanged. Followed is the main iteration routine STEPMC which performs Monte Carlo simulations for turbulent convection, diffusion, molecular mixing, and chemical reactions sequentially. ISAT is used to speed up kinetics calculations. Detailed input and output files and the associated manipulations by the post-processing tool are presented in Figure 19.

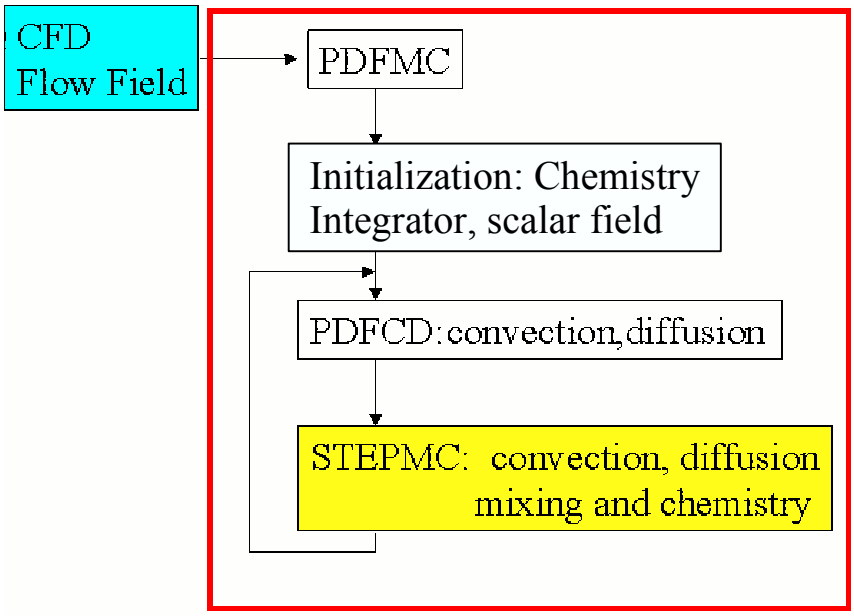

Figure 18. Schematic of PDF Post-Processing Tool Showing that Results from CFD are Read in and the Main Routine Starts the Monte Carlo Simulations.

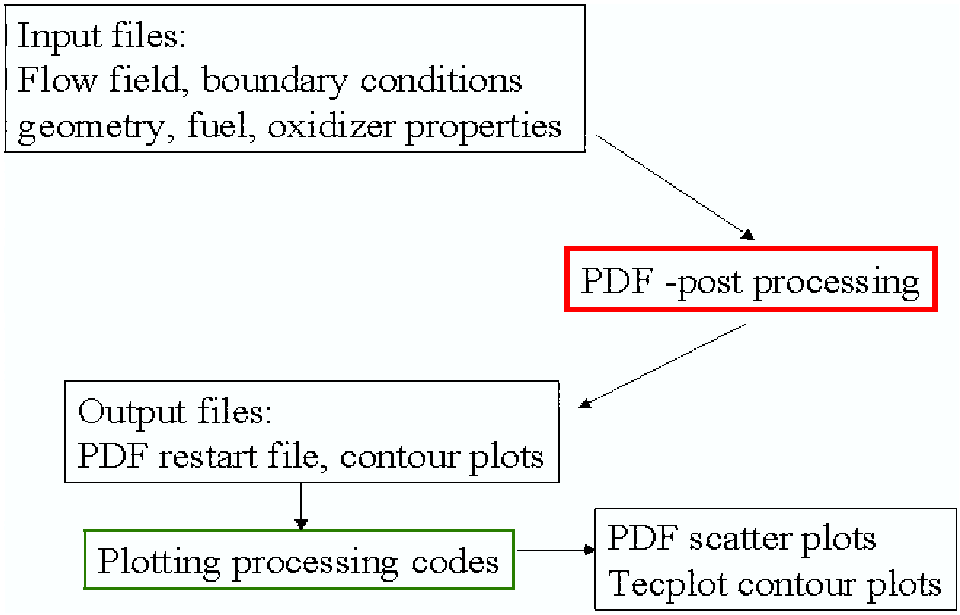

Figure 19. Schematic of Details of PDF Post-Processing Tool Showing Various Input and Output Files Associated with Different Parts of the Process.

8.0 Implementation of New Techniques in VULCAN

8.1 VULCAN Overview

VULCAN is a Navier-Stokes flow solver that is currently maintained and distributed (restricted to the U.S.) by the Hypersonic Airbreathing Propulsion Branch of NASA Langley Research Center. For details, see the Vulcan home page (http://vulcan-cfd.larc.nasa.gov/) (White & Morrison, 1999).

VULCAN is a multigrid, multiblock, structured, finite-volume code, developed for solving the spatially elliptic and parabolized forms of the equations governing 3-D, turbulent, calorically perfect and nonequilibrium chemically reacting flows. Space marching algorithms developed to improve convergence and/or reduce computational cost were implemented as well as elliptic methods for solving flows with large regions of subsonic flow. A full approximate storage, full multigrid scheme was also implemented to accelerate convergence of either the elliptic or space marching schemes. Compressibility corrected forms of the *k-* and *k-* , two equation turbulence models, were implemented that are suitable for high-speed flows. In addition, a compressible, pressure gradient corrected turbulent law-of-the-wall matching function was implemented that decreased wall grid spacing sensitivity. Turbulence-chemistry interaction models were also implemented using the assumed PDF methods.

For the simulations completed in this work, turbulence was modeled with the Menter (1992) baseline (BSL) two-equation turbulence model. The Menter BSL model couples the standard forms of the *k-* and *k-* models. The BSL model invokes the *k-* model near solid surfaces and smoothly transitions to the *k-* model in the outer portion of the boundary layer and in regions of free shear. At solid surfaces, the wall matching procedure of Wilcox (1989) was employed. Also, the compressibility correction of Wilcox (1993) was used to model the reduction in mixing associated with high convective Mach numbers.

8.2 Implementation of Reduced Mechanisms

To implement reduced mechanisms in the VULCAN code, a numerical Jacobian capability was first implemented in VULCAN. This was necessary because the implicit treatment of chemical source terms in VULCAN requires the Jacobian matrices of the reaction rates, allowing VULCAN to use the (nonanalytical) chemical rate source terms from CARM-formulated reduced mechanisms. CARM produces a subroutine that calculates chemical source terms for a given set of conditions, rather than terms which fit an analytical form such as Arrhenius rate coefficients.

The numerical Jacobian has been implemented into VULCAN including both the species derivative and temperature derivative contributions. It is calculated using the formula

$$\frac{f}{} \quad \frac{f(\ldots,\quad) \quad f(\ldots,\ )}{}, \tag{13}$$

where is given by: 10^{7} 10^{6} .

The implementation has been checked with two hand calculations using a conventional seven-specie, seven-reaction Arrhenius hydrogen-air model. The numerical values agreed to 10 significant figures for the species derivative and to 3 significant figures for the temperature derivative. Also, the terms of the numerical Jacobian have been compared to the corresponding terms of the analytical Jacobian as implemented into VULCAN. Good agreement was found between the terms of the analytical Jacobian in VULCAN and the new numerical Jacobian.

The implementation was then tested for an ignition delay case (= 0.25, T = 1000 K, P = 1 atm) using the seven-specie seven-reaction Arrhenius-form hydrogen-air model. Ignition delay was taken as the time for the temperature to increase 400 K. The ignition delay calculated using Chemkin and the seven-by-seven hydrogen-air model was 1.580E-04 s. In VULCAN, a three-stage Runge-Kutta method was used. The ignition delay values obtained with analytical and numerical Jacobians were 1.566e-4 s and 1.564e-4 s, respectively. Figure 20 shows the time history of temperature for the calculations. The solutions with the two methods are very close.

With the numerical Jacobian capability added to VULCAN, the implementation of the reduced mechanism is straightforward. The gas temperature, pressure and species mass fractions are passed to the reduced mechanism subroutine, CKWYP, and the chemical source terms are returned.

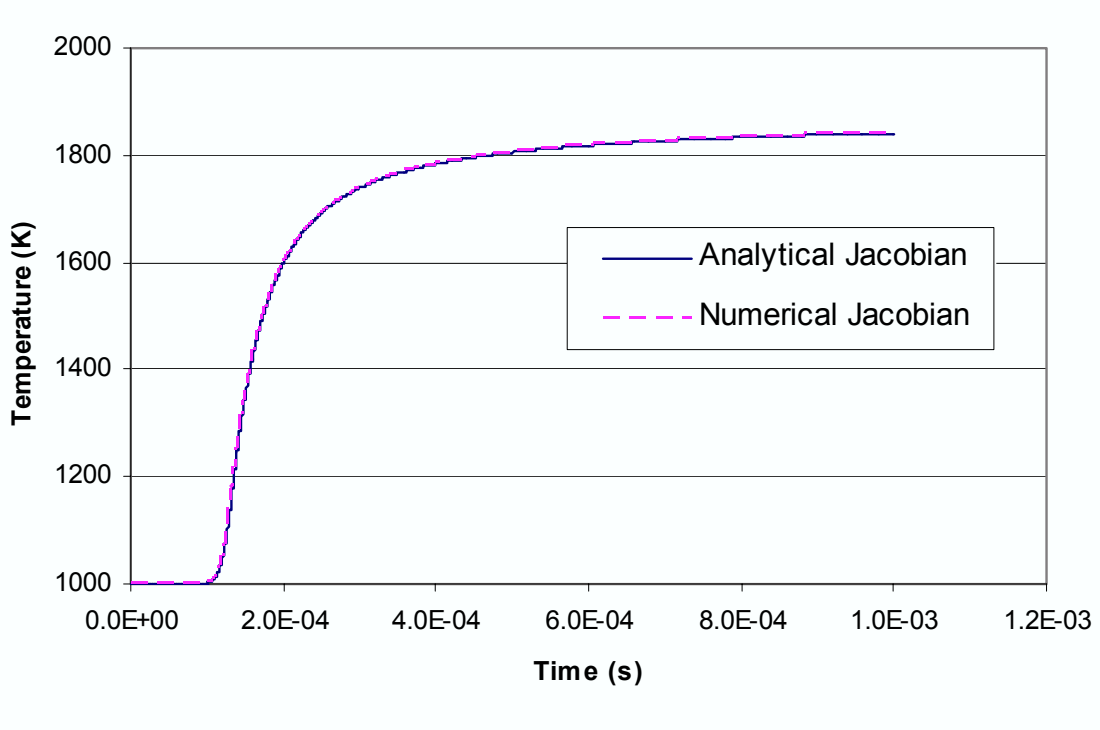

Figure 20. Temperature Versus Time Using Analytical Jacobian and Numerical Jacobian for an Ignition Delay Calculation.

8.3 Implementation of ISAT

Figure 21 shows the overview of the interconnection between a reactive flow code, the ISAT algorithm, and the reduced mechanism. The CFD code passes the species mass fractions, temperature, and pressure to the ISAT routine. The ISAT routine then traverses the existing binary tree table. If an entry within the ellipsoidal of accuracy is found, an interpolation is performed and the interpolated reaction rates and the Jacobian matrix used for interpolation are returned to VULCAN. If such an entry is not found, the ISAT routine then calls CKWYP to calculate the reaction rates and Jacobian. A new entry is added to the table, and the reaction rates and Jacobian are returned to VULCAN. The implicit method used in VULCAN requires the evaluation of the Jacobian matrix of the chemical source term, which is available in the ISAT table. It thus saves significant CPU time for the ISAT subroutine to return not only the reaction rate vector, but the Jacobian matrix required by VULCAN. The only additional cost introduced by ISAT is traversing the binary tree data structure to search for a close entry to the inquiry vector. The cost of this operation is very small compared to direct evaluation of the reaction rates.

The memory size, M, occupied by the ISAT table can be estimated as $M = 8N(n^2+6n+14)$ bytes, where n is the number of species, and N is the number of table entries. For a 20-specie mechanism and a table size of 50,000, the memory size occupied by the table is approximately 214 MB. It was found that the ISAT table size increases very fast in the early stage of the simulations due to the fast change in species concentrations and temperature. Many table entries created early are rarely used in the later iterations or time

steps. A tree-trimming method was developed to control the table size. An upper limit is set for the size of binary tree. Once the tree is full, the table entries that have never been used during the most recent few time steps are trimmed from the table.

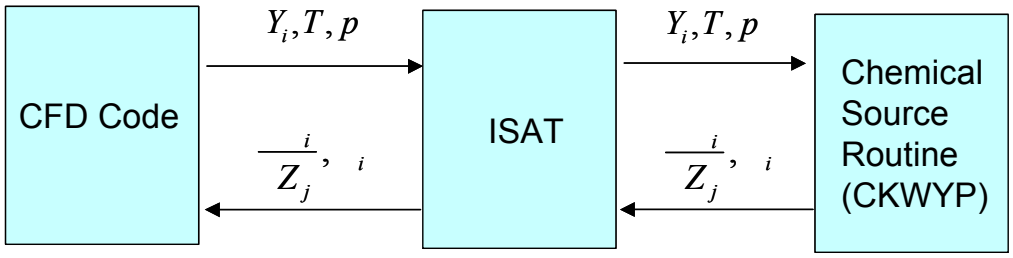

Figure 21. Overview of the Interconnection between a Reactive Flow Code, ISAT, and a Reduced Mechanism.

8.4 Implementation of EDC Model

Implementation of the EDC model in VULCAN is very similar to that of the reduced mechanism, as shown in Figure 22. The target functions of ISAT are the turbulent mean reaction rates, and the independent variables for ISAT are species mass fractions, pressure, temperature, and the life time of the fine structures. Utilizing the EDC model without ISAT is very CPU intensive, due to the large number of calls to the reduced mechanism routine in order to integrate the mean reaction rates. Thus, the efficiency of ISAT is expected to be significantly better than when using laminar chemistry.

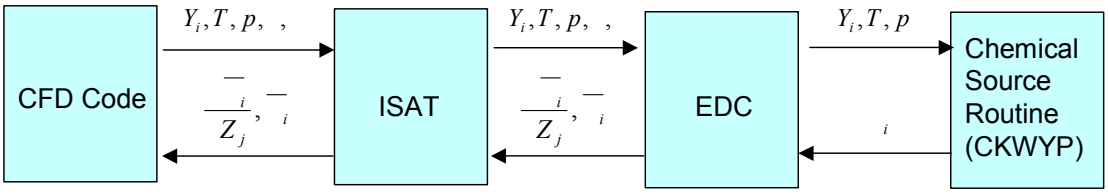

Figure 22. Overview of the interconnection between a reactive flow code, ISAT, EDC model, and a reduced mechanism.

9.0 Evaluation of New Techniques in VULCAN

Initial evaluations of the reduced mechanism and ISAT implementations into VULCAN were performed for 2-D supersonic reacting flows. This allowed debugging and examination of stability, accuracy, and parallelization issues to be performed on cases with comparatively small CPU demands. These reactions are discussed in Section 9.1. Simulations were completed to investigate impacts of turbulence-chemistry interactions on calculation of the mean chemical reaction rates. A discussion of these results is provided in Section 9.2.

9.1 Evaluation of Reduced Mechanisms with ISAT

The case considered is the coaxial jet flow experiment conducted by Evans et al. (1978). The experiment consisted of coaxial injection of a cold, Mach 2, hydrogen jet at matched pressure into a hot, Mach 1.9, vitiated air stream. Figure 23 is a schematic of this experiment.

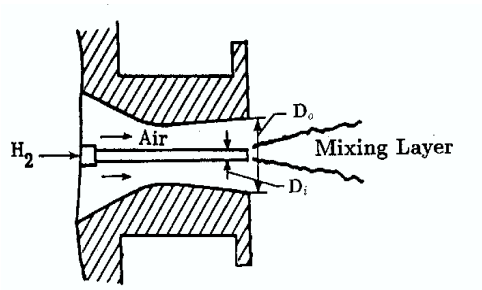

Figure 23. Schematic of the Supersonic Diffusion Flame Experiment of Evans et al. (1978).

The fuel nozzle was conical with a 5° exit half-angle. The computational domain extended seven jet diameters (d = 0.009525 m) upstream of the nozzle exit to capture the flow angularity at the inner nozzle exit and to include a boundary layer in the exit profiles. Modeling the flow upstream of the jet exit was found to yield better agreement with the experimental data. The computational domain also extended 30 diameters downstream of the nozzle exit and 2 diameters in the transverse direction. The modeled flow conditions are given in Table 3. The computational grid downstream of the nozzle exit plane that was used for the majority of the calculations was discretized with 120 and 68 cells in the streamwise and transverse directions, respectively. Calculations were performed with grids containing 240×136 and 60×34 cells to assess grid sensitivity in the results. Complete grid independence was not obtained, but differences between the solutions on the medium and fine grids were minor. The results shown in the succeeding figures were obtained on the medium grid (120×68).

Table 3. Conditions for Supersonic Jet Flame Simulations.

Specified condition	Fuel jet	Outer jet
Mach number	---	1.9
Temperature (K)	---	1495
Pressure, p (bar)	---	1.0
Total temperature (K)	452	---
Total pressure (bar)	8.6068	---
O_2 mass frac.	0.0	0.241
N_2 mass frac.	0.0	0.478
H_2O mass frac.	0.0	0.281
Fuel mass frac.	1.0	0.0

Solutions were obtained in three steps. First, flow upstream of the jet nozzle exit plane was calculated. The resulting solution was used as the inflow boundary condition for the flow calculation downstream of nozzle exit plane. A no-slip, adiabatic boundary condition was applied at the injector lip, a symmetry boundary condition was applied along the centerline, and zeroth order extrapolation was used at the outflow boundary and at the upper domain boundary. Secondly, the coaxial jet flow field calculation was advanced with reactions disabled. Finally, the calculation was continued with the reactions enabled. This same procedure was followed for both the CARM-produced and global Arrhenius-form models. Similar convergence behavior was observed in both cases.

9.1.1 Supersonic Hydrogen Flame Simulations

Solutions were obtained for both reduced and detailed H_2-air kinetics models. The detailed mechanism was a subset of the GRI 3.0 mechanism (GRI mech web page) and included the nine species H_2, O_2, H_2O, OH, O, H, HO_2, H_2O_2, and N_2. All of the reactions involving these species from GRI 3.0 were included except one, which was omitted because pressure-dependent reactions are currently not supported by VULCAN. The resulting mechanism had 27 reactions.

For comparison purposes, two mechanisms were evaluated. The first is the CARM-produced reduced kinetic mechanism using the seven species H_2, O_2, H_2O, O, H, HO_2, and N_2, which was described earlier. The second is a global mechanism obtained by eliminating HO_2 and H_2O_2 from the mechanism of Jachimowski (1988), which yields a seven-step, seven-species Arrhenius-form mechanism which we refer to in the following as the seven-by-seven mechanism.

Contours of the Mach number, temperature, fuel-air E.R., and the ratio of turbulent-to-laminar viscosity from the solution with the CARM seven-species reduced mechanism are shown in Figure 24. The hydrogen jet expanded from sonic conditions to a nominal Mach number of 2.0 at the nozzle exit. Further expansion elevated the Mach number to a maximum of 2.72. The hydrogen jet turned back toward the centerline at $x/D \sim 1.0$,

recompressing the jet. The minimum Mach number at the exit of the domain (x/D = 30) was 1.26.

A mixing layer formed in the wake behind the nozzle lip between the hydrogen jet and the vitiated air stream. The wake also generated relatively high levels of turbulent kinetic energy, and thus, high eddy viscosity values, which were convected downstream. The fuel-air E.R.s indicate a thin surface of approximately stoichiometric proportions along the outer edge of the shear layer that formed between the two streams. Ignition was observed at x/D ~ 2. The flame occurred near the stoichiometric surface. Contours of the O_2, N_2, H_2O, and H_2 mass fractions from the same solution are shown in Figure 25.

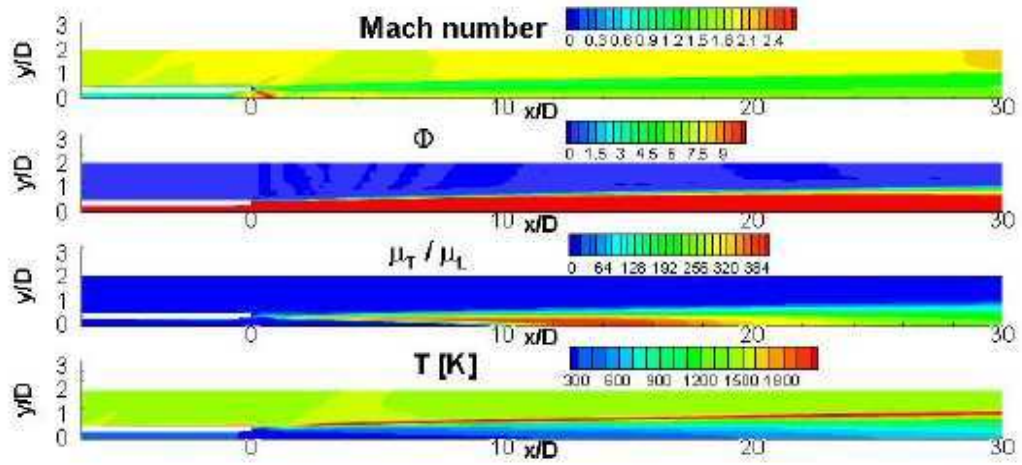

Figure 24. Contours of Mach Number, Fuel-Air E.R., Ratio of Turbulent to Laminar Viscosity and Temperature for the Solution Obtained with the CARM Seven-Species Reduced Chemical Kinetic Mechanism.

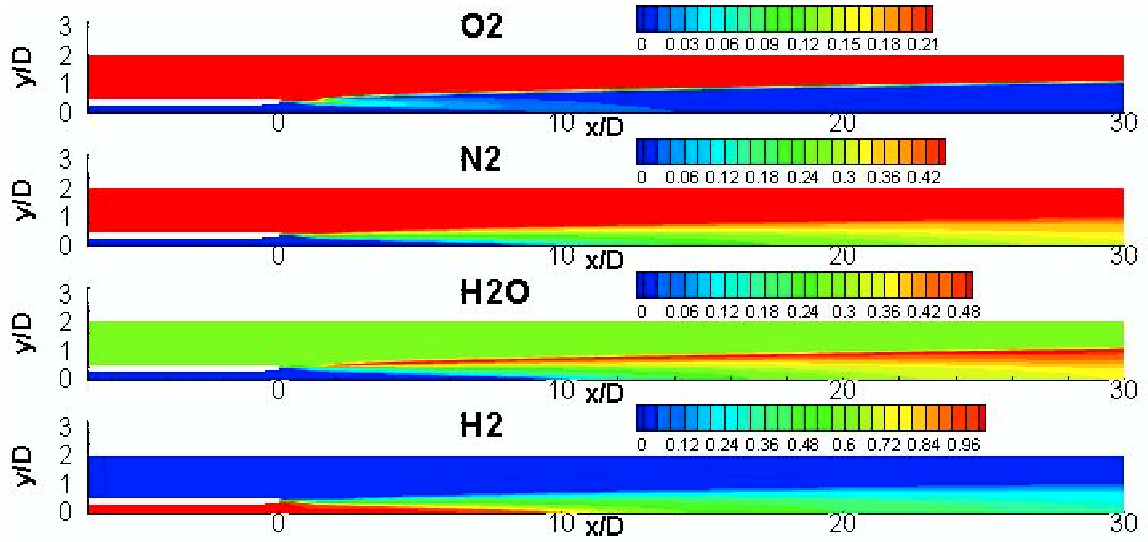

Figure 25. Contours of Mass Fraction of O_2, N_2, H_2O, and H_2 for the Solution Obtained with the CARM Seven-Species Reduced Chemical Kinetic Mechanism.

Oxygen penetrated into the fuel-rich region upstream of the flame surface. This oxygen diffused into the fuel jet and reacted with the fuel. Downstream of ignition, little oxygen penetrated through the flame zone. N_2, H_2O, and H_2 diffuse in the region below the flame surface. Contours of H_2O reveal that little diffusion occurs above the shear layer due to low values of turbulent viscosity at the outer edge of the shear layer.

Profiles of the mass fraction of the major species O_2, N_2, H_2O, and H_2 are compared for the solutions with three kinetics models and the experimental data in Figure 26. Experimental data for other species and temperature were not available. As reflected in the N_2 profiles, near the centerline, the shear layer mixing is slightly underpredicted at the first measurement station but predicted well at the succeeding three stations. However, the extent of mixing near the edge of the shear layer ($x/d \sim 0.7$) is greater in the calculations than in the experimental data. The measured values for O_2 and H_2O in the vitiated stream ($x/d > 1.2$) are observed to deviate from their nominal values. As seen in Figure 25, oxygen penetrated into the fuel rich region, and positive values of oxygen mass fraction are predicted below the flame at $x/d = 8.26$. Each of the kinetics models predicted more oxygen than was observed in the measurements, with the CARM reduced model predicting the least oxygen and the seven-by-seven model the most. Both the CARM reduced mechanism and the detailed model predicted negligible O_2 at the last three stations in accord with the measurements, while the seven-by-seven model predicted significant levels of O_2. This demonstrates the presence of kinetic effects retained in the CARM model and detailed chemistry, but absent from the seven-by-seven mechanism.

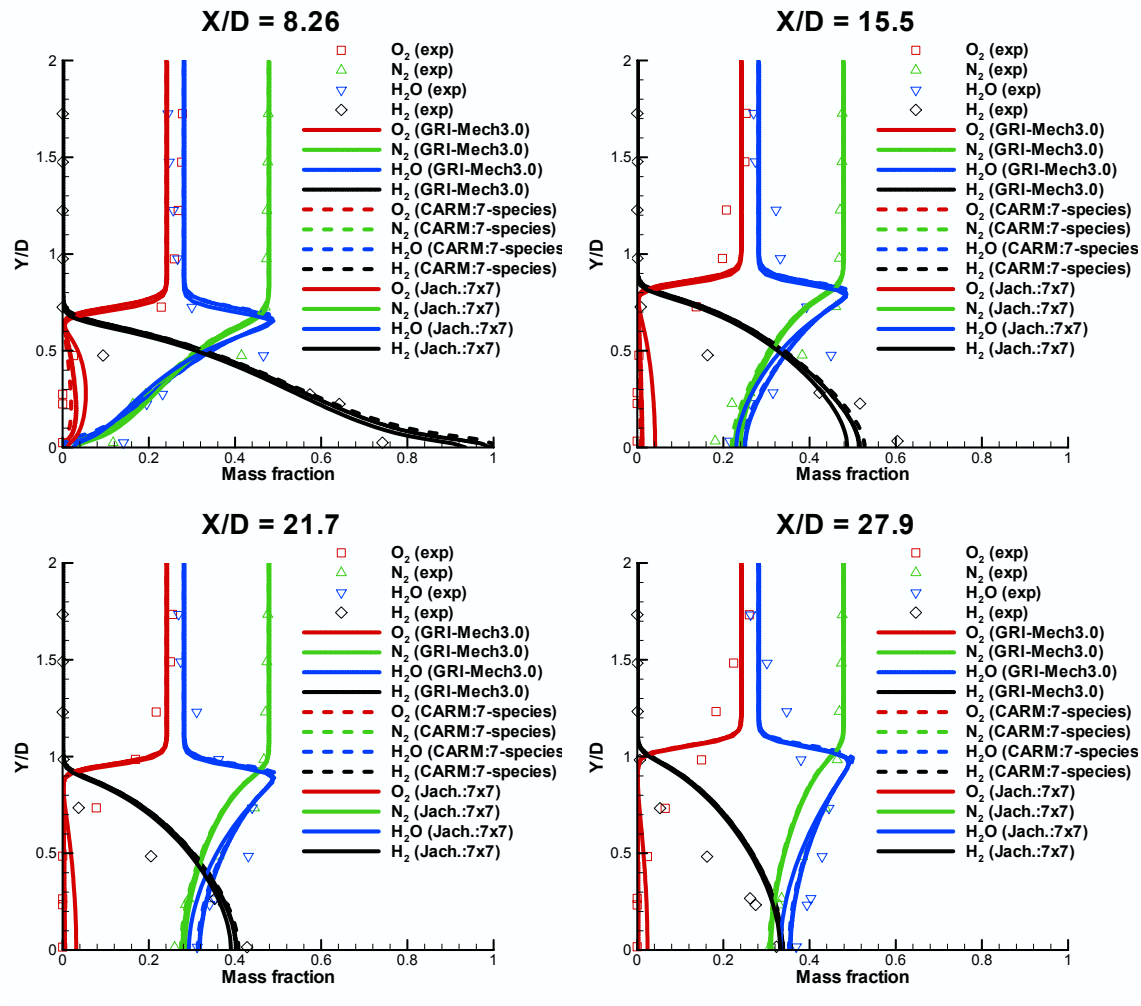

Figure 26. Comparison of Species Profiles between Calculation and Experiment.

9.1.2 Supersonic Ethylene Flame Simulations

Calculations using the same geometry and boundary conditions were repeated with ethylene (C_2H_4) as the fuel using the 20-species reduced mechanism described previously. The total pressure and temperature of the C_2H_4 jet were the same as for the H_2 jet to again produce matched pressure conditions. No numerical stability problems were encountered. Shown in Figure 27 are contours of the temperature and the mass fractions of O_2, N_2, CO_2, and C_2H_4. The standoff flame distance has increased from $x/d \sim 2.0$ to $x/d \sim$ in the hydrogen-air flame and $x/d \sim 17.0$ in the ethylene-air flame. The calculation demonstrates the capability for modeling high-speed combustion problems using hydrocarbon fuels with CARM-produced kinetic mechanisms in a state-of-the-art CFD solver. Unfortunately, very little experimental data is available for supersonic hydrocarbon flames.

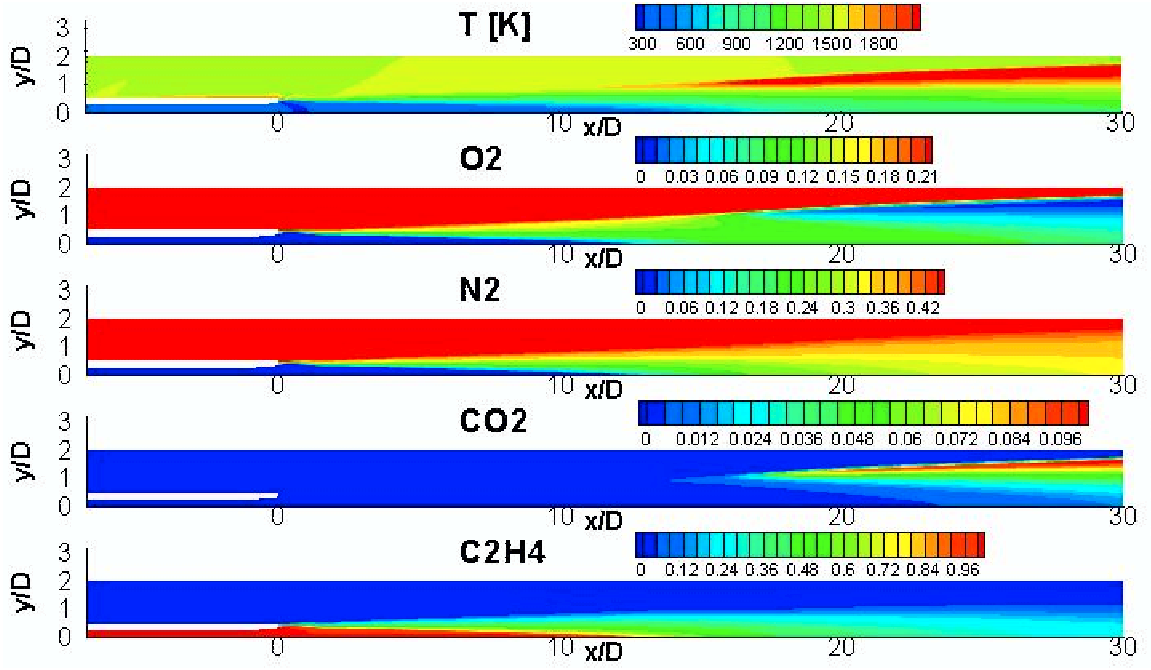

Figure 27. Contours of Temperature and Mass Fraction of O_2, N_2, CO_2, and C_2H_4 for the Solution Obtained with the 20-Species C_2H_4 Reduced Chemical Kinetic Mechanism.

The error tolerance for ISAT for both cases was set to 0.02, with a maximum table size of 50,000 entries. After several hundred iterations, the table size stabilized at around 30,000 entries. The number of new entries added to the table at each time step was less than 10. The average CPU time per time step for the mechanism is listed in Table 4. For the hydrogen flame, the CPU cost of the reacting flow simulation with directly evaluated reaction rates was only 1.8 times that of the nonreacting case. Still, a speedup factor of 1.34 was achieved with ISAT. For the ethylene flame case, the CPU cost of the reacting flow simulation without ISAT is about 82 times that of nonreacting flow. Numerically evaluating the reaction rate Jacobian matrix is extremely expensive for the CARM-produced reduced mechanisms. More than 98% of the total CPU time was consumed by the reduced mechanism subroutine. Using ISAT, the total CPU time was cut by a factor of 36, making the reacting flow comparable in CPU time to the nonreacting flow simulation.

Table 4. Average CPU Time for a Single Time Step for the Jet Flame Simulations.

Mechanism	7-specie H_2	20-specie C_2H_4
CPU, nonreacting	0.35 s	0.93 s
CPU, reacting, direct	0.63 s	76.4 s
CPU, reacting, ISAT	0.47 s	1.8 s
ISAT speedup factor	1.34	36.4

Calculations of the Evans et al. (1978) diffusion flame geometry case have been repeated for comparison to other ethylene kinetic models. A solution was obtained with a six species, three-reaction ethylene mechanism which has been used previously in scramjet combustor simulations (Baurle & Eklund, 2002). The CPU time compared to the 20-species ethylene reduced kinetics model with and without the use of ISAT is shown in Table 5. The timings were obtained on a single Compaq SC-45 processor for each of the three calculations. ISAT reduced the CPU time by a factor of 42.

Table 5. CPU Times for Calculations Performed on One Processor.

Mechanism	Seconds per iteration
C2H4 (6 by 3)	0.54
C2H4 (reduced 20 specie)	76.4
C2H4 (reduced 20 specie) +ISAT	1.8

9.1.3 Parallelization

Further calculations were performed using the 20-species C2H4 reduced mechanism and ISAT, but using multiple processors on a Compaq SC-45. The results of the timings are shown in Table 6. The relatively poor speedup is due to the small grid employed (121 by 69) and the consequent large relative ratio of communication to computation, which increases as the number of processors increases.

Table 6. CPU Times for 2-D Ethylene Jet Flame Calculations (with ISAT) on Multiple Processors.

Processors	Seconds per iteration	Speedup
1	1.8	---
2	1.1	1.6
4	0.7	2.6
8	0.5	3.5
12	0.5	3.6
24	0.8	2.3

No convergence problems were encountered using multiple processors, as shown in Figure 28, which shows the residual histories for the solutions obtained using the reduced kinetics model with ISAT and various number of processors. The solution labeled DIRECT refers to the solution obtained without ISAT.

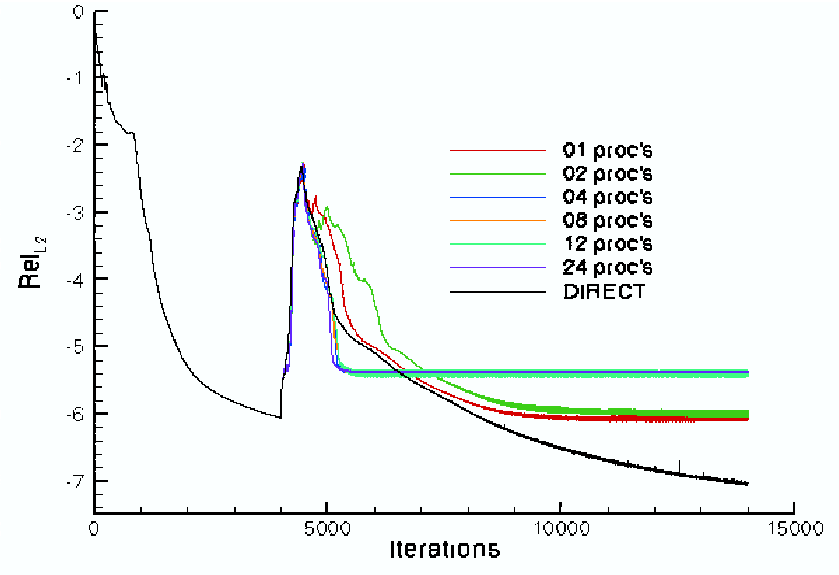

Figure 28. Residual History for Solutions obtained with ISAT and without ISAT (DIRECT).

Discrepancies were initially observed among solutions obtained using different numbers of processors. Figure 29 displays contours of OH mass fraction for the solution obtained with the reduced kinetics model without ISAT, while Figures 30 and 31 show contours of OH mass fraction in the vicinity of the flame region for the solutions using ISAT. The solution with ISAT and one processor (red contours) is indistinguishable from the solution without ISAT (black contours); however, the solutions with multiple processors are clearly different from each other.

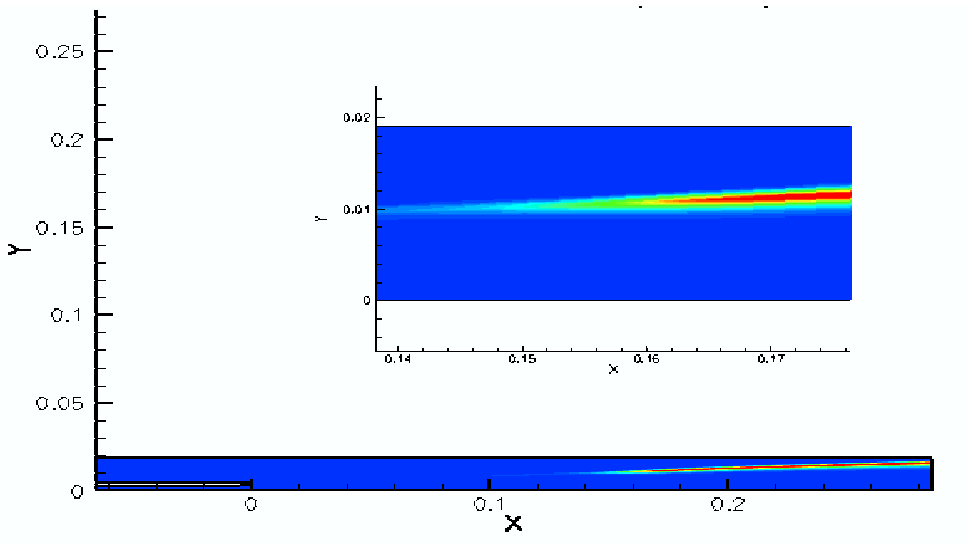

Figure 29. Contours of OH Mass Fraction Obtained with the Reduced Kinetics Model without ISAT.

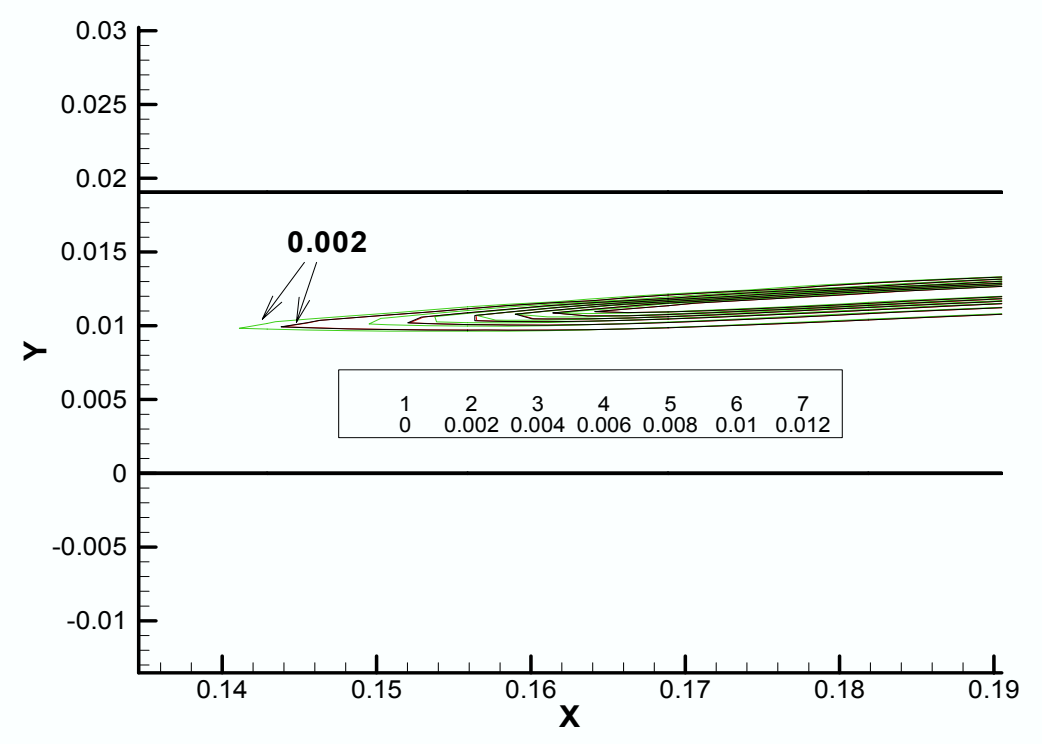

Figure 30. Contours of OH Mass Fraction Obtained with ISAT Using 1 and 2 Processors and without ISAT (DIRECT). See Figure 28 for the color key.

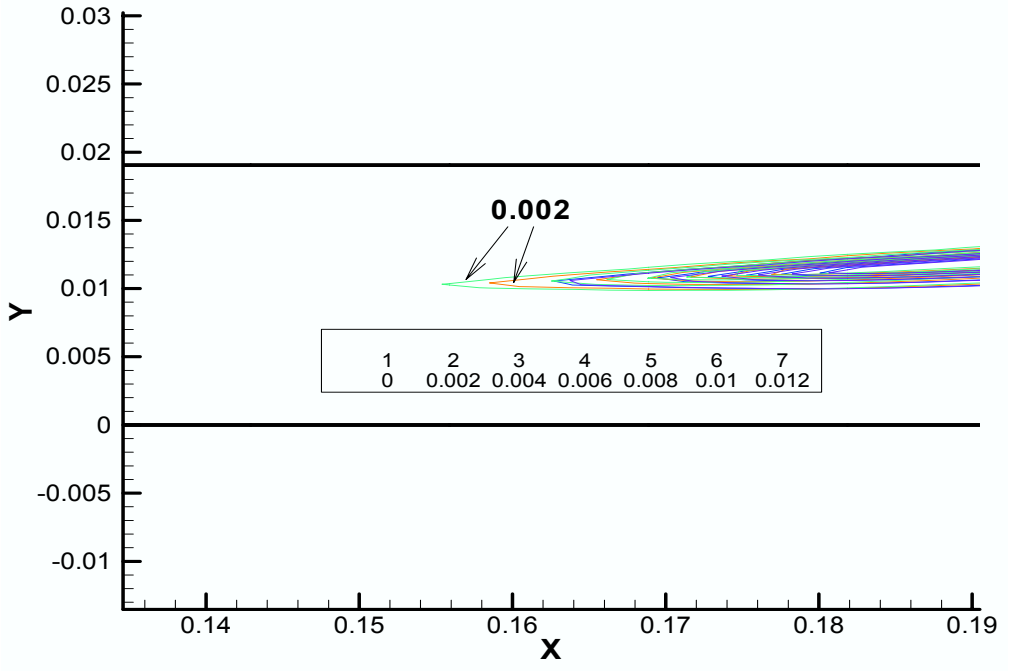

Figure 31. Contours of OH Mass Fraction Obtained with ISAT using 4, 8 12 and 24 Processors. See Figure 28 for the color key.

Differences in the solutions are more clearly apparent in Figures 32 and 33, which show profiles of OH mass fraction at two axial locations. The values of OH mass fraction above the flame region ($y > 0.013$ m in Figure 30 and $y > 0.017$ m in Figure 31) are nonzero for the solutions obtained with multiple processors. The calculation was repeated with four processors and with ISAT the error tolerance tightened from 0.05 to 0.01. Shown in Figure 34 is the residual history. Figure 35 displays the contours of OH mass fraction and Figures 36and 37 show the OH mass fraction profiles. The solution with the tighter ISAT error tolerance is now indistinguishable from the solution obtained without ISAT.

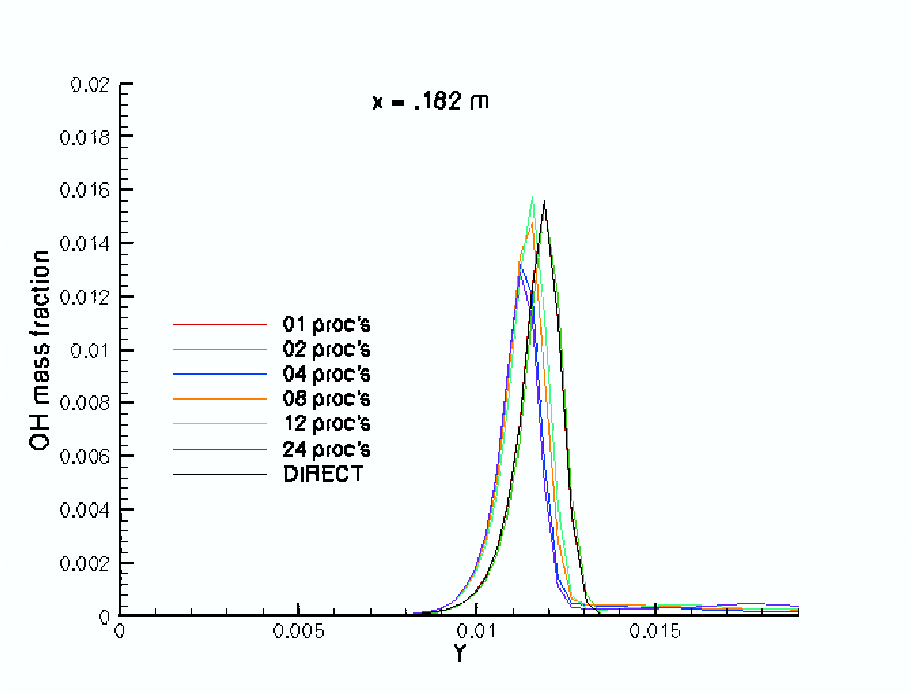

Figure 32. OH Mass Fraction Profiles at x = 0.182 m.

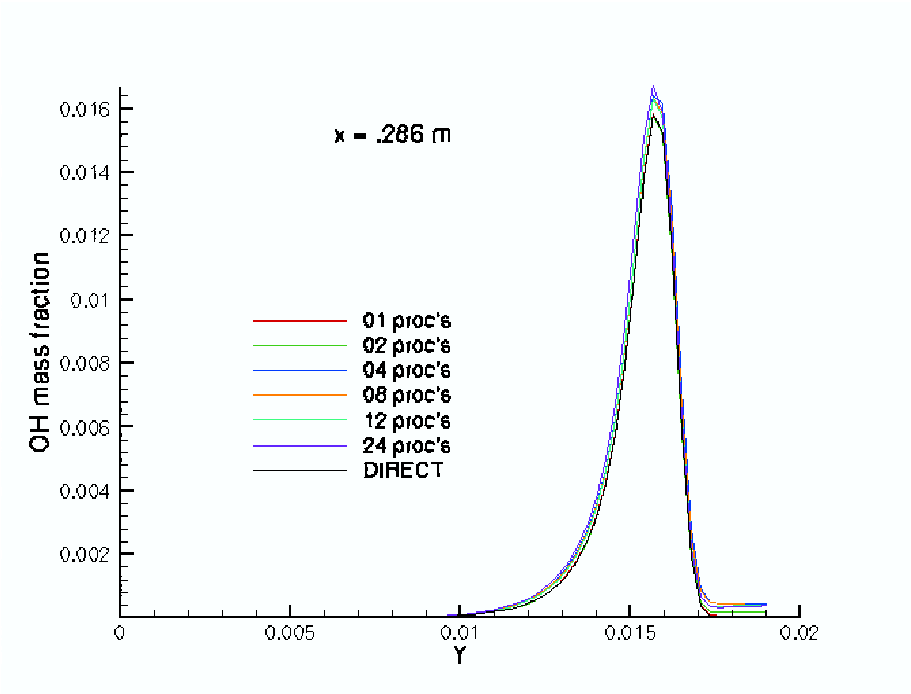

Figure 33. OH Mass Fraction Profiles at x = 0.286 m (exit of the domain).

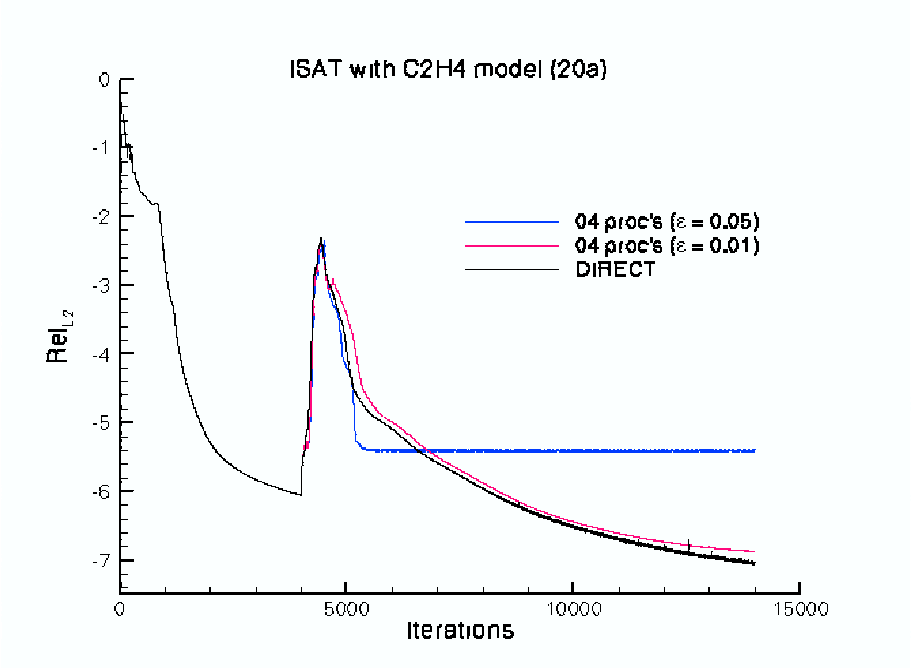

Figure 34. Residual History with the ISAT Error Tolerance Reduced to 0.01.

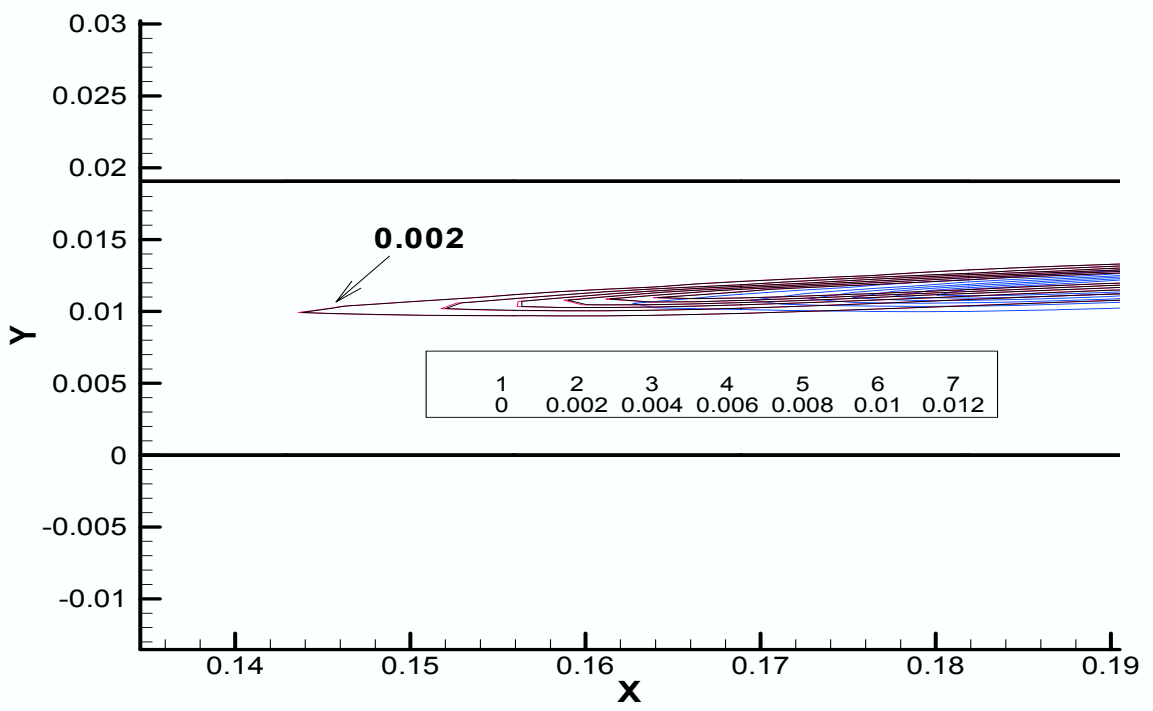

Figure 35. Contours of OH Mass Fraction obtained with ISAT and the Error Tolerance Set to 0.05 and 0.01 and Without ISAT (DIRECT). See Figure 34 for the color key.

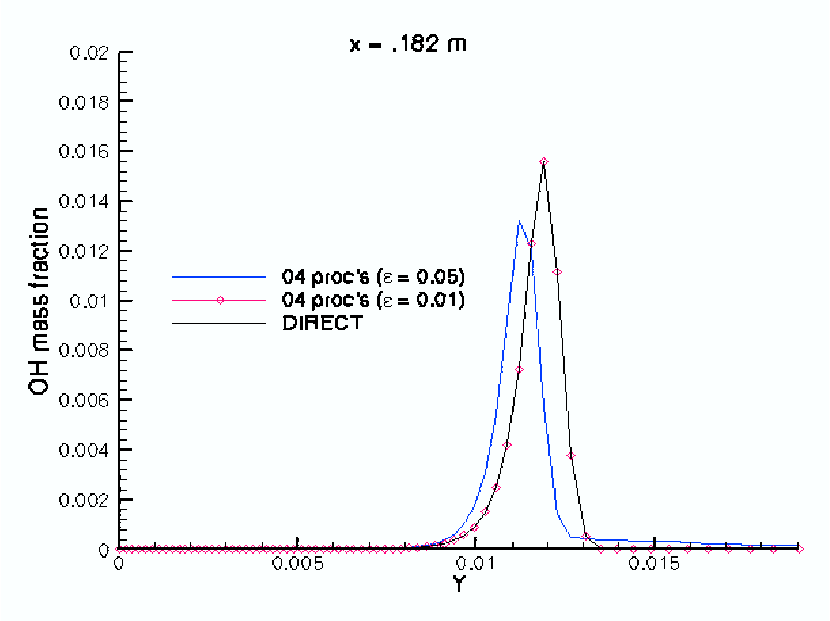

Figure 36. OH Mass Fraction Profiles at x = 0.182 m with the Error Tolerance Reduced to 0. 01.

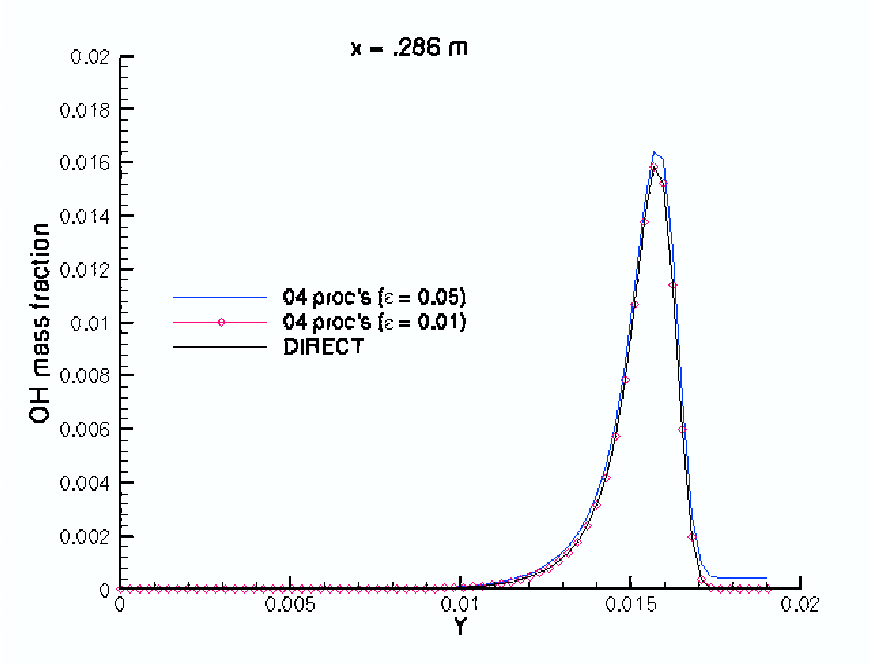

Figure 37. OH Mass Fraction Profiles at x = 0.286 m with the Error Tolerance Reduced to 0. 01.

It is believed that the solution differences seen using ISAT and multiple processors are due to separate ISAT tables that are generated for each processor. Differences among the tables will require a tighter overall tolerance on the ISAT interpolation to achieve the same results. Reducing the error tolerance caused the CPU time to increase from 0.7 seconds/iteration to 1.2 seconds/iteration.

Finally, a 3-D grid was used to further evaluate the parallel speedup of the ISAT routine. The grid was obtained from the axisymmetric grid by sweeping 180° in 36 intervals; the resulting grid size was 121 by 69 by 37 cells. Shown in Figure 38 is a cross section of the 3-D grid. The CPU timings for the ISAT routine on the 3-D grid are given in Table 7. Note that for the parallel computations both the axisymmetric and 3-D grids were split in the axial direction.

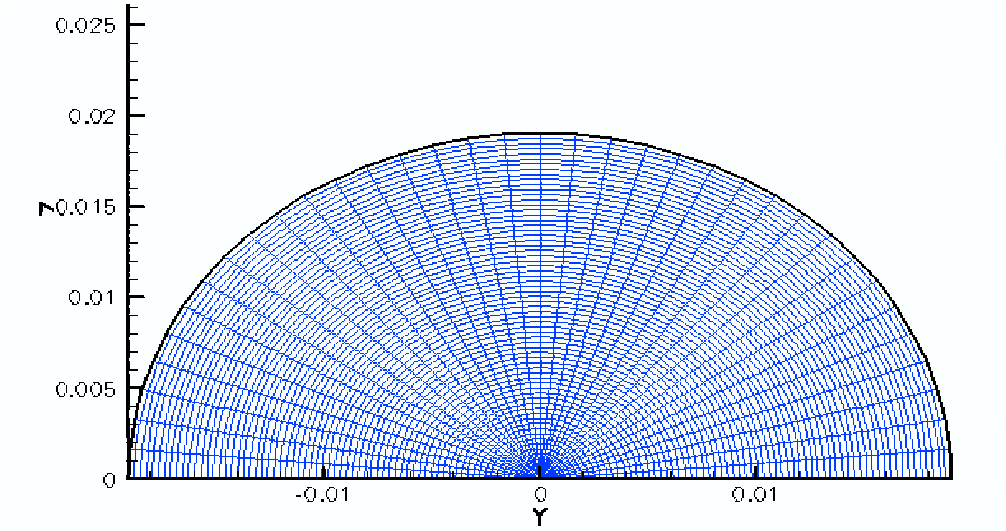

Figure 38. Outflow Plane for the 3-D Grid.

Table 7. CPU Times for Calculations Performed on Multiple Processors Using a 3-D Grid.

Processors	Sec. per iteration	Speedup	Efficiency
1	73.6	---	1.0
2	41.1	1.8	0.90
4	25.1	2.9	0.73
8	16.2	4.5	0.57
12	11.3	6.5	0.54
24	8.63	8.5	0.36

9.1.4 2-D *N*-Heptane Case

The 19-species *n*-heptane reduced mechanism has been successfully applied to simulate the axisymmetric diffusion flame using VULCAN. The inflow conditions of the flame simulation are similar to the experimental setup of Evans et al. (1978) except that the static temperature of the air jet was again increased by 200 K to facilitate the ignition of the flame. The grid size for the simulation is 144 by 69 cells. Shown in Figure 39 are the contour plots of static temperature and mass fractions of the species C_7H_{16}, O_2, and H. The speedup factor when using ISAT for this case is approximately 10.

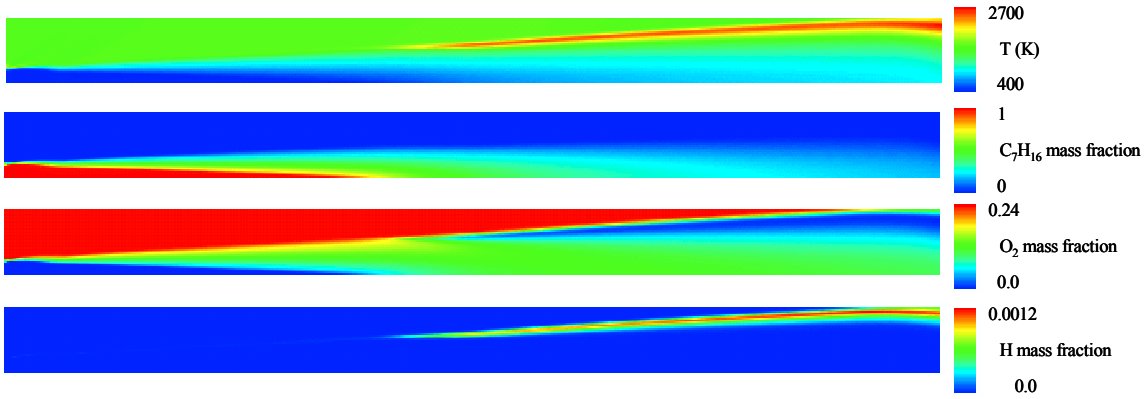

Figure 39. Contour Plots of Static Temperature and C_7H_{16}, O_2, and H Mass Fractions for the 2-D Heptane Diffusion Flame.

9.1.5 2-D JP-8 Case

The 35-species JP-8 reduced mechanism has been successfully applied to simulate the axisymmetric diffusion flame with VULCAN. The inflow conditions of the flame simulation are again similar to the experimental setup of Evans et al. (1978) except that the static temperature of the air jet was increased by 200 K to facilitate the ignition of the flame. The grid size for the simulation is 144 by 69 cells. Shown in Figure 40 are contour plots of static temperature, Mach number, and mass fractions of the six species in the fuel surrogate, O_2, CO, and CO_2. This case demonstrates the capability, developed during this project, of taking a large, complex mechanism and fuel surrogate from the literature and creating a reduced mechanism that can be incorporated into CFD simulations.

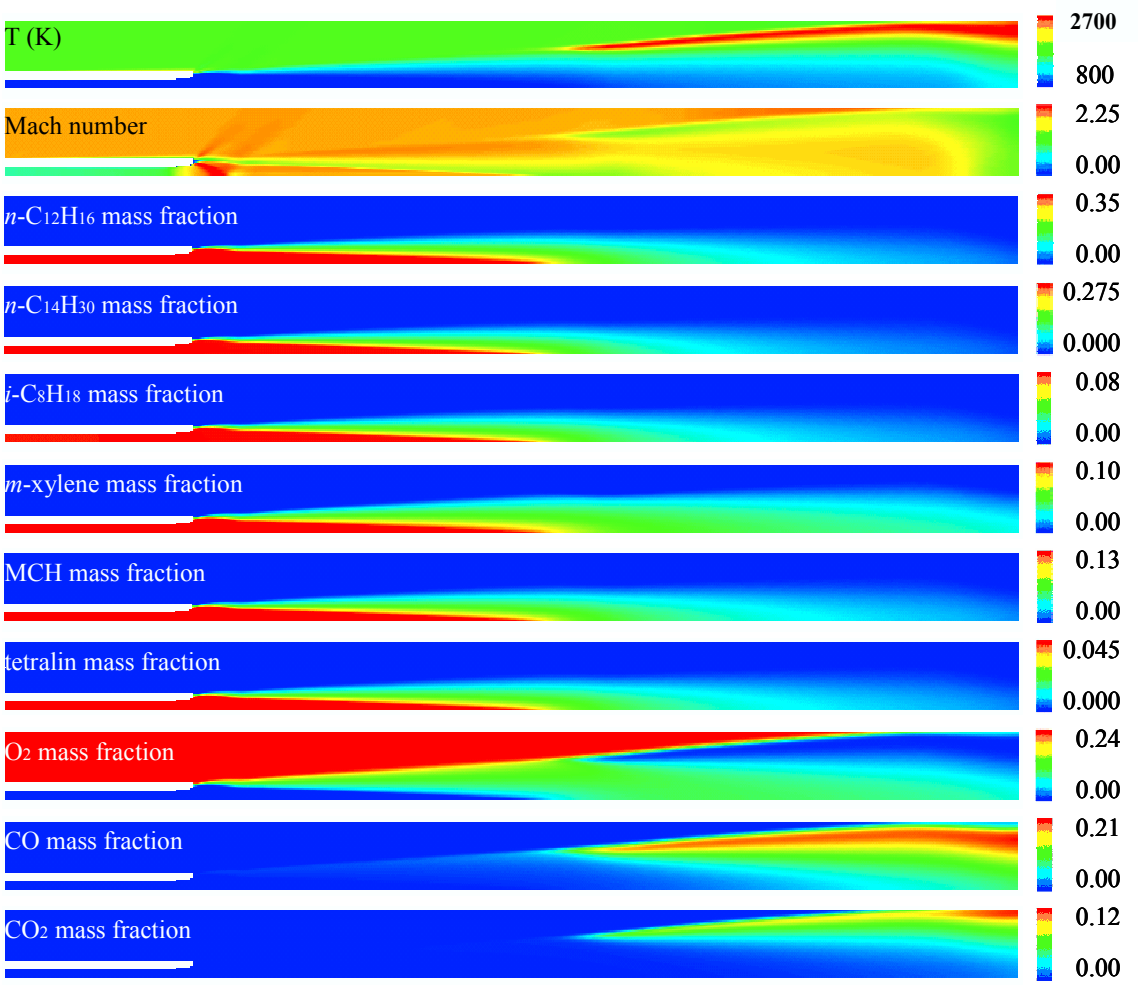

Figure 40. Contour Plots of Static Temperature, Mach Number, and Species Mass Fractions for the 2-D JP-8 Diffusion Flame.

9.1.6 ISAT Impacts for Complex Fuels

The CPU times of simulations of the *n*-heptane and JP-8 flames are summarized in Table 8. Note that the computer platform used to run the two cases is different from that for the H_2 and C_2H_4 case shown earlier in this section. For comparison purposes, the CPU times for C_2H_4 case are also listed in the table. The error tolerance for each of the three cases was 2%. The speedup factors of ISAT for the *n*-heptane and JP-8 flames are 11 and 12, respectively. Both are much smaller than the factor of 36 achieved in the C_2H_4 case. The ratio of CPU times between the reacting case and the mixing case, which can be used as an indicator of how expensive the mechanism is, is 72, 15, and 34, respectively, for the three mechanisms. A smaller speedup factor is expected for the relatively inexpensive *n*-heptane mechanism. In VULCAN, the implicit method requires the inversion of the Jacobian matrix, the chemical source term, of which the computational cost is proportional to n^3, where n is number of species. In the 35-specie JP-8 mechanism, the CPU cost for the inversion is about 5 times that of the 19-specie *n*-heptane mechanism.

This cost remains the same with and without ISAT. It results in a lower speedup for the JP-8 flame case. The exact measurement of the CPU time consumed by different procedures in VULCAN, however, is not available at this time. The CPU time of the reacting case for each of the mechanisms, is within 3 times the CPU time of the mixing case.

Table 8. Average CPU Times for a Single Time Step of Simulations of C_2H_4, n-Heptane, and JP-8 Flames.

Mechanisms	Mixing	Reacting w/o ISAT	Reacting w/ ISAT	Speedup
C_2H_4, 20-specie	1.43	102.9	2.82	36
N-Heptane, 19-species	1.32	19.6	1.72	11
JP-8, 35-species	2.11	72.1	5.94	12

9.1.7 Summary of 2-D Implementation

The 2-D cases described in this section demonstrate that detailed chemical kinetic mechanisms can be reduced using CARM and successfully integrated into VULCAN. Use of these reduced mechanisms has been demonstrated to include kinetic information that is lost when using comparable simplified Arrhenius-form models. Reduced mechanisms for larger hydrocarbons can be very slow to evaluate, but the use of ISAT makes the CPU time needed for CARM reduced mechanisms comparable to that of similarly sized global kinetics. The speedup for multiple processors when using ISAT is not as large as anticipated, but the speedup improves for 3-D cases. 2-D cases that were run using reduced mechanisms for *n*-heptane and JP-8 demonstrate the feasibility of creating and implementing reduced kinetics for large hydrocarbons into VULCAN. Unfortunately, no experimental data are available for comparison.

9.2 Turbulence-Chemistry Interaction

9.2.1 EDC Model

The EDC turbulent combustion model was applied to simulate the hydrogen and ethylene flames described in Sections 9.1.1 and 9.1.2. The grid size for all the cases shown here is 61 by 35 cells. For the hydrogen flame simulations, Figure 41 compares the temperature and H_2 mass fraction fields predicted with the EDC model and laminar chemistry. The flame structures look very similar for both cases. The flame is detached in both cases. The liftoff height of the flame predicted with the EDC model is slightly larger than that with laminar chemistry. This implies that the turbulence-chemistry interaction might be important when the flame is close to blowout conditions.

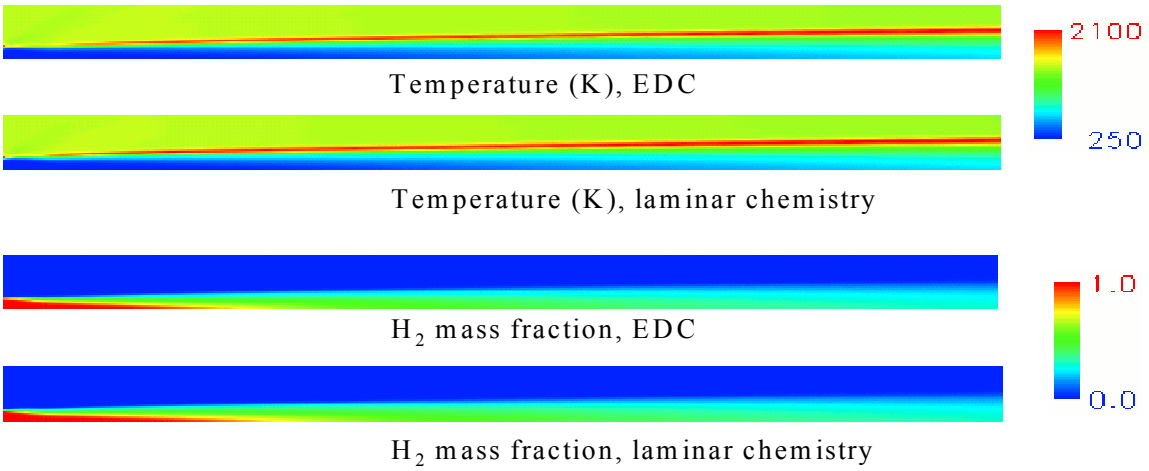

Figure 41. Temperature and H_2 Mass Fraction Fields Predicted with EDC Model and Laminar Chemistry.

The H_2 mass fraction along the centerline is shown in Figure 42. The potential core of the EDC flame is slightly shorter than that of laminar chemistry, and the downstream centerline H_2 mass fraction is slightly lower than that of laminar chemistry downstream.

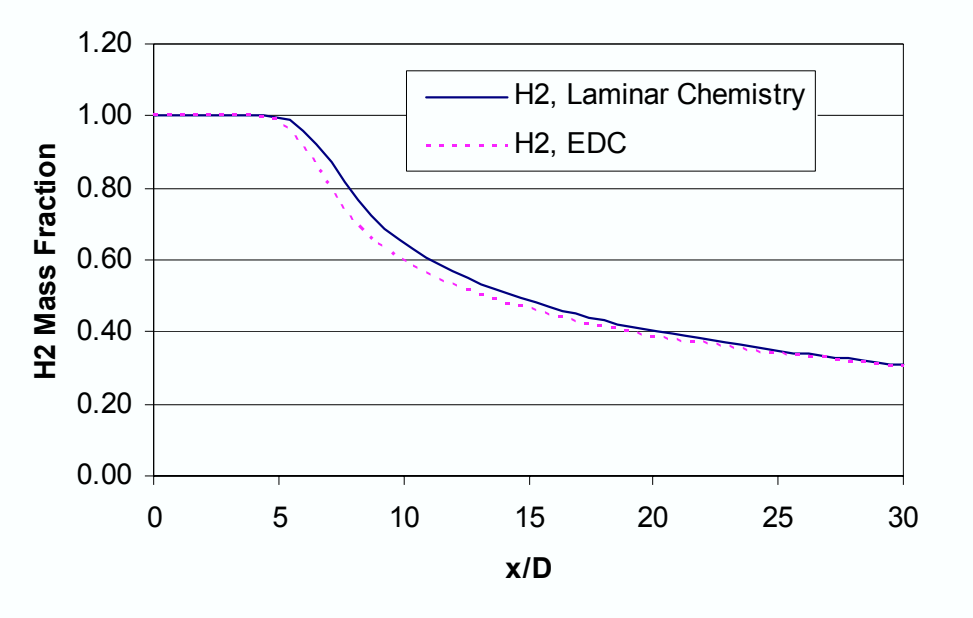

Figure 42. Distribution of H_2 Mass Fraction Along the Centerline.

Figures 43 and 44 show the radial profiles of H_2 and O_2 mass fractions at two axial locations, respectively. Again one sees very similar flame structure. The larger liftoff height of the EDC model allows more air mixed into the fuel stream, which results in higher O_2 concentration near the centerline.

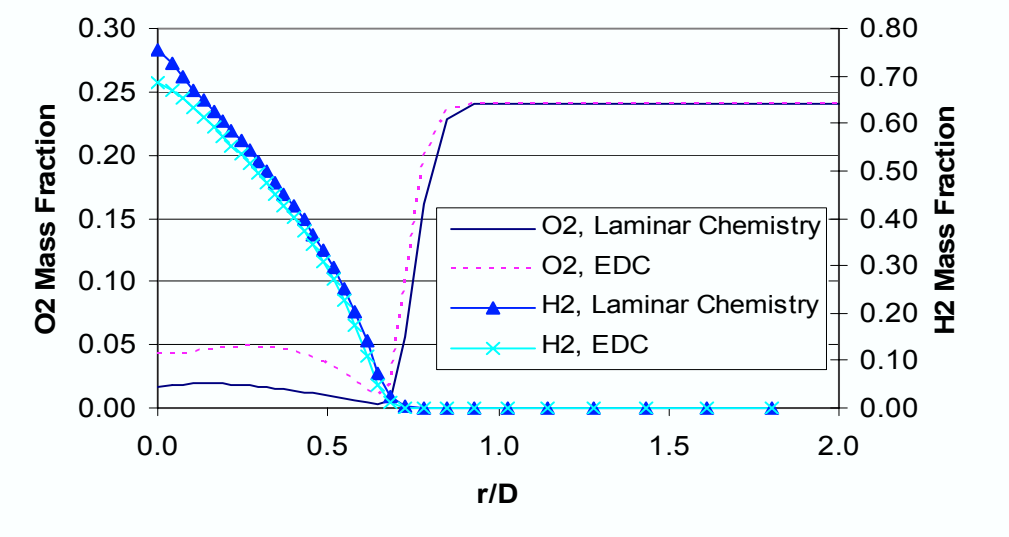

Figure 43. Radial Distribution of H_2 and O_2 Mass Fractions at x=8.26D.

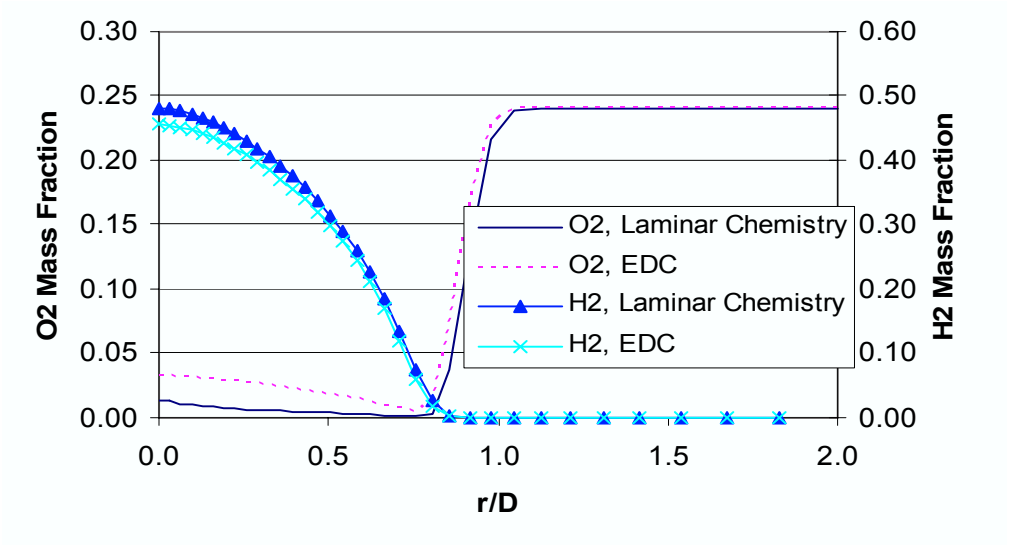

Figure 44. Radial Distribution of H_2 and O_2 Mass Fractions at x=15.5D.

In Figure 45, two important parameters in the EDC model, the life time of fine structures, , and the fraction of the regions occupied by the fine structures, are shown. The parameter is smaller inside the core of the jet, and larger outside. Throughout the computational domain, it is on the order of 10^{-5} seconds, which is much smaller than the typical ignition delay time of the hydrogen. As discussed in Section 7.1, the averaged reaction rate from Equation (11) is expected to be close to the laminar reaction rate. The small values of the life time of the fine structures, which resulted from the high-speed nature of the jet, are insignificant in their contribution to the mean reaction rate. The

fraction of the fine structure, , is close to 1 outside the jet shear layer, where turbulence is not very strong. Just downstream of the hydrogen duct, there is a region where is very small. This results in a small turbulent mean reaction rate, and delayed ignition of the flame.

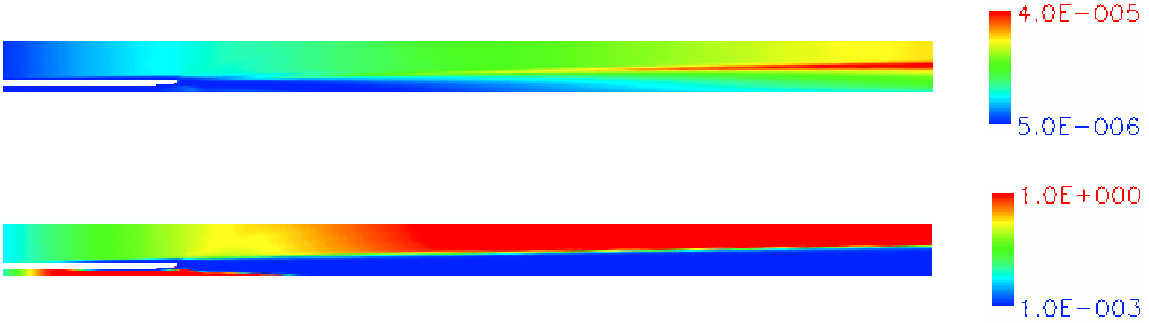

Figure 45. Contour Plots of EDC Model Parameters, (top, in seconds) and (bottom).

Comparisons of predicted temperature and C_2H_4 mass fraction fields of the ethylene flame simulations with and without the EDC model are shown in Figure 46. The effect of turbulence-chemistry interaction on the ignition of the flame is even more significant for the ethylene flame. For the case with laminar chemistry, the flame was ignited half way through the computational domain, while for EDC model, the flame is barely started at the end of the computational domain. The distribution of C_2H_4 in both cases is similar because the amount of C_2H_4 consumed in the two cases is very small due to the high speed of the jet.

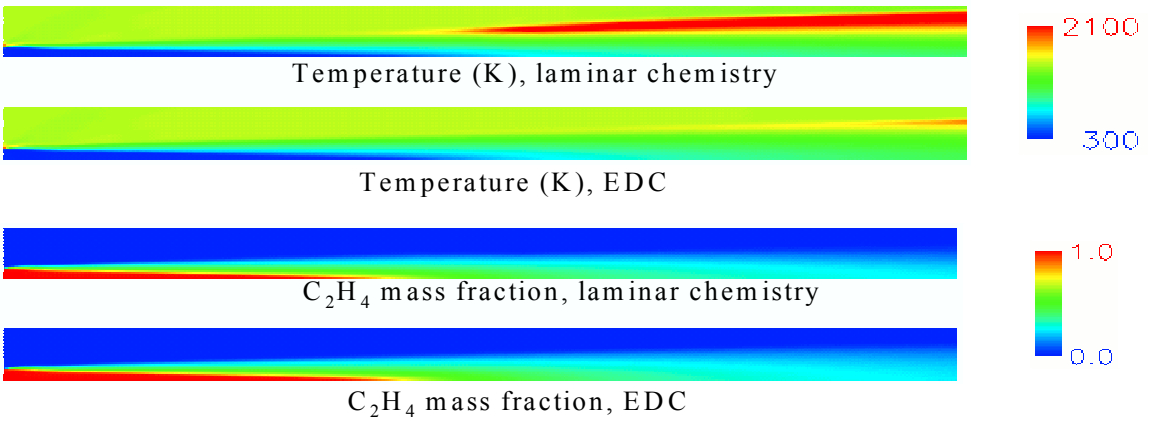

Figure 46. Temperature and C_2H_4 Mass Fraction Fields Predicted with EDC Model and Laminar Chemistry.

The CPU timings of the EDC model for the hydrogen and ethylene flames are shown in Table 9.

Table 9. CPU Time (in seconds) Per Time Step for Simulations with EDC Model Compared with Laminar Chemistry.

Mechanisms	Lam. Chem. w/o ISAT	Lam. Chem. w/ ISAT	EDC w/o ISAT	EDC w/ ISAT
H_2, 7-specie	0.254	0.147	11.2	0.431
C_2H_4, 20-specie	18.7	0.51	908.1	3.21

As previously discussed, there are only two steady-state species in the reduced hydrogen mechanism. Calculation with and without ISAT is relatively inexpensive. The CPU time including the EDC model without ISAT is 11.2 seconds per time step, 44 times that for laminar chemistry without ISAT. With ISAT, the CPU time for the EDC model is reduced to 0.431 seconds, a speedup factor of 26.

The 20-specie C_2H_4 mechanism is significantly more expensive. The CPU time of the EDC model without ISAT is 908.1 seconds per iteration. It is reduced to 3.21 seconds per time step with ISAT. The speedup factor is 282. The CPU cost for a simulation with the EDC model and ISAT for the ethylene flame is approximately 6 times that using laminar chemistry with ISAT. The tremendous CPU savings from the ISAT makes it feasible to perform a 3-D simulation with a practical fuel.

9.2.2 PDF Post-Processor

The axisymmetric hydrogen flame was chosen as the test case for the PDF post-processor to limit the tremendous CPU cost involved in PDF simulations. The reduced chemical mechanism is the seven-specie H_2 mechanism. A curvilinear coordinate system is used in VULCAN. However, the PDF post-processor requires Cartesian coordinates. The predicted velocity, density, and turbulent kinetic energy and its dissipation rate from the VULCAN simulation were interpolated to a 61 by 51 Cartesian grid. Those variables were fixed in the post-processor, while the species concentrations and temperature were recalculated. Two mixing models were applied in the post-processor: a well-mixed model (no turbulence-chemistry interaction) and a modified Curl's model (Curl, 1963). For Curl's model, the model constant C , which is the mechanical-to-scalar timescale ratio, is set to 2, a typical value in PDF simulations.

The predicted mean temperature and H_2 and O_2 mass fractions with the well-mixed model are shown in Figure 47. The results agree well with the results from VULCAN using laminar chemistry (see Figure 41), although the PDF post-processor predicts a slightly larger flame liftoff height. Since different numerical schemes are employed in VULCAN and the post-processor, a perfect match is not expected.

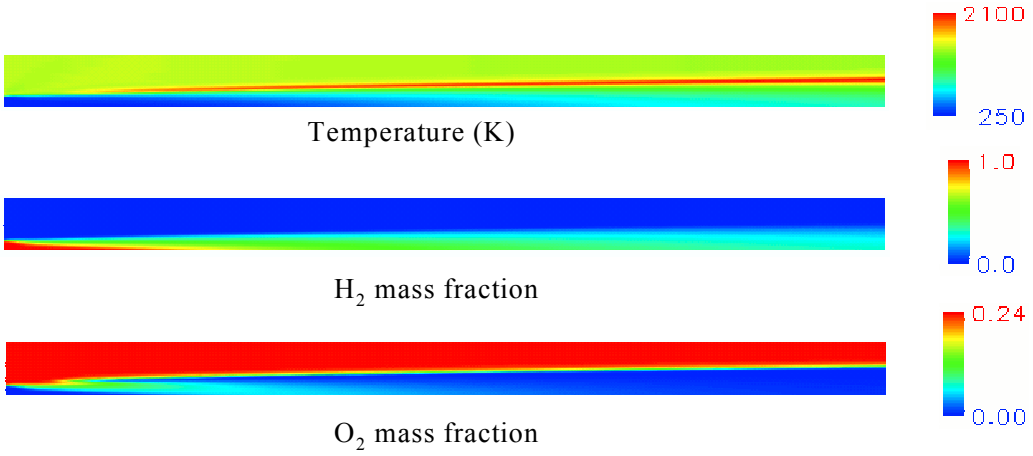

Figure 47. Contour Plots of Mean Temperature and H_2 and O_2 Mass Fractions for the Well-Mixed Model.

The results predicted with the modified Curl's model are shown in Figure 48. It is surprising to see that the flame is quenched in this case. The maximum temperature in the jet was slightly higher than that of the air stream. To understand the reason for the extinction, the turbulent time scale, $_t$, which is calculated from $_t \quad k/ \quad$, is plotted in Figure 49. This variable was used to determine the mixing frequency in the Curl's model, which is given by

$$\frac{C}{t}. \qquad (14)$$

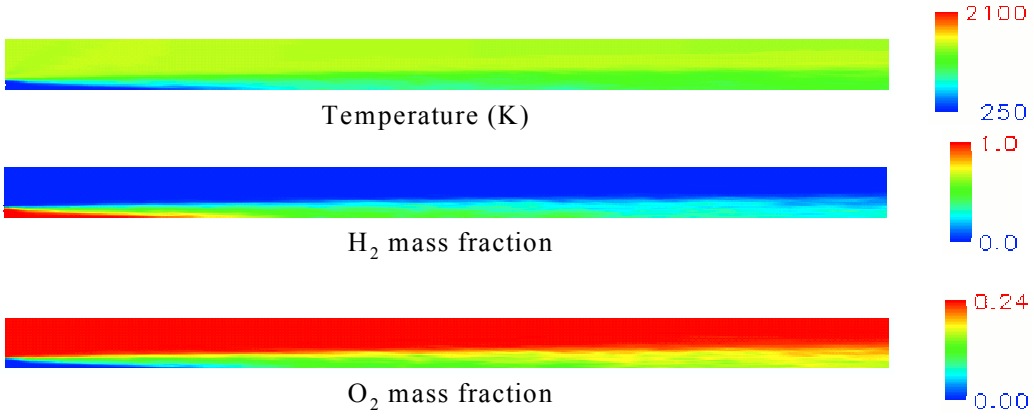

Figure 48. Contour Plots of Mean Temperature and H_2 and O_2 Mass Fractions for the Modified Curl's Model.

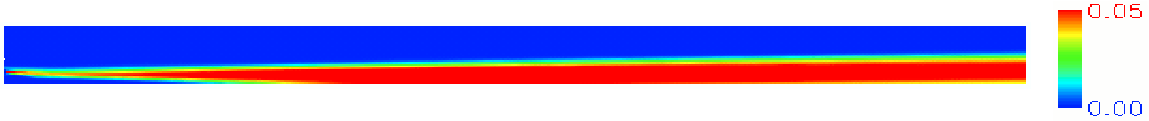

Figure 49. The Turbulent Time Scale, $_t \quad k/ \quad$ (in seconds).

Inside the jet shear layer where mixing between the hydrogen and air takes place, the time scale is on the order of 10^{-2} seconds. The residence time, defined as the time for a fluid particle to walk through the whole computational domain from the inlet to the outlet, is approximately 1.5×10^{-4} seconds (the length of the computational domain is 0.28 m, and the averaged axial velocity is approximately 2000 m/s). Thus, residence time is 2 orders of magnitude smaller than $_t$. This implies that the molecular-level mixing between the particles from the hydrogen and air streams is very slow compared to the convection speed of the jet.

We define a new variable, unmixedness:

$$\frac{\overline{f^{\,2}}}{1 \quad \overline{f}\,\overline{f}}, \tag{15}$$

where $\overline{f}$ and f are the mean and variation of the mixture fraction, respectively. The variable is 0 in the well-mixed region, and it is 1 in the region where the fluids are totally unmixed. Figure 50 shows the unmixedness for the well-mixed model and modified Curl's model. For the well-mixed model, is 0 everywhere. For the modified Curl's model, it is 1 inside the jet shear layer, and 0 in the pure air and hydrogen regions.

Figure 50. Contour Plots of Unmixedness for Well-Mixed Model (top) and Modified Curl's Model (bottom).

The turbulent time scale defined by *k*/ as predicted in VULCAN, is large. It results in the extinction of the hydrogen flame. To study the effect of the time scale on the PDF calculation, the time scale was artificially decreased by a factor of 100 such that its value inside the jet shear layer is in the same order of magnitude as the residence time. The predicted flame using the modified Curl's model is shown in Figure 51. With the improved molecular-level mixing between the particles, the flame is stabilized. The liftoff height is larger than that of the well-mixed case, which is consistent with the predictions of the EDC model.

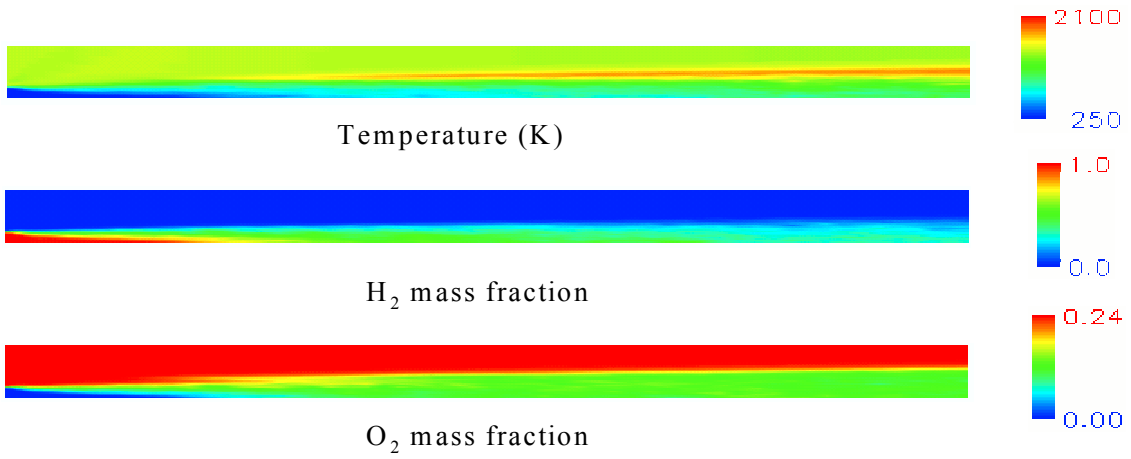

Figure 51. Predicted Mean Temperature and H_2 and O_2 Mass Fractions Using an Artificially Increased Turbulent Time Scale.

These simulations indicate that the turbulent time scale is very important in determining the molecular-level mixing process in the PDF methods.

9.2.3 Difference Between Turbulence-Chemistry Interaction Models

Evans et al. (1978, Appendix B) described a method for calculating the profiles of k and based on Prandtl's mixing length equation. Although the method was applied only to provide an initial profile for their simulations, it can also give us an estimation of the magnitudes of k and throughout a jet shear layer. The turbulent kinetic energy and its dissipation rate estimated by Evans et al. peaked at approximately 10^5 m^2/s^2 and 10^{11} m^2/s^3, respectively (See Evans et al., 1978, Figure 1 (b)). While the peak value of k predicted by VULCAN is in the same order of magnitude as the Evans estimate, the value of is significantly lower, with peak values of only 10^7 m^2/s^3. The apparent under-prediction of in VULCAN results in a very low value of mixing frequency, which results in the flame being quenched in the PDF post-processor simulations.

In the EDC model, k and are used to calculate the volume fraction of flow occupied by fine structures, , and the lifetime of the fine structures, . For low values of , and approach 1 and 0, respectively. From Eq. (7-6), the turbulent reaction rate approaches the laminar reaction rate, which is consistent with the results shown earlier in this section. It is expected that, with a higher calculated value of , the flame structures predicted using EDC model and PDF method will be much closer to each another.

In summary, simulations with both the EDC and PDF methods showed the effect of turbulent mixing on flame structure, i.e. larger lift-off height and a lower maximum temperature inside the flame. Both models rely on the accuracy of the turbulence model within the CFD code to predict the turbulent kinetic energy and dissipation rate.

10.0 3-D Scramjet Simulations

Two of the previously described reduced mechanisms, those for ethylene and *n*-heptane have been used to run 3-D simulations of a scramjet cavity flameholder. Results of these simulations are reported in this section. These simulations were performed on a Compaq ES-45 computer using sixteen processors. Each simulation required about 250,000 iterations and about one month of computer time to converge. The grid for these simulations had 334,558 cells.

10.1 Ethylene

The ethylene reduced chemical kinetic mechanism previously incorporated into VULCAN was tested for a 3-D simulation. The test model is a cavity-based flameholder with an injection port at the back of the cavity-ramp wall, which corresponds to the experimental research of AFRL/PRA Test Cell 19 facility. Although there were 10 injection ports in the back cavity-ramp wall, current numerical simulation consisted of the study of the flow fields of one of the injector ports, as shown in Figure 52. In addition, no side-wall effects are considered in these simulations. The freestream Mach number is 2.0, with the total temperature and pressure of ethylene fuel at the injector exit at 311 K and 12 psia, respectively.

In the numerical simulation, the ethylene fuel was first injected into the cavity so that the mixing between the fuel and air in the cavity could be established. An ignition source was then applied in the cavity region to initiate combustion. Once combustion had been established based on increased temperature and production of CO_2 and H_2O in the cavity region, the ignition source was turned off. The simulation was then continued to determine whether the flame in the cavity would be self-sustaining. In the Test Cell 19 experimental setup, spark plugs were used for ignition. Experimental results have shown that the flame is able to self-sustain under these conditions. Numerical results using the CARM reduced mechanism also showed that the flame was able to sustain itself in the cavity, as shown in Figures 53 through 57. Previous efforts to simulate these conditions with global ethylene kinetics models have incorrectly predicted flame extinction at these conditions. This demonstrates CARM's ability to incorporate more chemical kinetic information into a model than curve fitting of global reaction rates can.

The temperature contours (Figure 53) show high temperature regions in the cavity, which indicate combustion taking place. Note that the low temperature zone in the center of the cavity is due to very fuel rich conditions. This can be observed from the E.R. contours (Figure 54). CO_2 and OH mass fractions are depicted in Figures 55 and 56. Regions of high concentrations of these species show that the chemical reaction is taking place near the stoichiometric surface (shown in Figure 54). The pressure contours and streamlines are shown in Figure 57. The recirculation region in the cavity facilitates mixing of fuel and air as well as hot, radical-containing flame gases with unburned fuel-air mixture, which sustains the flame, even under high Mach number freestream conditions.

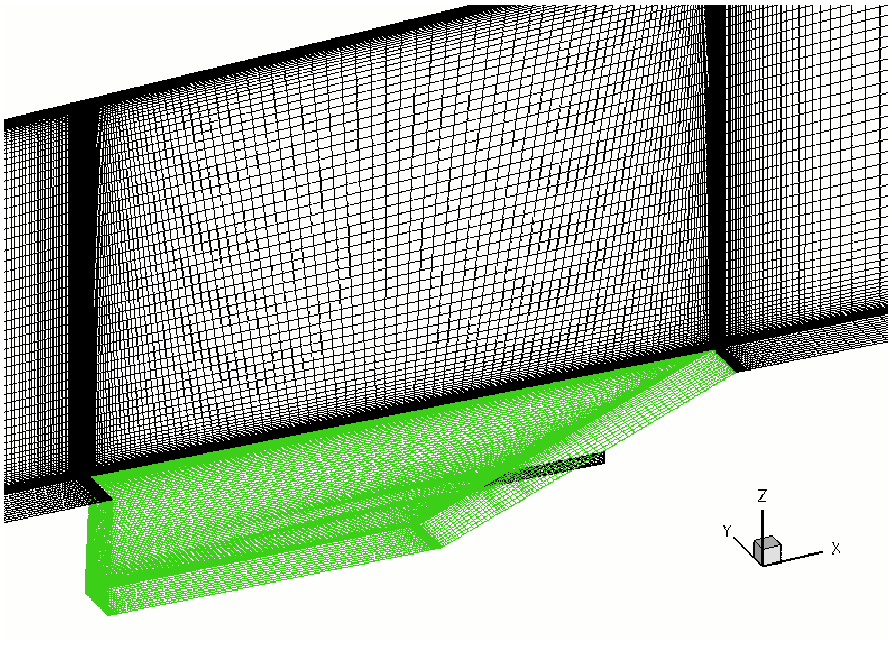

Figure 52. Computational Domain with Cavity and Injector Port.

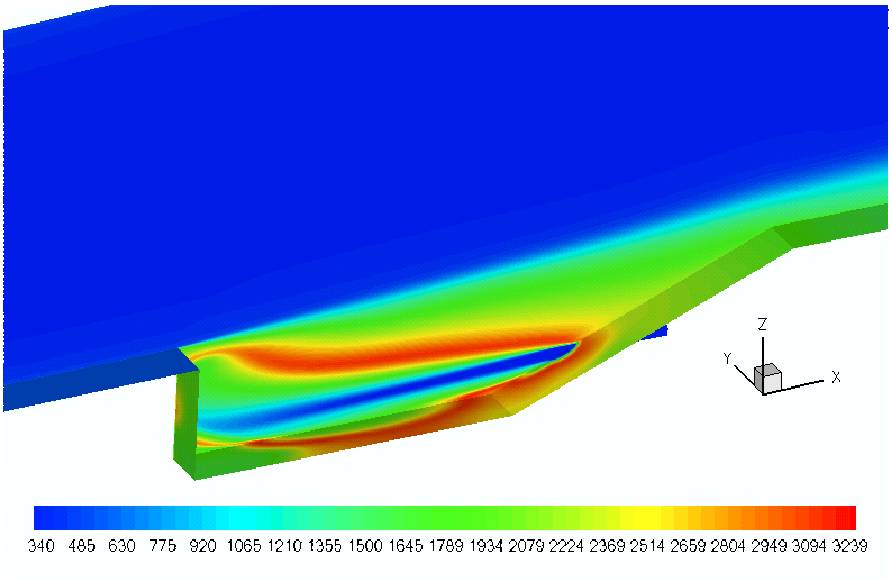

Figure 53. Temperature Contours (K) in the Vicinity of the Cavity.

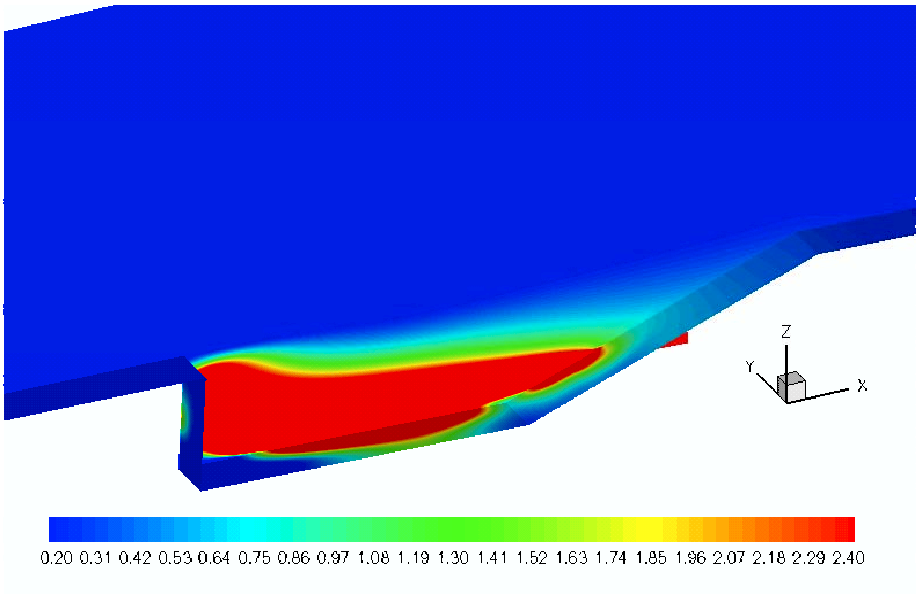

Figure 54. E.R. Contours in the Cavity Region.

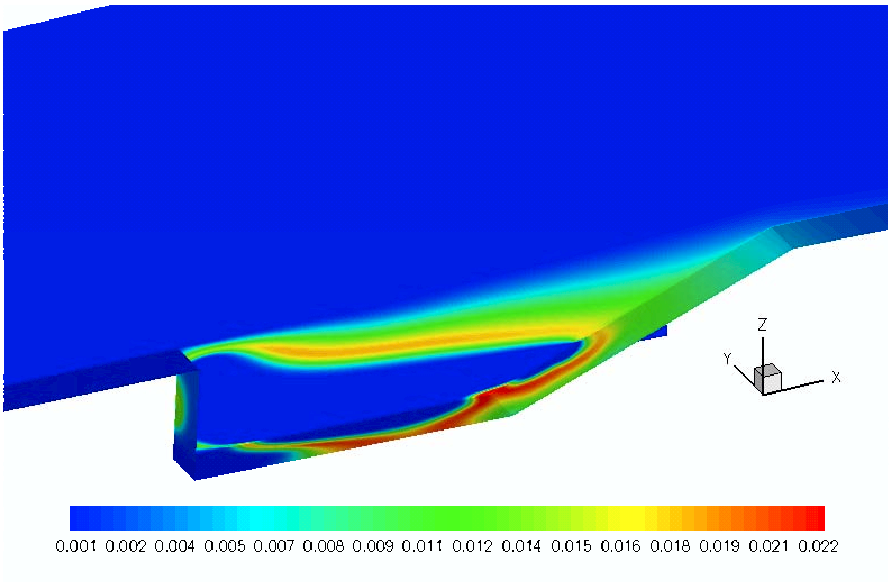

Figure 55. CO_2 Mass Fraction Contours in the Cavity Region.

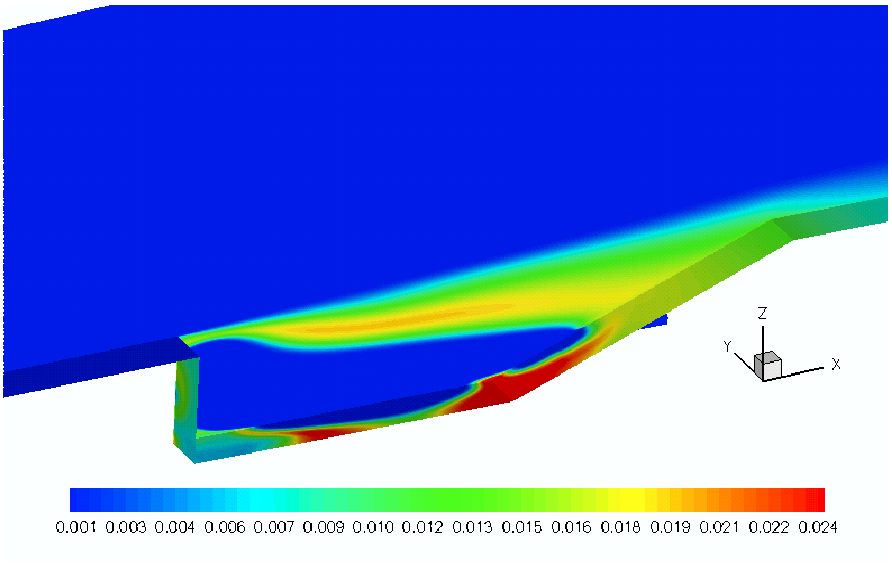

Figure 56. OH Mass Fraction Contours in the Cavity Region.

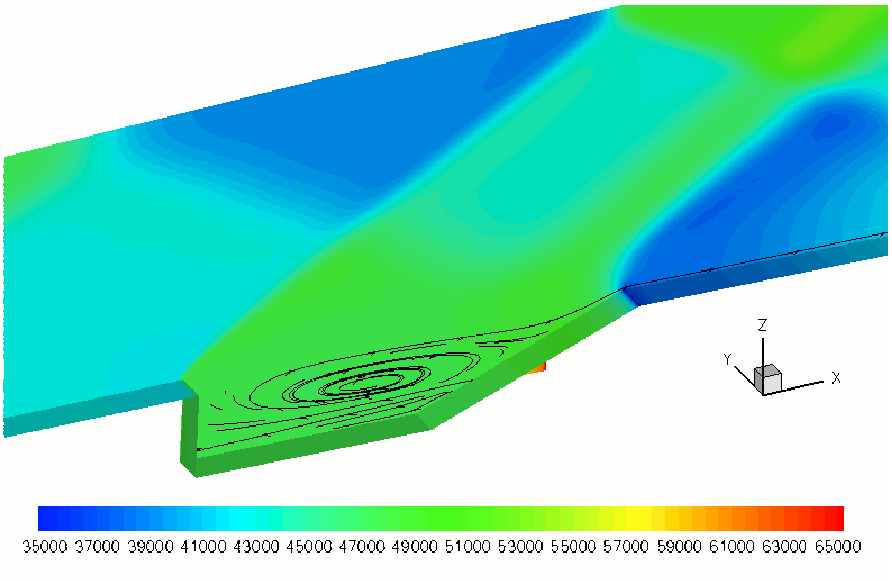

Figure 57. Pressure Contours and Streamlines in the Cavity Region.

10.2 *N*-Heptane

The *n*-heptane reduced mechanism described in previous reports has been used to model a 3-D flameholder case. The conditions were similar to those of the ethylene case. Once again stability problems due to the reduced mechanism were not observed, and a self-

sustaining simulated flame was achieved. Results of this calculation are shown in Figures 58 through 61.

The test model is a cavity-based flameholder with an injection port at the back of the cavity-ramp wall, similar to the ethylene case. However, no experimental data is available for comparison for the *n*-heptane case. In the ethylene simulation, the total pressure and temperature of the injector was provided by AFRL/PRA Test Cell 19 facility, and the data corresponds to 82.74 kPa (12 psia) and 316.46 K (110 °F), respectively.

Extensive effort was required to choose appropriate boundary conditions at injector port entrance for the *n*-heptane gas. Two analytical approaches were used to calculate the pressure coming out of the injector, while keeping the total temperature (316.46 K) the same as in the ethylene case. The first attempt was to assume that the mass flow rate and injector area of the ethylene and heptane gases are the same out of the injector port. Then the total pressure of the *n*-heptane gas can be computed using Equation (16), where *w* and *A* are the mass flow rate and injector area, respectively:

The values of and *R* were 1.26 and 83.1493 J/kg K, based on the temperature and the molecular weight of the *n*-heptane gas. The total pressure was found to be 43.33 kPa. These total properties were used at the entrance of the injector boundary condition. However, in this simulation, the static pressure at the injector entrance was lower than at the injector exit, i.e., at the flameholding cavity. Thus, the air inside the cavity was flowing into the injector port, instead of the heptane gas flowing into the cavity.

$$\frac{w}{A}_{\max} \quad \sqrt{\frac{}{R}\ \frac{2}{1}}^{\frac{1}{1}}\ \frac{P_0}{\sqrt{T_0}} \tag{16}$$

The second approach used the isentropic relation and assumed that the flow was choked at the injector exit. The static pressure was set to be 56 kPa, which corresponded to the injector exit for the ethylene case. Thus, the total pressure was found to be 101.3 kPa, while the total temperature remained at 316.46 K. In this case, the numerical solution showed that the flow was choked inside the injector port. The *n*-heptane gas was initially at a supersonic flow and became subsonic inside injector port. Eventually, this solution diverged. Different total pressure values were tested for the injector entrance. Unfortunately, these solutions were either not promising and/or diverging.

To reduce the complexity of the fuel inflow boundary condition, the injector itself was eliminated from the model, and a fixed boundary condition was imposed at the injector exit. A top-hat velocity profile was assumed. Initially, the total pressure was set to 43.33 kPa, which provided the same mass flow rate as the ethylene case. However, the solution for these conditions did not converge due to the low static pressure at the vicinity of the injector exit. After trial-and-error, the static pressure was increased to 160 kPa with exit velocity of 180 m/s. The simulation using this boundary condition has shown promise. First, a nonreacting flow simulation was performed to establish a mixing solution. Then,

the ignition zone was increased gradually inside the cavity with a constant static temperature of 1500 K to start a reacting solution. Once combustion had been established based on increased temperature and production of CO_2 in the cavity region, the ignition source was turned off to determine whether the flame in the cavity would self-sustain. Although the computation has not completed, the preliminary result shows that the flame was able to self-sustain in the cavity, as shown in Figures 58 through 61.

The temperature contours (Figure 58) show high temperature regions in the cavity, which indicate that combustion is taking place there. The high temperature zones are located near the front of the cavity and center of the bottom walls. The temperature is lower at the center of the cavity due to fuel-rich conditions. This can be observed from the E.R. contours (Figure 59) Mass fractions of CO_2 and H are depicted in Figures 60 and 61. Regions with high concentrations of these species show where chemical reactions were taking place. This simulation demonstrates the capability of CARM to produce a reduced mechanism for a large hydrocarbon fuel that can be implemented and run in a 3-D VULCAN case.

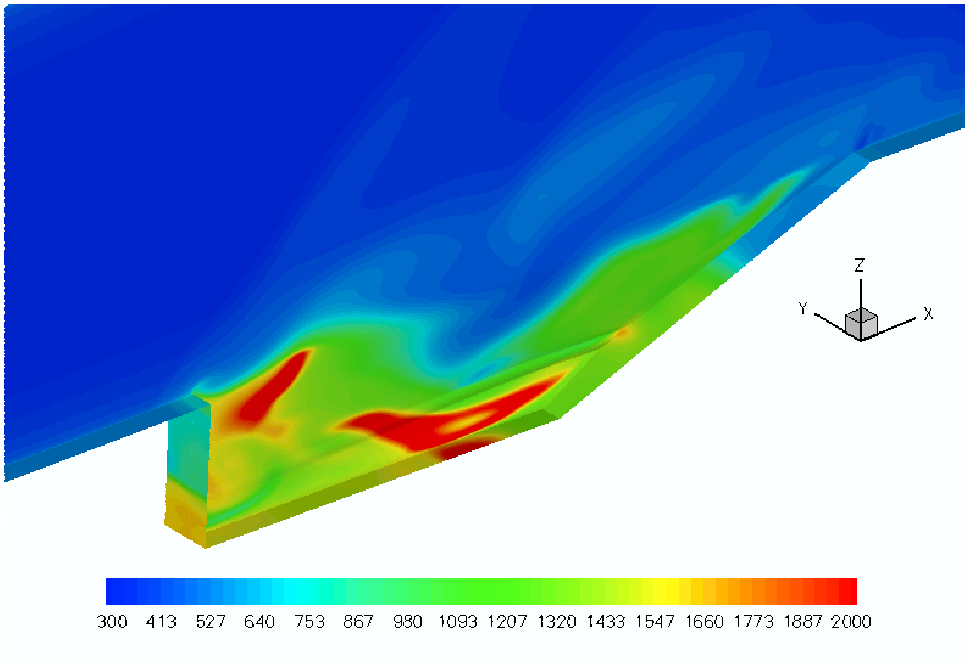

Figure 58. Temperature Contours (K) in the Vicinity of the Cavity.

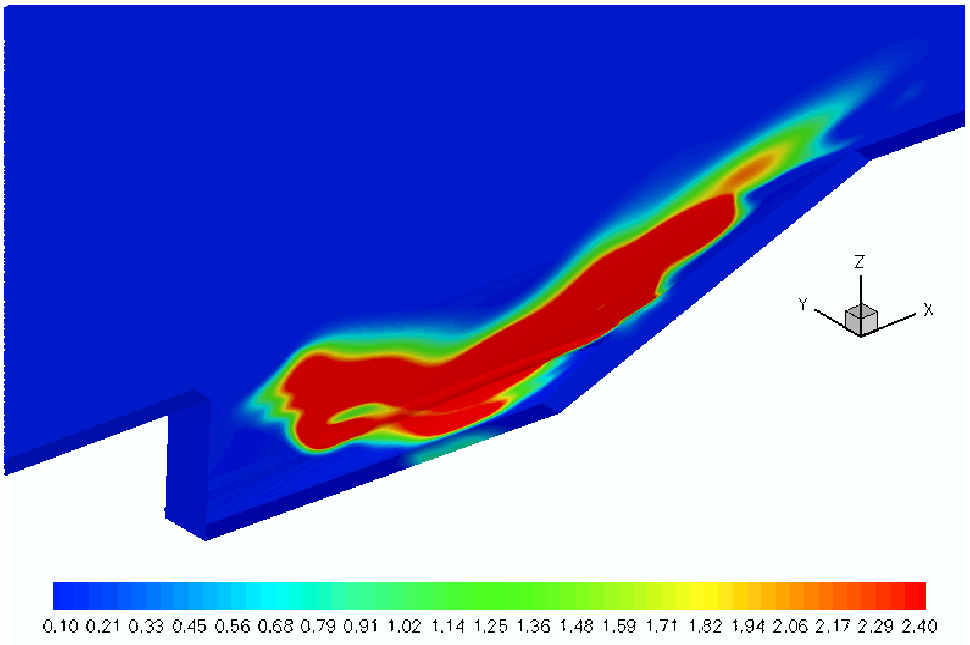

Figure 59. E.R. Contours in the Cavity Region.

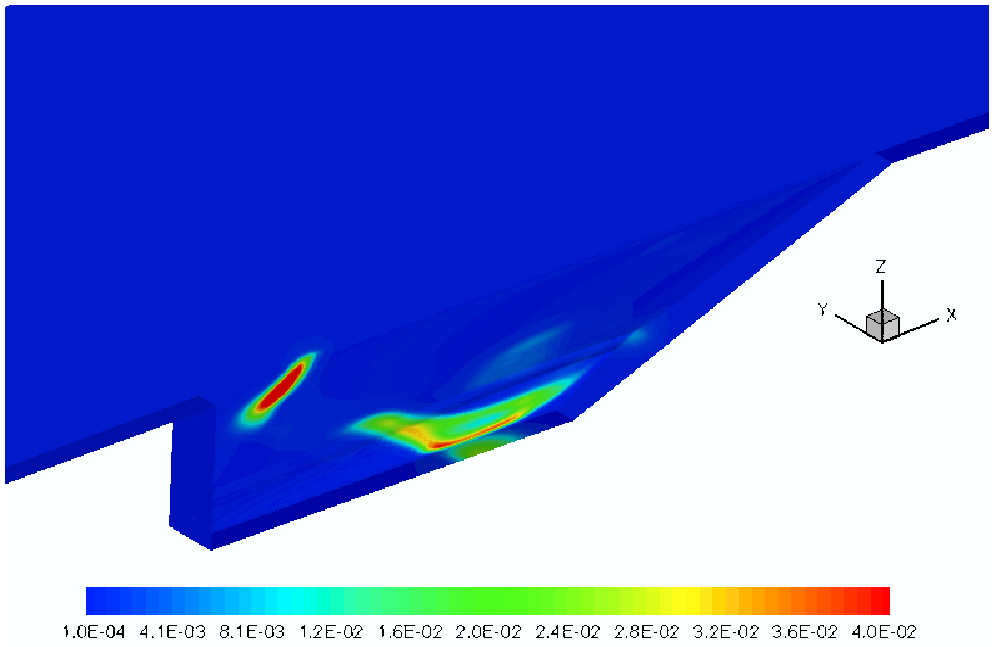

Figure 60. CO_2 Mass Fraction Contours in the Cavity Region.

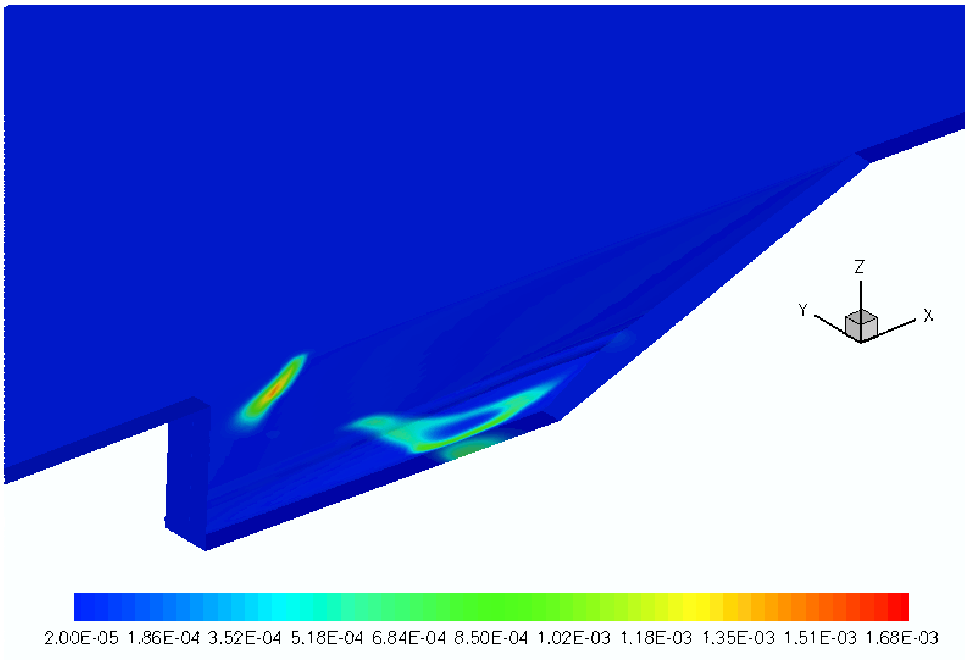

Figure 61. H Mass Fraction Contours in the Cavity Region.

11.0 Conclusions

This project has addressed existing limitations regarding our ability to represent complex hydrocarbon combustion chemistry within 3-D simulations of high-speed combustion of complex aviation fuels. This project focused on the implementation of several key recent developments into existing state-of-the-art CFD software that is currently utilized in the design of scramjet combustors. The developments that were utilized in this project are as follows:

Detailed chemistry for aviation fuels
Software (CARM) for generating accurate reduced mechanisms for aviation fuels
Sophisticated tabulation techniques (ISAT) that reduce the CPU time required for modeling hydrocarbon combustion
Techniques (EDC & PDF) to model the impacts of turbulence on calculation of the mean reaction rates
Software (VULCAN) for modeling high-speed hydrocarbon combustion.

This project integrated these components to demonstrate a process for: 1) developing accurate reduced chemical kinetic mechanisms for aviation fuels, 2) integrating them with ISAT and EDC into VULCAN, and 3) simulation of combusting flows with complex aviation fuel chemistry in scramjet combustor geometries. Data for the 2-D and 3-D cases is very limited particularly for aviation fuels. This project focused on utilizing simple configurations for verification of accuracy in cases where data were available.

The key results from the Phase II work included:

Development of accurate reduced mechanisms for combustion kinetics of hydrogen, ethylene, *n*-heptane, and a six-specie surrogate blend representing JP-8
Improvements to CARM software for automated reduction of chemical kinetic mechanisms resulting in improved robustness and decreased computational times
Implementation of four reduced mechanisms into VULCAN
Implementation of ISAT chemical rate tabulation technique into VULCAN
Implementation of EDC turbulence model (with ISAT) into VULCAN
Completion of simulations demonstrating improved chemical descriptions from reduced mechanisms compared to previously used global chemistry models
ISAT results showing speed increases up to a factor of 42
2-D combustion simulations in VULCAN demonstrating this approach for hydrogen, ethylene, *n*-heptane, and JP-8 (up to 35 species in the reduced mechanism)
3-D scramjet combustor simulations run for ethylene and *n*-heptane (up to 20 species in the reduced mechanism), demonstrating that this process can be used for CFD simulations of realistic 3-D scramjet geometries with aviation fuels.

The CARM software has proven to be a powerful tool for reducing large detailed kinetic mechanisms modeling the combustion of hydrocarbon fuels from the literature to a form that can be implemented into a CFD code. ISAT is a necessary companion

technology which is needed to reduce the computational cost of source term evaluation when using CARM-reduced mechanisms.

Modeling turbulence-chemistry interactions for high-speed reacting flows remains a challenge due to both the computational cost of the models and the uncertainties of the models themselves. Both the EDC and PDF models tested during this project gave the expected results of increasing the flame liftoff distance and reducing the maximum flame temperature. However, the models gave very different predictions. These differences can be traced to the ways the models use the information, such as turbulent time scales, from the fluid turbulence model. The results suggest that further work is needed to improve both turbulence models and turbulence-chemistry interaction models for high-speed reacting flows.

12.0 Future Directions

REI has been actively developing and applying reduced chemistry to 3-D simulation for a wide range of industrial applications involving low-speed combustion and incineration and will continue to do so. There are also a number of potential follow-on opportunities associated with simulation of high-speed reacting flows related to the work completed on this project that could be pursued. Some specific areas are summarized here.

12.1 Development of a Reduced Mechanism for JP-7

JP-7 is a highly refined hydrocarbon fuel originally developed for the SR-71 (Edwards & Maurice 2001) but now of interest as a scramjet fuel. Kinetics for JP-7 have been developed (Mawid et al., 2003) but they are proprietary and their distribution may be problematic. It is likely that a suitable surrogate could be formulated using compounds available in the Violi et al. (2002) mechanism, from which a JP-8 reduced mechanism was successfully created during this project. It is also possible that the present JP-8 reduced mechanism could work for JP-7 with a surrogate fuel containing species in the JP-8 mechanism but in different proportions. Agreement among interested parties on a suitable detailed mechanism and fuel surrogate would be necessary before starting work on the development of a reduced mechanism.

12.2 Incorporation of ISAT/CARM Methodology into Metacomp's CFD++

VULCAN is not the only CFD code used by Air Force personnel for simulation of high-speed combusting flows. Metacomp's CFD++ is a well-developed commercial code that could see significant benefit from incorporation of ISAT and reduced mechanism capability. This would require an agreement between REI and Metacomp, possibly allowing REI access to at least some source code. It may also require a C code output option from CARM.

12.3 Improvements in ISAT Table Access Methods

Several possibilities exist for improving the efficiency of the ISAT algorithm. Among these are periodic table restructuring and multitable methods. Possibilities also exist for improving the performance of ISAT on multiple processors. Investigation into the sensitivity of accuracy and speedup to alternate definitions of the Region of Accuracy could also be beneficial.

12.4 Turbulence-Chemistry Interaction Methods for High-Speed Flows

This is a difficult but important area of research. New ideas that improve on a constant Schmidt number approximation would be valuable to the high-speed flow community. Novel ideas could involve aspects of existing models for turbulent mixing, including Kerstein's LEM.

References

Baker, J. A., and Skinner, G. B., "Shock-Tube Studies on the Ignition of Ethylene-Oxygen-Argon Mixtures," *Combustion and Flame* 19:347-350, 1972.

Baurle, R. A., Alexopoulos, G. A., and Hassan, H. A., "Analysis of Supersonic Combustors with Swept Ramp Injectors," *Journal of Propulsion and Power* 13:327-328, 1997.

Baurle, R.A., Fuller, R.P., White, J.A., Chen, T.H., Gruber, M.R., and Nejad, A.S., "An Investigation of Advanced Fuel Injection Schemes for Scramjet Combustion," AIAA Paper 98-0937, 1998a.

Baurle, R.A., Mathur, T., Gruber, M.R., and Jackson, K.R., "A Numerical and Experimental Investigation of a Scramjet Combustor for Hypersonic Missile Applications," AIAA Paper 98-3121, 1998b.

Baurle, R. A., Tam, C.-J., and Dasgupta, S., ``Analysis of Unsteady Cavity Flows for Scramjet Applications," AIAA Paper 2000-3617, July 2000.

Baurle, R. A., and Eklund, D. R., "Analysis of Dual-Mode Hydrocarbon Scramjet Operation at Mach 4-6.5," *Journal of Propulsion and Power*, 18 (5):990-1002, 2002.

Bendtsen, A.B. Glarborg, P., and Dam-Johansen, K., "Visualization Method in Analysis of Detailed Chemical Kinetics Modeling," *Computers and Chemistry*, 25:161-170, 2001.

Bockelie, M., Wang, D., Cremer, M., Tang, Qing, and Chen, J.-Y. , "A Newton-Krylov Based Solver for Modeling Finite Rate Chemistry CFD Modeling," presented at the 2003 SIAM Conference on Computational Science and Engineering, San Diego, CA, USA, February 10-13, 2003.

Chen, J.-Y., Workshop on Numerical Aspects of Reduction in Chemical Kinetics, CERMICS-ENPC, Cite Descartes - Champus sur Marne, France, Sept. 2, 1997. available at http://www.reaction-eng.com/downloads/carmpaper.pdf

Chen, J.-Y., Blasco, J. A., Fueyo, N., and Dopazo, C., "An Economical Strategy for Storage of Chemical Kinetics: Fitting *In Situ* Adaptive Tabulation with Artificial Neural Networks," *Twenty-Eighth Symposium (International) on Combustion*, 2000.

Colket, M. B., and Spadaccini, L. J., "Scramjet Fuels Autoignition Study," ISABE Paper No. 99-7069, 14th International Symposium on Air Breathing Engines, Florence, Italy, Sept. 5-10, 1999.

Cremer, M. A., Montgomery, C. J., Wang, D. H., Heap, M. P., and Chen, J.-Y. "Development and Implementation of Reduced Chemistry for CFD Modeling of Selective Noncatalytic Reduction," *Proceedings of the Combustion Institute*, 28:2427-2434, 2000a.

Cremer, M., Adams, B., Wang, D., and Heap, M., "CFD Modeling of NOx Reduction Technologies in Utility Boilers," FACT-Vol. 23/HTD-Vol. 367, Combustion, Fire, and Computational Modeling of Industrial Combustion Systems, ASME, 57-68, 2000b.

Cremer, M. A.,Wang, D. H., Montgomery, C. J., and Adams, B. R., "Utilization of Reduced Mechanism Methods in CFD Simulations for Improved NOx Predictions in Utility Boilers and Furnaces," Joint AFRC/JFRC/IEA International Combustion Symposium, Kauai, HI, Sept. 9-12, 2001.

Curl, R. L., *AIChE Journal*, 9:75, 1963.

Curran, H.J., Gaffuri, P., Pitz, W. J., and Westbrook, C. K., "A Comprehensive Modeling Study of *n*-Heptane Oxidation," *Combustion and Flame* 114:149-177, 1998; and also Curran, E.T., Heiser, W.H., and Pratt, D.T., *Annu. Rev. Fluid Mech.* 28:323-360, 1996.

Dagaut, P., Reuillon, M., Boettner, J.-C., and Cathonnet, M., "Kerosene Combustion at Pressures up to 40 Atm: Experimental Study and Detailed Chemical Kinetic Modeling," *Twenty-Fifth Symposium (International) on Combustion*, 919-926, 1994.

Denison, M. K,., Montgomery, C. J., Sarofim, A. F., Bockelie, M. J., and Webster, A. G., "Computational Modeling of a Chemical Demilitarization Deactivation Furnace System," submitted to *Environmental Engineering Science*, 2003.

Douté, C., Delfau, J.L., Akrich, R., and Vovelle, C., *Combustion Science and Technology* 106(4-6):327-344, 1995.

Edwards T., and Maurice, L. Q., "Surrogate Mixtures to Represent Complex Aviation and Rocket Fuels," *Journal of Propulsion and Power,* 17:461-466, 2001.

Evans, J. S., Schexnayder, C. J. Jr., and Beach, H. L. Jr., "Application of a Two-Dimensional Parabolic Computer Program to Prediction of Turbulent Reacting Flows," NASA TP 1169, 1978.

Freeman, G. and Lefebvre, A. H., "Spontaneous Ignition Characteristics of Gaseous Hydrocarbon-Air Mixtures," *Combustion and Flame* 58:153-162, 1984.

GRI Mech web site, http://www.me.berkeley.edu/gri_mech/version30/text30.html

Gran, I. R. and Magnussen, B. F., "A Numerical Study of a Bluff-body Stabilized Diffusion Flame. Part 2. Influence of Combustion Modeling and Finite Rate Chemistry," *Combustion Science and Technology*, 119:191-217, 1996.

Heiser, W. H., and Pratt, D. T., *Hypersonic Airbreathing Propulsion*, AIAA, Washington, DC, 1994.

Held, T. J., Marchese, A. J., and Dryer, F. L., "A Semi-Empirical Reaction Mechanism for *n*-Heptane Oxidation and Pyrolysis," *Combustion Science and Technology,* 123:107-146, 1997.

Jachimowski, C. J., "An Analytical Study of the Hydrogen-Air Mechanism with Application to Scramjet Combustion," NASA TP 2791, 1988.

Magnussen, B. F., "Modeling of Pollutant Formation in Gas Turbine Combustors Based on the Eddy Dissipation Concept," *Eighteenth International Congress on Combustion Engines*, International Council on Combustion Engines, Tianjin, China, 1989.

Marinov, N. M., Pitz, W. J., Westbrook, C. K., Vincitore, A. M., Castaldi, M. J., and Senkan, S. M., "Aromatic and Polycyclic Aromatic Hydrocarbon Formation in a Laminar Premixed *n*-Butane Flame," *Combustion and Flame,* 114:192-213, 1998.

Mawid, M., Park, T., and Sekar, B., "Development and Validation of Detailed and Reduced JP-8 Fuel Chemistry Models," AIAA Paper 2002-3876, 38th AIAA/ASME/SAE/ASEE Joint Propulsion Conference, 2002.

Mawid, M. A., Park, T. W., Sekar, B., Arana, C., and Aithal, S. M., "Development of a Detailed Chemical Kinetic Mechanism for Combustion of JP-7 Fuel," AIAA 2003-4939, July, 2003.

Maurice, L.Q., Ph.D. thesis, Dept. of Mechanical Engineering, University of London, 1996.

Menter, F. R., "Improved Two-Equation k-omega Turbulence Models for Aerodynamic Flows," NASA TM-103975, Oct. 1992.

Mercier, R.A., and Ronald, T.M.F., "U.S. Air Force Hypersonic Technology Program (HyTech)," AIAA 7th International Spaceplanes and Hypersonics Systems and Technology Conference, Norfolk, VA, Nov. 18-22, 1996.

Montgomery, C. J., Swensen, D. A., Harding, T. V., Cremer, M. A., and Bockelie, M. J., "A Computational Problem Solving Environment for Creating and Testing Reduced Chemical Kinetic Mechanisms," *Advances in Engineering Software,* 33:59-70, 2002a.

Montgomery, C. J., Cremer, M. A., Chen, J.-Y., Westbrook, C. K., and Maurice, L. Q., "Reduced Chemical Kinetic Mechanisms for Hydrocarbon Fuels," *Journal of Propulsion and Power*, 18:192-198, 2002b.

Montgomery, C. J., Cannon, S. M., Mawid, M. A., and Sekar, B., "Reduced Chemical Kinetic Mechanisms for JP-8 Combustion," AIAA 2002-0336, Jan., 2002c.

Montgomery, C. J., Sarofim, A. F., Eddings, E. G., Marsh, N., and Palotas, A., "Multifunctional Fuel Additives for Reduced Jet Particulate Emissions," Phase I SBIR Final Report, Contract Number F33615-02-M-2254, 2003a.

Montgomery, C. J., Zhao, W., Eklund, D. R., and Chen, J.-Y., "CFD Simulations of Supersonic Hydrocarbon Combustion Using Reduced Mechanisms and ISAT," AIAA 2003-3547, June, 2003b.

Mullins, B. P., "Autoignition of Hydrocarbons," AGARDograph No. 4, 1955.

Peters, N., *Turbulent Combustion*, Cambridge University Press, Cambridge, UK, 2000.

Pope, S. B. "Computationally Efficient Implementation of Combustion Chemistry Using *In Situ* Adaptive Tabulation," *Combustion Theory and Modeling,* 1:42-63, 1997.

Soyhan, H.S., Lovas, T., and Mauss, F., "Stochastic Simulation of an HCCI Engine Using an Automatically Reduced Mechanism," *ICE*, Vol. 37-2, 2001 Fall Technical Conference, ASME, 2001.

Spalding, D. B., "Mixing and Chemical Reaction in Steady Confined Turbulent Flames," *Thirteenth Symposium (International) on Combustion,* The Combustion Institute, Pittsburgh, 649-657, 1971.

Spalding, D. B., "Development of Eddy-break-up Model of Turbulent Flames," *Sixteenth Symposium (International) on Combustion,* The Combustion Institute, Pittsburgh, 1657-1663, 1976.

Tham, Y. F., and Chen, J. Y., "Recent Advances on Automatic Generation of Simplified Mechanisms," Paper 03F-49, Combustion Institute Western States Section Fall Meeting, Los Angeles, CA, Oct. 20-21, 2003.

Violi, A., Yan, S., Eddings, E. G., Sarofim, A. F., Gratata, S., Faravelli, T., and Ranzi, E., "Experimental Formulation and Kinetic Model for JP-8 Surrogate Mixtures," *Combustion Science and Technology,* 174:339-417, 2002.

VULCAN Web Page: http://vulcan-cfd.larc.nasa.gov/

Wang, H., and Frenklach, M., "Detailed Reduction of Reaction Mechanisms for Flame Modeling," Combustion and Flame, 87:365-370, 1991.

Wang, H., Laskin, A., Djurisic, Z. M., Law, C. K., Davis, S. G., and Zhu, D. L., "A Comprehensive Mechanism of C_2H_x and C_3H_x Fuel Combustion," Eastern States Section of the Combustion Institute Meeting, Raleigh, NC, Oct., 1999.

White, J. A., and Morrison, H. "A Pseudo-Temporal Multi-Grid Relaxation Scheme for Solving the Parabolized Navier-Stokes Equations," AIAA 99-3360, Jan. 1999.

Wilcox, D. C., "Wall Matching, a Rational Alternative to Wall Functions," AIAA Paper 89-0611, Jan., 1989.

Wilcox, D. C., *Turbulence Modeling for CFD*, DCW Industries, Inc., 1993.

Yang, B., and Pope, S.B., "Treating Chemistry in Combustion with Detailed Mechanisms – *In Situ* Adaptive Tabulation in Principal Directions – Premixed Combustion," *Combustion and Flame* 112:85-112, 1998.

List of Acronyms

Acronym	Description
2-D	two dimensional
3-D	three dimensional
BSL	baseline
CARM	computer-assisted reduction mechanism
CFD	computational fluid dynamic (or dynamics)
CPU	central processing unit
DDASAC	Double precision Differential-Algebraic Sensitivity Analysis Code
DoD	Department of Defense
DR	detailed reduction
E.R.	equivalence ratio
EBU	eddy breakup
EDC	eddy dissipation concept
EOA	ellipsoid of accuracy
GRI	Gas Research Institute
H-O	hydrogen-oxygen
ISAT	in situ adaptive tabulation
KIVA	not an acronym
LEM	linear eddy model
LU	lower-upper
NSF	National Science Foundation
ODE	ordinary differential equation
PDF	probability density function
PFR	plug flow reactors
PSE	problem solving environment
PSR	perfectly stirred reactor
r/D	radius divided by diameter
QSS	quasi-steady state
REI	Reaction Engineering International
UNICORN	UNsteady Ignition and COmbustion with ReactioNs
VULCAN	Viscous Upwind aLgorithm for Complex flow ANalysis